Investigation Relative to the Roentgen Satellite (ROSAT)

NASA Grant NAG5-1536

Semiannual Report Nos. 4 and 5

For the Period 15 October 1992 through 15 October 1993

Principal Investigators
(See Attached)

January 1994

Prepared for:

National Aeronautics and Space Administration
Goddard Space Flight Center
Greenbelt, Maryland 20771

Smithsonian Institution
Astrophysical Observatory
Cambridge, Massachusetts 02138

The Smithsonian Astrophysical Observatory is a member of the Harvard-Smithsonian Center for Astrophysics

The NASA Technical Officer for this grant is Dr. Robert Petre, Code 666, Laboratory for High Energy Astrophysics, Space Sciences Directorate, Goddard Space Flight Center, Greenbelt, MD 20771.

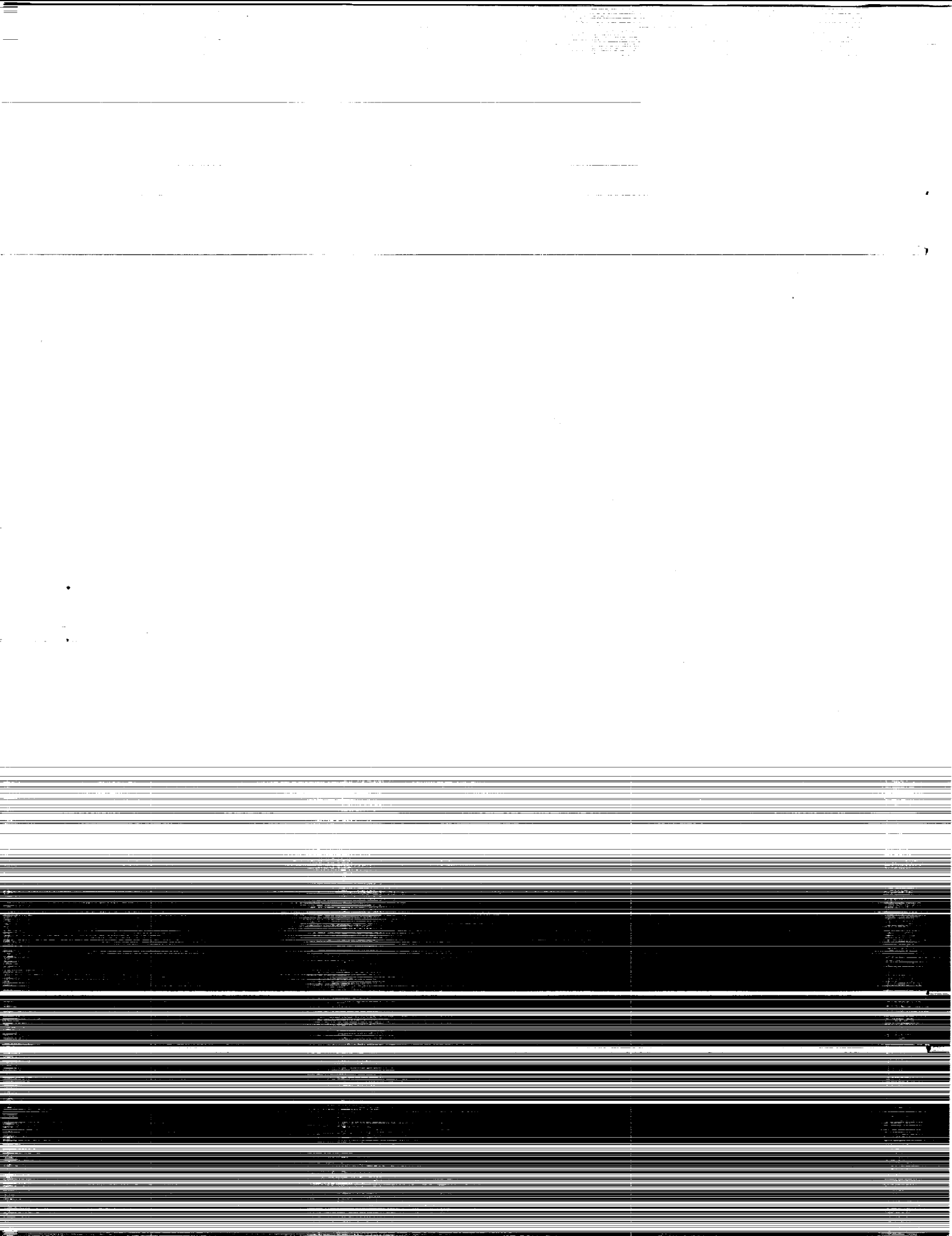

1 Investigation Relative to ROSAT

1.1 PR 666-27127 (P.I.: Martin S. Elvis)

Papers were written describing several major results as a result of this program. Others are in preparation.

1. P2095-5-89RI — What Does a Normal Quasar Look Like in X-rays?
   Objects observed in this program have been combined with those in a study by A. Laor et al. to increase the sample size and will be reported there. A paper is in preparation on the combined sample.

2. P2094-5-89RI — complexity in Quasar X-ray Spectra: XUV Excesses
   This work proceeds well and a paper is in preparation indicating a high energy excess. This program has been critically dependent on the energy calibration of the PSPC, and indeed our investigations have assisted significantly in understanding that calibration through our discussions with GSFC and MPE.

3. P2121-5-89RI — Structure of Seyfert Galaxies with Known X-ray Extent
   Paper on NGC1068 published in Ap.J. 1992. Demonstrated that ~50% of the soft x-ray emission in NGC1068 is extended on a galaxy sized scale, and is not nuclear. The HRI hardness ratio shows the extended emission is stronger at 1 keV than at 0.25 keV, suggesting that the emission from Fe-L lines seen in BBXRT is extended and thermal. Our A01 observation of NGC 4151 was not scheduled until A04 (May 93) and the data has not been receive yet.

4. P2079-5-89RI — Quasar Spectra Beyond the Redshift "Cut-Off"
   One paper has been published in Ap.J.(Letters) 1992, another is in press with Ap.J. They describe the results on six high redshift quasars, including the discovery of unexpected absorption toward these objects. The implications of these results are discussed in detail. A third paper describing the multiwavelength properties of these quasars from x-ray to radio is in preparation.

Refereed Papers

An X-ray Image of the Seyfert Galaxy NGC1068 (A.S. Wilson, M. Elvis, A. Lawrence, and J. Bland-Hawthorn), *Ap.J.(Letters)*, 391, L75.

PKS0438-436: A High Redshift Quasar with Strong X-ray Absorption (B.J. Wilkes, M. Elvis, H. Tananbaum, J.C. McDowell, and A. Lawrence), *Ap.J. (Letters)*, 393, L1.

Absorption in X-ray Spectra of High Redshift Quasars (M. Elvis, F. Fiore, B.J. Wilkes, J.C. McDowell, and J. Bechtold, *Ap.J.* **422**, in press (Feb. 10).

1.2 PR 666-27036 (P.I.: Francis A. Primini)

P2092-5-89RI — High Resolution Observations of the Central Region of M31

A comprehensive study of the X-ray source population in the central bulge of M31 appeared in Vol. 410 of the Astrophysical Journal (June 20, 1993). This study includes X-ray source identifications, luminosity measurements, luminosity functions for all the total source population and for X-ray globular clusters, estimates for individual source variability, and a preliminary measurement of the unresolved X-ray emission with 1 kpc of the nucleus of M31.

1.3 PR 666-27513 (P.I.: Giuseppina Fabbiano)

P2096-5-89RI — The X-ray Emission of Low-X-ray-Luminosity Early-Type Galaxies: Gas Versus Compact Sources

Two papers submitted to Ap.J.: The first reporting the results of the ROSAT observations of NGC4365 and NGC4382, the second discussing these results in the context of an evolutionary model for the ISM. Copies of these papers are included in Appendix A.

1.4 PR 666-27512 (P.I.: Daniel E. Harris)

P2098-5-89RI — Interaction Between Cluster GAs and Radio Features of Cygnus A

Although this was a ROSAT AO-1 project, the data were not delivered until Nov 1992. Preliminary evaluation of the image demonstrated: (a) the "6-month aspect offset syndrome" is present in the data, with an amplitude of approximately 15″; (b) there is discreet emission from the regions of the radio hot-spots; and (c) there appears to be a diminution of emission coincident with the radio lobes.

C. Carilli, CoI from NRAO visited the CfA for a week to work on data reduction (Feb, 93). We performed 3 operations to improve the spatial characteristics of the image. First we examined the PHA distribution of the main cluster gas, the features in the radio hotspot region, and the background. We found that if we cut channels 8–15, we would loose 3% of the source counts, but 21registration we performed two independent shifts. In the first, we used a smoothed version of each of the 29 obis to measure the peak of the main cluster emission, and then shifted each obi and coadded. In the second method, we divided the data into 5 time segments: 91apr, 91nov, 91dec, 92apr, and 92may. The position of a weak unresolved source 4′ off axis was then used to calculate the required shifts.

Analysis of the hotspot emission showed that the East spot is resolved with gross structure similar to the radio morphology. Counts were measured with "gun-sight" binning. Following conversion to flux with Obstime software, we used the observed radio spectrum to predict the synchrotron self Compton (SSC) contribution to the x-ray emission and found agreement with the measurements. We have been in contact with Biermann and Mannheim (Germany) to discuss the relevance of their model for emission from "proton induced cascades". This is a 'sister' process to the SSC emission. Perley, another Co-I from the NRAO visited for

a week in April '93, and pursued Gould's and Marscher's published methods for dealing with SSC emission. Harris has obtained code which uses numerical methods for calculating SSC spectra, and this will be used to check our analytic estimates. We also estimated the parameters to explain the hotspot emission as an extension of the radio synchrotron spectrum or as thermal emission. Both of these possibilities appear unlikely.

Thermal emission from the bow shock has been evaluated, and we are also investigating explanations for the decrease in emission coincident with the inner parts of the radio lobes. Perley and Harris met with D. Clarke to discuss a collaboration on numerical simulations to model the jet evolution and lobe structure to see if we can reproduce some of the details of the interaction between the gas and radio features. We have performed a King model subtract, which emphasizes the effect of the "cavity" in the to gas, as well as accentuating the hot spot emission and the core source which is apparently unresolved and coincident with the optical galaxy.

We plan a first paper which will concentrate on the hotspot emission. Subsequent papers will deal with the lobe/gas interaction and other aspects of the data. Results are also being reported at a variety of talks by the investigators.

1.5 PR 666-27514 (P.I.: Christine Jones-Forman)

P2124-5-89RI — Hot Gas and Dark Halos in Early-Type Galaxies

We are now completing a paper for submission to the Astrophysical Journal in which we report the results of our analysis of a deep 29 ksec ROSAT PSPC observation of the Fornax cluster which was centered on NGC1399. We use the observed x-ray surface brightness profile and gas temperature profile to determine the distribution of gravitating mass. The x-ray parameters required for measuring the gravitational mass can be traced to a distance of 18/arcmin from NGC1399, a distance of 126 kpc, assuming a distance modulus of 31.9 (equivalent to 24.0 Mpc; Ferguson 1989). We derive and discuss the radial distributions of the mass components of the system–the gas mass, the stellar mass in galaxies, and the dynamical mass. For the gaseous corona around NGC1399, we also measured the iron abundance to be approximately solar and constant with radius.

P2099-5-89RI — A Gravitational Lens in X-rays - 0957+461

The gravitational lens 0957+561 is comprised of a quasar at a redshift of 1.41 that is lensed by an intervening galaxy and surrounding cluster at a redshift of 0.36. A paper "ROSAT Images of the Gravitationally Lensed Quasar 0957+561" by Chartas, Falco, Forman, Jones, Schild and Shapiro was presented at the 31st Liege International Astrophysical Colloquium "Gravitational Lenses in the Universe" and will be submitted to the conference proceedings. From our analysis of the ROSAT observations, we find that the x-ray flux ratio of th two quasar images is significantly greater than the optical flux ratio. Our observations suggest that one of the quasar images may be microlensed by stars in the lensing galaxy. From analysis of a ROSAT PSPC observation, obtained from the archive, we find that the energy spectra of the quasar images is extremely soft.

1.6 PR 666-27511 (P.I.: Ginevra Trinchieri)

P2102-5-89RI — How Massive are Early-Type Galaxies?

The spatial analysis of PSPC data of NGC4636, a bright early type galaxy at the outskirts of the Virgo Cluster, indicates that the source is extended, with a smoothly decreasing radial profile out to $r/sim6' - -8'$, after which radius the profiles flattens significantly and an be detected out to $r/sim18'$, or roughly the round support structure of the PSPC.

A thin thermal spectrum with low energy absorption is used to fit the spectral count distribution. Several concentric annuli are analyzed separately, to obtain information on the spectral parameters in different regions. We cannot fit a single temperature model to the data, if we assume a gas with 100% cosmic abundances: multitemperature fits are required in the innermost $2'$. This requirement is relaxed for low (20%) cosmic abundances. A temperature gradient is observed in the inner $4' - 6'$, for kT increasing outwards from $\sim$0.5 to $\sim$1 keV.

A paper containing the details of the analysis and the results in upon completion. Preliminary results have been presented at the ROSAT Data Analysis and Science workshop held in November 1992 in Boston, and at the Kiel meeting in Germany (Mary 8-12, 1993).

1.7 PR 666-27229 (P.I.: Leon Golub)

P2106-5-89RI — Coronal Physics of the Lower Main Sequence: Relationships Among X-rays, Radio Emission and Magnetic Fields

No new input was given for this report.

1.8 PR 666-27509 (P.I.: Jay Bookbinder)

P2108-5-89RI — X-ray Observations of the Eclipsing Millisecond Pulsar

No new input was given for this report.

1.9 PR 666-27126 (P.I.: Frederick D. Seward)

P2114-5-89RI — Three Crab-Like SNR in the Large Magellanic Cloud

One HRI observation was approved from this proposal. The exposure was made in July 1990. The purpose was to detect the outer shell of a SNR in the LMC. The observation is difficult because the remnant has an x-ray bright interior where an energetic 50 millisecond pulsar resides. The observation was success. The shell was observed and delineated. 23% of the x-rays originate in the shell. Measured properties of the shell ware used to derive the energy release of the supernova explosion. A paper describing these results has been written and submitted to the Astrophysical Journal.

1.10 PR 666-27508 (P.I.: Martin V. Zombeck)

P2116-5-89RI — X-ray Detection of A-Type Stars

No new input was given for this report.

1.11 PR 666-27193 (P.I.: Saeqa Dil Vrtilek)

P2136-5-89RI — Soft X-ray Emission from Boundary Layers in Cataclysmic Variables

Many cataclysmic variables and low-mass X-ray binaries show HeII line emission at λ1640 and λ4686. As recombination lines of an ion requiring 55 eV for ionization, these lines cannot be attributed to gravitational heating in the disk, but could be due to reprocessed 55 eV to 280 eV X-rays which may be produced in a boundary layer at the disk/star surface. We undertook a search for this soft component using the Position Sensitive Proportional Counter (sensitive between 0.1-2.4 keV) on ROSAT. The photon fluxes we observe are not sufficient to produce the HeII λ1640 fluxes observed by IUE. If we assume that the X-ray luminosity is due to emission from a boundary layer then the observed quiescent luminosity is one quarter of the total accretion luminosity as determined by optical and ultraviolet observations rather than the half that is predicted by some theories. An additional very soft component (e.g. an $\approx$ 10-20 eV blackbody) could provide sufficient photons in the 0.055 - 0.100 keV band to produce the observed HeII fluxes and contribute the additional luminosity from the boundary layer while remaining hidden to the PSPC and IUE. Alternatively, the high HeII line fluxes could be evidence for high temperature collisionally ionized material. We also find evidence for line emission at $\approx$0.9 keV consistent with L-shell emission from highly ionized iron.

Concurrent data on the optical state of the systems observed by ROSAT (TV Col, RU Peg, WW Cet, AB Dra, and SU Uma) were acquired from the AAVSO. The optical data of SU Uma revealed that X-ray observations existed immediately preceding and during an outburst. SU UMa is a dwarf nova with a binary period of 1.83 hours. It exhibits both normal and superoutbursts. SU UMa was observed by ROSAT for 6500 seconds. The allocated time was divided into three observations to maximize the efficiency of the ROSAT observatory. The X-ray count rate during the optical outburst was 0.31 cts/s compared with 0.93 cts/s during optical quiescence: i.e. the X-ray flux *decreased* during optical outburst. Both quiescent and outburst spectra are well fit to a thermal Bremsstrahlung with a line at 1 keV and a temperature of 2 keV. The column density during outburst increases from Mass accretion onto white dwarf increases during the outburst for all current theories; the prediction that X-ray efficiency should decrease during an outburst has been difficult to test due to the lack of simultaneous X-ray and optical observations. These may be the first observations that support current theories: our observation of a decrease in X-ray flux during outburst suggests that for SU UMa mass-accretion has increased to the point where the boundary layer becomes optically thick, quenching the production of X-rays.

Papers submitted or in print since December 1992:

ROSAT Observations of Boundary Layers in Cataclysmic Variables, (S.D. Vrtilek, A. Silber, J. C. Raymond, & J. Patterson), *Ap. J.*, submitted.

Concurrent X-ray and Optical Observations of SU Uma During a Dwarf Nova Outburst A. Silber, S.D. Vrtilek, & J. C. Raymond, *Ap. J.*, submitted.

A Papers submitted to the Astrophysical Journal

Contents

1 Investigation Relative to ROSAT 1

1.1 PR 666-27127 (P.I.: Martin S. Elvis) 1
1.2 PR 666-27036 (P.I.: Francis A. Primini) 2
1.3 PR 666-27513 (P.I.: Giuseppina Fabbiano) 2
1.4 PR 666-27512 (P.I.: Daniel E. Harris) 2
1.5 PR 666-27514 (P.I.: Christine Jones-Forman) 3
1.6 PR 666-27511 (P.I.: Ginevra Trinchieri) 4
1.7 PR 666-27229 (P.I.: Leon Golub) 4
1.8 PR 666-27509 (P.I.: Jay Bookbinder) 4
1.9 PR 666-27126 (P.I.: Frederick D. Seward) 4
1.10 PR 666-27508 (P.I.: Martin V. Zombeck) 5
1.11 PR 666-27193 (P.I.: Saeqa Dil Vrtilek) 5

A Papers submitted to the Astrophysical Journal 7

ROSAT PSPC Observations of two X-ray-faint Early-type Galaxies: NGC 4365 and NGC 4382

G. Fabbiano
Harvard-Smithsonian Center for Astrophysics

D.-W. Kim
Chungnam National University, Daejeon, Korea
and
Harvard-Smithsonian Center for Astrophysics

and G. Trinchieri
Osservatorio Astrofisico di Brera, Milano, Italy
and
Harvard-Smithsonian Center for Astrophysics

August 30, 1993

Submitted to Ap. J.

Abstract

We present the results of ROSAT PSPC observations of the two early-type galaxies NGC 4365 and NGC 4382. These galaxies are among those observed with *Einstein* to have the lowest X-ray to optical flux ratios of early-type galaxies. The PSPC data show that these galaxies have complex X-ray spectra, different from those observed in X-ray bright ellipticals. Confirming earlier *Einstein* results, we find that the spectral data can be fitted with two thermal components: a very soft component, with kT$\sim$0.2 keV, and a hard component with kT$>$1.5 keV. While the hard component may be indicative of the integrated emission of a population of low-mass X-ray binaries, the nature of the very soft component is more speculative. Candidates include the emission of late-type stars, supersoft X-ray sources, and a 'warm' ISM.

1. Introduction

Observations of early-type galaxies with the *Einstein* satellite (Giacconi et al 1979) have revealed that these galaxies can retain large amounts (up to $\sim 10^{11} M_{\odot}$) of hot (T$\sim 10^7$K) Interstellar Medium (ISM; Forman, Jones and Tucker 1985; Canizares, Fabbiano and Trinchieri 1987). However, it was also observed that early-type galaxies of the same optical luminosity can have X-ray luminosities differing up to a factor of $\sim$ 100 (e.g. Fabbiano, Kim, and Trinchieri 1992). While there are convincing observational and theoretical arguments that suggest that the X-ray emission of X-ray bright galaxies is dominated by the hot ISM, the origin of the emission of X-ray faint galaxies is less certain (Canizares, Fabbiano and Trinchieri 1987; Fabbiano, Gioia and Trinchieri 1989; see Fabbiano 1989 and refs. therein). These galaxies may have not been able to retain their hot ISM, which may have been either expelled through winds (e.g. Ciotti et al 1991; David et al 1991) or stripped through interaction with a hot Intracluster Medium (e.g. White and Sarazin 1991).

A recent analysis of the *Einstein* IPC data of elliptical galaxies in different ranges of X-ray to optical ratio (L_X/L_B) has shown significant differences in the average spectral properties of the X-ray emission (Kim, Fabbiano and Trinchieri 1992), which may support these conclusions. While X-ray bright galaxies ($\log(L_X/L_B)$ >30.3, where L_X/L_B is in erg s$^{-1}/L_{\odot}$) have average spectra that can be fitted with thermal Raymond models with kT$\sim$1 keV, decreasing L_X/L_B the spectra become virtually indistinguishable from those of spiral galaxies, which are significantly harder (kT>3 keV), and whose emission is dominated by populations of evolved X-ray sources (see Fabbiano 1989). However, an unexpected very soft component of the X-ray emission is apparent in the average X-ray spectrum of the X-ray faintest galaxies [Group 1 in Kim, Fabbiano and Trinchieri 1992; $\log(L_X/L_B)$=29.3–30.0] as a significant excess of counts in the lowest spectral channels.

To confirm the existence of this very soft emission in X-ray faint early-type galaxies, and to determine its characteristics, we have observed two of these galaxies, NGC 4365 and NGC 4382, with the ROSAT (Trümper 1983) PSPC (Pfeffermann et al 1987). In this paper, we report the results of these observations, and we discuss briefly their implications. In the companion paper (Pellegrini and Fabbiano 1993), these results are compared with detailed model predictions.

2. Observations, Data Analysis and Results

Table 1 summarizes the characteristics of our two X-ray faint galaxies and gives the ROSAT PSPC observation log.

2.1 Contour Plots

The data were analyzed using the PROS ('xray') package of IRAF, developed at SAO for the analysis of X-ray data. Fig. 1a,b shows contours plots of the central parts of the two PSPC images, containing the target galaxies. Data from spectral

channels 7 to 240 were used. The PSPC data were binned in 5" pixels and smoothed with 15" Gaussians to obtain these plots. As it is readily visible from fig. 1, extended X-ray sources were detected in both cases, associated with the two galaxies. Other serendipitous sources are visible in the two fields. A comparison between the isophotes of point-like serendipitous sources, and those of the emission associated with the two galaxies, demonstrates qualitatively that the latter are not point-like. The emission of these galaxies could not be resolved with the *Einstein* IPC (see Fabbiano, Kim and Trinchieri 1992). In both cases the isophotes are well within the optical extent of the galaxies. The surface brightness distribution of NGC 4365 shows some azimuthal variations (see also §2.5). The surface brightness of NGC 4382 is more circularly symmetric, except for an elongation towards the South, which cannot be resolved as a separate emission region with the PSPC.

In NGC 4382 we resolve a point-like source at the N-W of the extended emission. This source was not resolved with the *Einstein* IPC, although the *Einstein* isophotes show a slight extension in this direction (Fabbiano, Kim and Trinchieri 1992). This source contributes ~74 counts to the image, and it would have an X-ray luminosity near 10^{40}erg s^{-1} were it at the distance of NGC 4382 (using the parameters of Table 4 below). However, it is possible that we are dealing with an interloper, and to be conservative we will treat it as such.

2.2 Background Subtraction and Extraction of Source Counts and Exposure Times

To extract counts for flux determination and for spectral analysis, and to study the radial behaviour of the X-ray surface brightness, the field background must be subtracted from the images. To this end, we have followed a method similar to that adopted by Fabbiano, Kim, and Trinchieri (1992) for the analysis of *Einstein* IPC images of galaxies. Using the broad-band images provided by the ROSAT pipeline processing, we have first subtracted all strong point sources detected in the fields, by excluding circular areas centered on these sources. These were determined both by inspection of the results of the pipeline processing of the data, which provides a list of sources, and by visual inspection of the data with the SAOimage tool. This done, radial profiles of the two fields were obtained, by binning the data around the centroids of the galaxy emission. These radial profiles were then compared with similarly binned profiles of the field background, provided by the pipeline processing. The case of NGC 4365 is shown in fig.2. For both observations it was evident that the radial profiles of the galaxy images flattened to a constant level at radii between 5' and 10', in a region when mirror vignetting effects are minor. That this is the case is shown quite clearly by the flatness of the field background at these radii. Because of this relatively small source extent, we derived the background locally in both cases, by using annuli surrounding the galaxy emission, from which we have excluded area containing other sources. In the case of NGC 4382 (see §2.1), there is a point source to the N-W of the extended emission, which falls within the optical extent of the galaxy. We give source counts with and without this source. The parameters used for

count extraction and the results are summarized in Table 2. This procedure resulted in 855.0±54.0 cts detected in NGC 4365, and 507.0±34.1 cts detected in NGC 4382 (without N-W point source) between 0.1 and 2.0 keV.

To calculate count rates, we also need to estimate the average exposure time in the region of interest. Because of local variations in the quantum efficiency of the PSPC, of vignetting, and the presence of the support structure (both ribs and wire mesh), the effective exposure time is a function of the position of the source in the instrumental field. At the center of the field, the exposure time is typically within ±2% of the instrument on-time (the time during which the data included in the image were collected). The instrumental effects that affect the effective exposure on the source are included in the exposure map, provided with the data package. By using the exposure map, we have estimated the average exposure time in the area used for source count extraction. We have also included an instrument dead-time correction of 97%. These times are given in Table 2.

2.3 Spectral Analysis

Counts for spectral analysis were extracted from the regions defined in §2.2 above. We fitted the data to different models using both the PROS spectral routines and XSPEC (provided by the NASA HEASARC). The spectral fit program in PROS rebins the spectral data (originally in 256 PHA bins) into 34 bins, covering an energy range of 0.07 to 2.48 keV. These data are then compared via χ^2 fits to models, convolved with the instrument and mirror response. We have excluded from the fits spectral bins with fewer than ~10 counts, because the software uses a gaussian approximation to calculate statistical uncertainties. We have also excluded the two lower spectral bins and the C-edge data, because the response function of the PSPC is less well determined in these regions (Hasinger et al 1992). The data used for the fits and the best-fit parameters are summarized in Table 3. Using different response matrices does not affect our results, because our uncertainties are dominated by statistics.

2.3.1 NGC 4365

Our first attempt was to fit the data with one-temperature optically thin Raymond models with solar abundances and line of sight absorption, calculated using the Morrison-McCammon (1983) cross sections. For this purpose we used the latest Raymond tables available (J. Raymond 1992, private communication), which are included in the PROS package. We find that the best-fit χ^2 is unacceptable (see Table 3). The spectral counts, compared with the best-fit spectrum are shown in fig.3a. A very significant improvement in the fit is found when a two-temperature model is used. The F-test gives a probability $P<<10^{-2}$ of exceeding F for two additional parameters. The best-fit spectrum and the two spectral components are compared with the data in fig.3b. The fit does not improve when a third component is added.

The best-fit parameters quoted in Table 3 were derived restricting the absorption column to be $> 10^{20}$ cm^{-2}, consistent with the line-of-sight neutral hydrogen column (see Table 1). However, if N_H is unrestricted the best-fit N_H tends to be lower than the line-of-sight HI values, but the change in χ^2 is small. Using the confidence contours for the *two* interesting parameters kT_1 and kT_2 (the temperatures of the two components) we find that the temperature of the soft component (kT_1) has well-determined values between 0.15 and 0.26 keV (at 90% confidence); the temperature of the hard component (kT_2) is less well defined, because of the spectral response of the PSPC, but values of kT_2 <1.5 keV are excluded. These contours were derived for log N_H=20.0, which is near the line-of-sight value, leaving all other parameters free to vary. However, if log N_H is allowed to be as low as 19.0, kT_1 may assume higher values (0.2 – 0.4 keV at 90% confidence). In this case, the preferred values of log N_H is 19.0. However, as said above, the improvement in the value of χ^2 is relatively small.

Assuming that N_H is only line-of-sight (and solar abundances), the spectral shape is completely defined by three parameters: kT_1, kT_2, and the ratio of the normalizations of the two components. In fig. 4, we show the 68%, 90% and 99% confidence contours for these *three* interesting parameters.

We attempted to fit the data with element abundances other than solar, but we did not find significant differences in our results for the range of abundances allowed by the PROS software. Lower values of abundance (~10% solar) tend to give more realistic values of the best-fit N_H, compatible with the line of sight value. However, the difference in χ^2 is very small. XSPEC allows more flexibility in varying the abundance. With XSPEC we found that a one-temperature model, with line of sight N_H gives a good fit to the data, for abundance values close to zero (<4% solar at 90% confidence for two interesting parameters, abundance and kT). In this case the temperature is between 0.6 and 1.1 keV (at 90% confidence) and the best fit χ^2 is 25.4 for 19 degrees of freedom. Unfortunately, with the limited band-width and spectral resolution of the ROSAT data we cannot distinguish between the two-temperature model, and the zero metal abundance model on the basis of the data alone. Other considerations will have to enter in our choice of model (see Discussion).

We searched for radial variations in the spectral parameters, by analyzing separately data from concentric annuli of increasing radii. No significant differences were found, except a possible softening of the spectrum at the outer radii (120"–250"). However, this result is likely to be due to an instrumental effect, that 'spreads out' soft photons (PI<25) between sets of adjacent PSPC cross-wires ('ghost images', Hasinger et al 1992).

2.3.2 NGC 4382

Similar results were found in the analysis of the spectral data of NGC 4382. The single component fit with solar abundance is unacceptable, while adding a second thermal component we find a good fit (Table 3, fig.5). The improvement in χ^2 is

highly significant. As in the case of NGC 4365, the low-temperature component is well defined (kT_1 between 0.18 and 0.31 at 90% confidence for the *two* interesting parameters kT_1 and kT_2); the values of the high-temperature component are less well defined, because of the fewer detected counts. Nonetheless, values of kT_2 <1.2 keV are excluded (at 90% confidence). The confidence contours for the *three* interesting parameters, kT_1, kT_2, and ratio of hard/soft normalizations are shown in fig.6. Notice that these confidence regions are less well defined than those of NGC 4365, reflecting the smaller statistical significance of the NGC 4382 data.

As for NGC 4365, we find that the data are also well fitted with a one-temperature Raymond model with very low metal abundances and line of sight N_H (minimum χ^2 =17.8 for ν =16 degrees of freedom). However, in this case the allowed parameter space is less extreme, reflecting the poorer counting statistics. We find a best fit abundance of 2% solar (<20% solar at 90% confidence for two interesting parameters, abundance and kT), and kT=0.30–0.65 keV (at 90%).

2.4 Fluxes and Luminosities

Table 4 gives flux and luminosities in the 0.1 – 2.0 keV range for the entire detected emission, using the best-fit two-component spectra, and for the soft and hard best-fit components separately. To obtain a rough measure of the uncertainty in the fluxes due to the uncertainties of the normalization of the spectral components, we have kept the temperatures of the two components fixed at 0.2 keV and 3.0 keV respectively, and we have used different sets of normalizations, to achieve an increase in χ^2 of ~10. This would correspond to a 99% confidence interval on the normalization (two interesting parameters). We find that the relative fluxes of the two components, which are comparable in the best-fit case, can vary up to a factor of two in each direction in NGC 4365. A similar exercise for NGC 4382 shows a similar uncertainty for the soft component. The luminosity of the hard component could vary upwards of up to a factor of three. If we consider the full allowed range of parameters (figs. 4 and 6), then the flux of the hard component could range from ~80% to ~6 times that of the soft component in NGC 4365, and from ~30% to 3 times, in NGC 4382.

2.5 Surface Brightness Profiles

We produced surface brightness profiles of the two galaxies, by binning the data in concentric 30" annuli centered on the peaks of the surface brightness distributions, determined with the aid of isointensity contour maps (see fig.1 and Table 2). The background was subtracted, as for the extraction of spectral counts. We first generated maps in energy intervals below and above the C edge (PI=40). We found that the soft profiles flatten at around 100", while the surface brightness keep decreasing with radius in the hard profiles. The broad-band profiles typically show a small flattening, which is the contribution of the soft data. To investigate if this flattening is the result of the 'ghost image' effect (see §2.3.1), we generated profiles by dividing the data in (PI 7-25) and (PI 26-247). The 'ghost images'

should not appear in PI channels above 25 (Hasinger et al 1992; R. Harnden 1993, private communication). We find that while the (PI 7-25) profiles are quite flat, the (PI 26-247) profiles are consistent with those we had generated in the 'hard' band, demonstrating that the flattening at 100" is an instrumental effect. In fig.7 we show the (PI 26-247) profiles for both galaxies. We remark that these profiles contain information on the spatial distributions of both soft and hard spectral components (see models in fig. 3b). The source at the N-W of NGC4382 (see fig.1b) is not included in the surface brightness profile of this galaxy. In fig.7 we also plot a representation of the ROSAT PSPC Point Response Function (Hasinger et al 1992). It is obvious that the galaxy emission is significantly extended in both cases.

The contour maps (fig. 1) suggest azimuthal asymmetries in both galaxies. We have explored differences in the profiles at different azimuthal angles. In NGC 4365 we find that the profile in 135-225 deg azimuthal pie is significantly different from the profiles in different pie bins. However, with the present data we cannot comment further on the nature of these asymmetries, and on the possible presence of background or foreground sources, superposed on the galaxy extended emission.

3. Discussion

The ROSAT PSPC observations of the two X-ray faint ellipticals NGC 4365 and NGC 4382 confirm the presence of very soft emission, suggested by the *Einstein* IPC data (Kim, Fabbiano, and Trinchieri 1992). Comparison with the ROSAT observations of X-ray bright ellipticals (e.g. Fabbiano 1993; Trinchieri et al 1993), shows significant differences in the spectral count distributions, in agreement with the earlier *Einstein* results. The ROSAT passband and spectral resolution are such that a unique spectral model cannot be found to describe our data. The same is true in the case of the X-ray bright galaxy NGC 4636 (Trinchieri et al 1993). A single temperature optically thin spectrum with solar abundances and at least line of sight absorption is excluded in our case. However, both a two-temperature model with abundances ranging from solar down to $\sim$10% solar, and a single temperature model with $<$4% solar abundance give acceptable fits to the data of NGC 4365. In the case of NGC 4382, both two-temperature and one-temperature low-abundance models fit the data well, but the constraints are less extreme because of the poorer counting statistics.

Although the ultimate solution of this puzzle requires obtaining better spectral data, such as the ASCA satellite may provide, at this point we are inclined to consider the two-temperature model to be the more realistic option.

A close to zero metal abundance, as required by the fit to the NGC 4365 data, is unphysical if the emission is due to a hot ($\sim$0.8 keV) ISM. Lower than solar metallicities have been reported from X-ray observations of early-type galaxies (e.g. Serlemitsos et al 1993), but not at these low values. Unless the thermally emitting medium is primordial metal-free medium suddenly accreted by a galaxy that has

been swept clean of its own ISM, metal enrichment from SNIa and stellar winds has to be expected (e.g. Renzini et al 1993). In the zero abundance model, of the order 10^8 $M_\odot$ of hot gas would be needed to explain the observed flux (see Trinchieri, Fabbiano and Canizares 1986). Only $10^7 M_\odot$ of wind from the evolving stars would be needed to pollute a metal free medium to ~10% solar abundances (assuming solar abundances for the stars). Given a crossing time of $\sim 10^8$years and a mass loss rate of $\sim 1 M_\odot$/year, it will take only 0.1 crossing times to achieve a 10% solar enrichment. Moreover, NGC 4365 has a counter-rotating core, suggesting that it is the product of a merger (Surma 1993). In this case, we would expect some enrichment in the ISM of the parent galaxies, and of the merger remnant itself, if the merger triggers a burst of star formation (Surma 1993; Schweizer 1993).

These considerations lead us to adopt the multi-temperature model for the X-ray spectrum of these two X-ray faint ellipticals. This conclusion is also in agreement with the spectral trends in elliptical galaxies suggested by the *Einstein* data (Kim, Fabbiano and Trinchieri 1992). There is a progression in the average *Einstein* spectral count distributions of early-type galaxies as a function of L_X/L_B, going from a distribution peaked near 1 keV, to a hard spectrum (Group 2), to the Group 1 spectrum, which can be represented as a hard spectrum with an added soft component. Given the similarity of the X-ray to optical ratios of Group 1 and 2 galaxies with those of spirals (and in particular bulge-dominated spirals), it is appealing to think that the X-ray luminosity of these galaxies contains a sizeable contribution from the (hard) emission of low-mass binaries (see also Fabbiano 1989; Fabbiano, Gioia and Trinchieri 1989; Canizares, Fabbiano and Trinchieri 1987; Fabbiano, Trinchieri and Van Speybroeck 1987; Trinchieri and Fabbiano 1985). The hard spectral distribution of Group 2 galaxies suggests that this baseline component is starting to appear, and in the two-temperature model it would also be present in the spectra of the yet X-ray fainter Group 1 galaxies, to whom our two galaxies belong.

In the two-temperature fit, the PSPC spectra of NGC 4365 and NGC 4382 consist of a low-temperature component with kT~0.2–0.3 keV, and high temperature components with kT>1.2–1.5 keV. ROSAT cannot determine the temperature of the hard component accurately. It can only establish its presence, and it can exclude that this emission is due to a hot ISM, of comparable properties to that present in X-ray bright ellipticals. The *Einstein* data suggested the presence of a ~1 keV hot gas in the latter (see Kim, Fabbiano and Trinchieri 1992), and recent analysis of ROSAT observations suggests that this ISM could be if anything slightly cooler, but still near 1 keV (e.g. Trinchieri et al 1993). Both the hardness of the spectrum, and the X-ray luminosities of the hard components of NGC 4365 and NCG 4382, which are comparable with those of spiral galaxies of similar optical luminosity, support the suggestion that the hard component may be due to the integrated emission of a population of low-mass X-ray binaries, similar to those present in spiral bulges.

The origin of the soft component is less clear. If these galaxies are stripped of their ISM by winds (see Ciotti et al 1991) or by interaction with the cluster medium (e.g. White and Sarazin 1991), the origin of the soft component ought to be related to the stellar population. Kim, Fabbiano and Trinchieri (1992) suggested the possibility that this component is the integrated emission of the M star population in the galaxies. We really don't know anything about the X-ray emission of M stars outside the solar neighborood, where these stars can be individually detected in X-rays (Schmitt et al 1990; Barbera et al 1993). To account for a few 10^{40}ergs s^{-1} we would need of the order 10^{12-13} M stars emitting $\sim 10^{27-28}$ergs s^{-1} each. More detailed considerations, taking into account the possible shape of the IMF in these galaxies, and an age effect which seems to reduce the L_X of M stars in the solar neighborood (Barbera et al 1993), suggest that late type stars may not account for the entire low-energy emission (Pellegrini and Fabbiano 1993). It is also possible, but very speculative at this point, that these galaxies contain a number of relatively bright very soft X-ray sources. Some of these sources have been reported in M31 (J. Trümper 1992, private communication). It would be interesting to look at the results of a full analysis of the observations of the bulge of M31, and compare the results with what we see in X-ray faint ellipticals. Pellegrini and Fabbiano (1993) speculate that supersoft sources, if present in elliptical galaxies, may be progenitors of SNIa.

Another possibility is that these galaxies have not been stripped of their ISM, and that the very soft emission is due to an ISM at lower temperatures than seen in X-ray bright galaxies. This possibility is explored fully by Pellegrini and Fabbiano (1993), in the context of the D'Ercole et al (1990) and Ciotti et al (1991) evolutionary models of the ISM of early-type galaxies. The results of the ROSAT observations of NGC 4365, presented in this paper (L_X, PSPC spectral count distribution, surface brightness profile), are there used to constrain model parameters, together with the optical characteristics of this galaxy (stellar velocity dispersion, surface brightness profile). The result of this exercise suggests that the X-ray emission of NGC 4365 could be explained by a combination of a hard low-mass X-ray binary component, a very soft component of stellar origin, and a hot ISM component. The latter is required to fit the shape of the X-ray surface brightness profile, which is more extended than that of the optical light distribution. The hot ISM models that agreed more closely with the data imply a SNIa rate $\sim$0.6 of the Tamman rate, and an extended dark halo, with dark/luminous mass ratio$\sim$9. Given the quality of the present data, this result is certainly not unique; however, it demonstrates the need of accurate spectral and spatial measurements of these galaxies in the X-rays.

4. Summary and Conclusions

We have observed with the ROSAT PSPC the two X-ray faint early-type galaxies NGC 4365 and NGC 4382. We detect extended X-ray emission from both galaxies, with similar count rates (0.06 cts s^{-1}) in the 0.1-2.0 keV band, corresponding to fluxes of 6-7$\times 10^{-13}$erg cm^{-2} s^{-1}, and luminosities of 5-6$\times 10^{40}$erg s^{-1}. The X-

ray spectra are well fitted with two thermal components with kT of ~0.2 keV and >1.5 keV respectively, which contribute to the emitted flux by comparable amounts. An alternate model that also fits the data well is a one-temperature low-abundance model. In the case of NGC 4365, which was detected with a higher signal to noise ratio, the abundance in this model is constrained to be <4% solar (at 90% significance). We believe that these low values are unrealistic, and that the two-temperature model is a more reasonable representation of the data.

These results confirm the earlier report of Kim, Fabbiano and Trinchieri (1992),who found differences in the average *Einstein* IPC spectra of early-type galaxies of different X-ray to optical ratios. In particular it is clear that the X-ray emission of X-ray faint galaxies is not due solely to the same type of hot ISM present in X-ray bright ellipticals.

We follow Kim, Fabbiano and Trinchieri (1992) in suggesting that the most plausible origin of the hard spectral component is the integrated emission of a population *of* low-mass X-ray binaries, similar to those responsible for the bulge emission of early-type spirals (see Fabbiano 1989). Several candidates exist for the very soft component. They include stellar emission of late-type stars, an unknown population of supersoft X-ray sources, and a hot/warm ISM. These are discussed in detail in the companion paper (Pellegrini and Fabbiano 1993).

These results demonstrate the importance of spectral data as a diagnostic of the X-ray emission properties and physical status of early-type galaxies. We hope to be able to explore more of the L_X/L_B plane of E and S0 galaxies with ROSAT and other X-ray satellites, to extend these studies and gather a more complete picture of the evolution of the ISM in these systems. In particular, observations with ASCA will remove the uncertainty on the spectral model that cannot be resolved with the present data. However, only with the spatial/spectral resolution of AXAF will we be able to investigate radial spectral variations, that may give direct evidence supporting the suggestion of an extended hot/warm ISM.

ACKNOWLEDGEMENTS

This work was supported by NASA grants NAG5-1937 (ROSAT) and NAGW-2681 (LTSA). GT aknowledges partial support from the Italian ASI. D-W Kim was partially supported by the Korean KOSEF international program. We thank the SAO PROS team and Chris Fassnacht for assistance in the data analysis; and Fabrizio Fiore, Silvia Pellegrini, Jay Gallagher, and Claude Canizares for useful discussions and comments.

REFERENCES

Barbera, M., Micela, G., Sciortino, S., Vaiana, G., Harnden, F. R., and Rosner, R. 1993, Ap. J., in press.

Canizares, C. R., Fabbiano, G. and Trinchieri, G. 1987, Ap. J., 312, 503.

Ciotti, L., D'Ercole, A., Pellegrini, S., and Renzini, A. 1991, Ap. J., 376, 380.

David, L. P., Forman, W., and Jones, C. 1991, Ap. J., 369, 121.

D'Ercole, A., Ciotti, L., Pellegrini, S., and Renzini, A. 1989, Ap. J. (Letters), 341, L9.

Fabbiano, G. 1989, Ann. Rev. Astr. Ap., 27, 87.

Fabbiano, G. 1993, in Structure, Dynamics, and Chemical Evolution of Elliptical Galaxies, Danziger, I. J., Zeilinger, W. W., and Kjär, K., eds., ESO Proceed. No. 45, p. 617.

Fabbiano, G., Gioia, I. M., and Trinchieri, G. 1989, Ap. J., 347, 127.

Fabbiano, G., Kim, D.-W. and Trinchieri, G. 1992, Ap. J. Suppl. 80, 531.

Fabbiano, G., Trinchieri, G., and Van Speybroeck, L. 1987, Ap. J., 316, 127.

Forman, W., Jones, C., and Tucker, W. 1985, Ap. J., 293, 102.

Giacconi et al 1979, Ap. J., 230, 540.

Hasinger, G., Turner, J. T., George, I. A., and Boese, G. 1992, OGIP Calibration Memo CAL/ROS/92-001, NASA-GSFC.

Kim, D.-W., Fabbiano, G., and Trinchieri, G. 1992, Ap. J., 393, 134.

Pellegrini, S. and Fabbiano, G. 1993, preprint.

Pfeffermann, E. et al 1987, Proc. SPIE, 733, 519.

Renzini, A., Ciotti, L., D'Ercole, A., and Pellegrini, S. 1993, Ap. J., submitted.

Schmitt, J., Collura, A., Sciortino, S., Vaiana, G., Harnden, F. R., and Rosner, R. 1990, Ap. J., 365, 704.

Schweizer, F. 1993, in Structure, Dynamics, and Chemical Evolution of Elliptical Galaxies, Danziger, I. J., Zeilinger, W. W., and Kjär, K., eds., ESO Proceed. No. 45, p. 651.

Serlemitsos, P. et al 1993, Ap. J., in press.

Surma, P. 1993, in Structure, Dynamics, and Chemical Evolution of Elliptical Galaxies, Danziger, I. J., Zeilinger, W. W., and Kjär, K., eds., ESO Proceed. No. 45, p. 669.

Trinchieri, G. and Fabbiano, G. 1985, Ap. J., 296, 447.

Trinchieri, G., Fabbiano, G., and Canizares, C. R. 1986, Ap. J., 310, 637.

Trinchieri, G., Kim, D.-W., Fabbiano, G., and Canizares, C. R. 1993, preprint.

Trümper, J. 1983, Adv. Space Res., 2, No. 4, 241.

White, E. W. III and Sarazin, C. L. 1991, Ap. J., 367, 476.

FIGURE CAPTIONS

Figure 1: Contour plots of the X-ray emission of NGC 4365 (a) and NGC 4382 (b). In both cases data from spectral channels 7-240 (~0.1–2.0 keV) were used. Data were binned in 5" pixels and smoothed with 15" Gaussians. Contour plotted are linearly spaced from 4% to 100% of peak in (a), and from 5% to 100% of peak in (b). The ellipses indicate the optical galaxies. Coordinates are J2000.

Figure 2: Radial distribution of surface brightness in the central part of the NGC 4365 field after subtraction of other sources in the field, compared with the radial distribution of the background map.

Figure 3: Comparison of the observed distribution of the PSPC spectral counts of NGC 4365 with (a) one-temperature best-fit; (b) two-temperatures best-fit. Both two-component spectrum, and each individual component are plotted.

Figure 4: Confidence contours for the three interesting parameters, two temperatures and normalization of the hard component relative to that of the soft component for NGC 4365. The temperatures are in keV and the ratio of normalizations (hard/soft) is in log units. (a) The two temperatures; (b) the temperature of the soft component (kT_1) and the ratio of normalizations; (c) the temperature of the hard component (kT_2) and the ratio of normalizations.

Figure 5: Comparison of the observed distribution of the PSPC spectral counts of NGC 4382 with (a) one-temperature best-fit; (b) two-temperatures best-fit.

Figure 6: Same as fig. 4, but for NGC 4382.

Figure 7: Hard-band radial surface brightness profile of NGC 4365 (a) and NGC 4382 (b); see text for details. The dashed line approximates the PSPC PRF.

TABLE 1

Galaxy and Observation Parameters

Name (NGC)	Type	RA,Dec (B1950)	RA,Dec (J2000)	D (Mpc)	N_H [a] (cm^{-2})	log L_X [b] (Eins)	log L_X/L_B [c] (Eins)	PSPC Start/Stop	On-time (sec)
4365	-5	12 21 56	12 24 29	27	1.6×10^{20}	40.42	29.61	15 Dec 91	14904
	E	+07 35 42	+07 19 05					16 Dec 91	
4382	-2	12 22 53	12 25 25	27	2.7×10^{20}	40.72	29.71	14 Dec 91	8632
	S0	+18 28 00	+18 11 25					24 Dec 91	

a) from Stark et al.

b) L_X is in units of erg s^{-1} (Fabbiano, Kim, and Trinchieri 1992)

c) L_X/L_B is in units of erg $s^{-1}/L_\odot$ (see Kim, Fabbiano, and Trinchieri 1992)

TABLE 2

Source Count and Exposure Time Extraction

Galaxy (NGC)	Source[a] x,y; radius	Background[a] x,y; radii	Excluded[a] x,y; radius	Net Counts (0.1–2.0 keV)	Exp. time (s)	Rate (ct/s)
4365	7630,7680; 250	7630,7680; 300–500	7350,6870; 110	855.0±54.0	14429	0.06
4382	7750,7700; 220	7750,7700; 300–500	7000,8290; 90 7930,8510; 90 7960,7970; 60 8270,7330; 90	507.0±34.1[b] 581.3±36.0[c]	8320	0.06

a) x and y are in instrument pixels; radii are in arcsec.

b) excluding the source at 7960,7970

c) including the source at 7960,7970

TABLE 3

Spectral Analysis

Galaxy (NGC)	Bins	Energy (keV)	Counts± error	1-temp. Raymond				2-temp. Raymond				
				log $N_H(cm^{-2})$	kT(keV)	χ^2	ν	log $N_H(cm^{-2})$	kT_1(keV)	kT_2(keV)	χ^2	ν
4365	3–11	0.11-0.47	812.18±	20.0	3.0	63.2	19	20.0	0.20	3.0	24.3	17
	13–25	0.11-1.50	52.91									
4382	3–10	0.11-0.42	463.50±	20.0	3.0	57.1	17	20.1	0.24	3.0	14.3	15
	13–24	0.52-1.41	32.66									

TABLE 4

Fluxes and Luminosities in the 0.1–2.0 keV Range

Galaxy (NGC)	2-comp. model f_X [a] (erg cm^{-2}s^{-1})	2-comp. model L_X [a] (erg s^{-1})	soft comp. f_X (erg cm^{-2}s^{-1})	soft comp. L_X (erg s^{-1})	hard comp. f_X (erg cm^{-2}s^{-1})	hard comp. L_X (erg s^{-1})
4365	6.4×10^{-13}	5.6×10^{40}	3.2×10^{-13}	2.8×10^{40}	3.3×10^{-13}	2.9×10^{40}
4382	7.3×10^{-13}	6.4×10^{40}	4.7×10^{-13}	4.1×10^{40}	2.5×10^{-13}	2.2×10^{40}

a) unabsorbed values, assuming log N_H from Table 3.

NGC4365

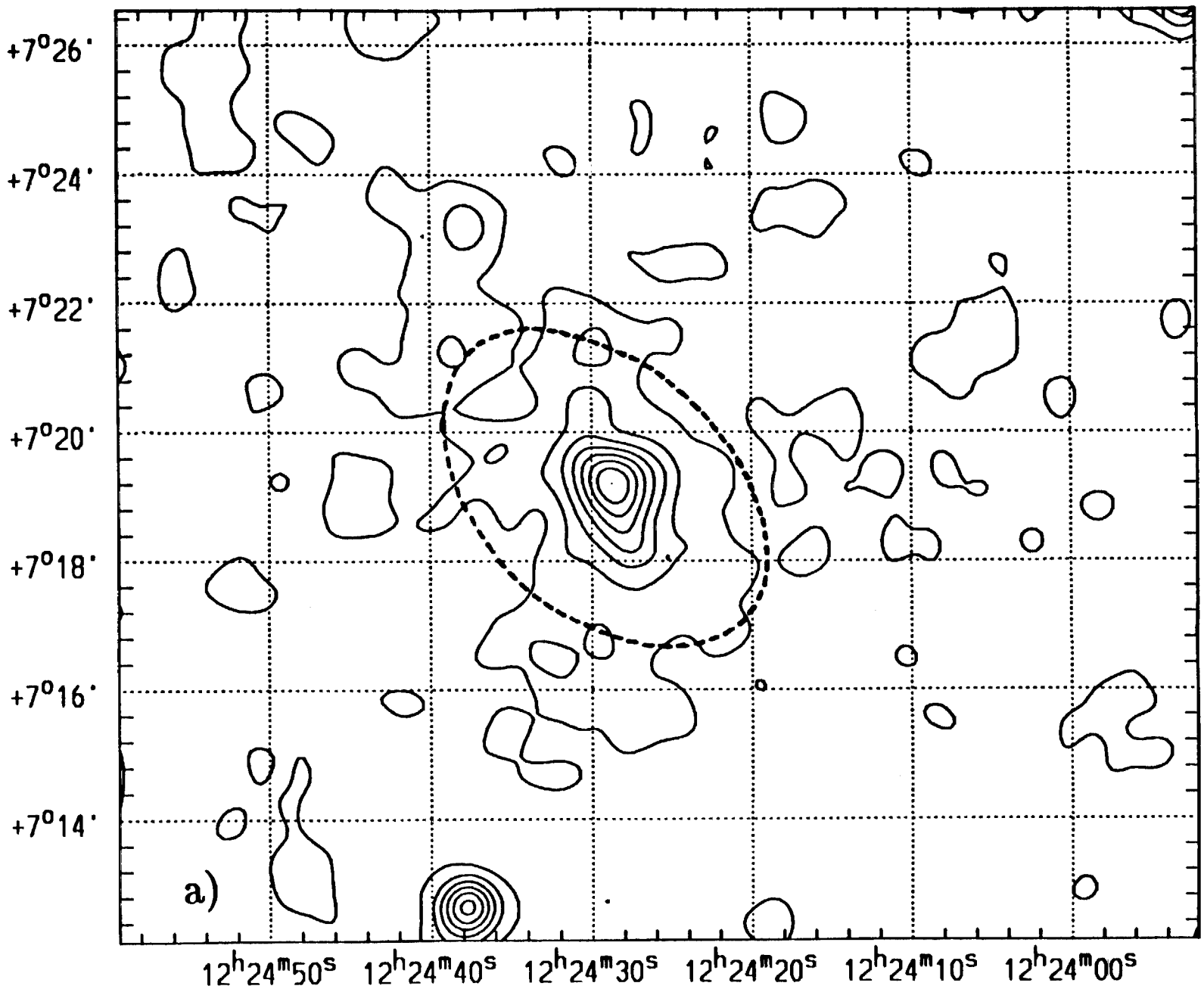
+7°26'
+7°24'
+7°22'
+7°20'
+7°18'
+7°16'
+7°14'
a)
12h24m50s
12h24m40s
12h24m30s
12h24m20s
12h24m10s
12h24m00s

NGC4382

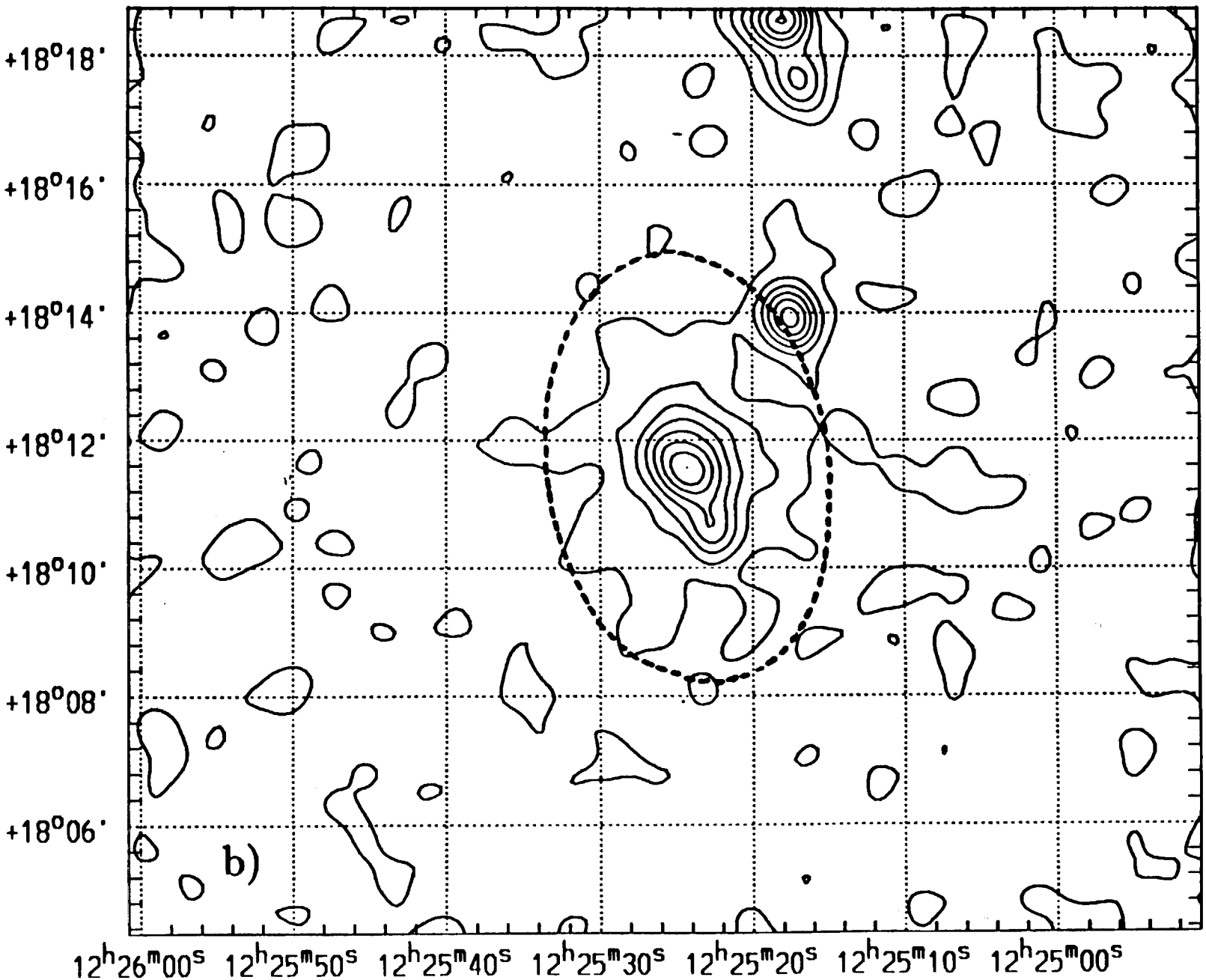
+18°18'
+18°16'
+18°14'
+18°12'
+18°10'
+18°08'
+18°06'
b)
12h26m00s
12h25m50s
12h25m40s
12h25m30s
12h25m20s
12h25m10s
12h25m00s

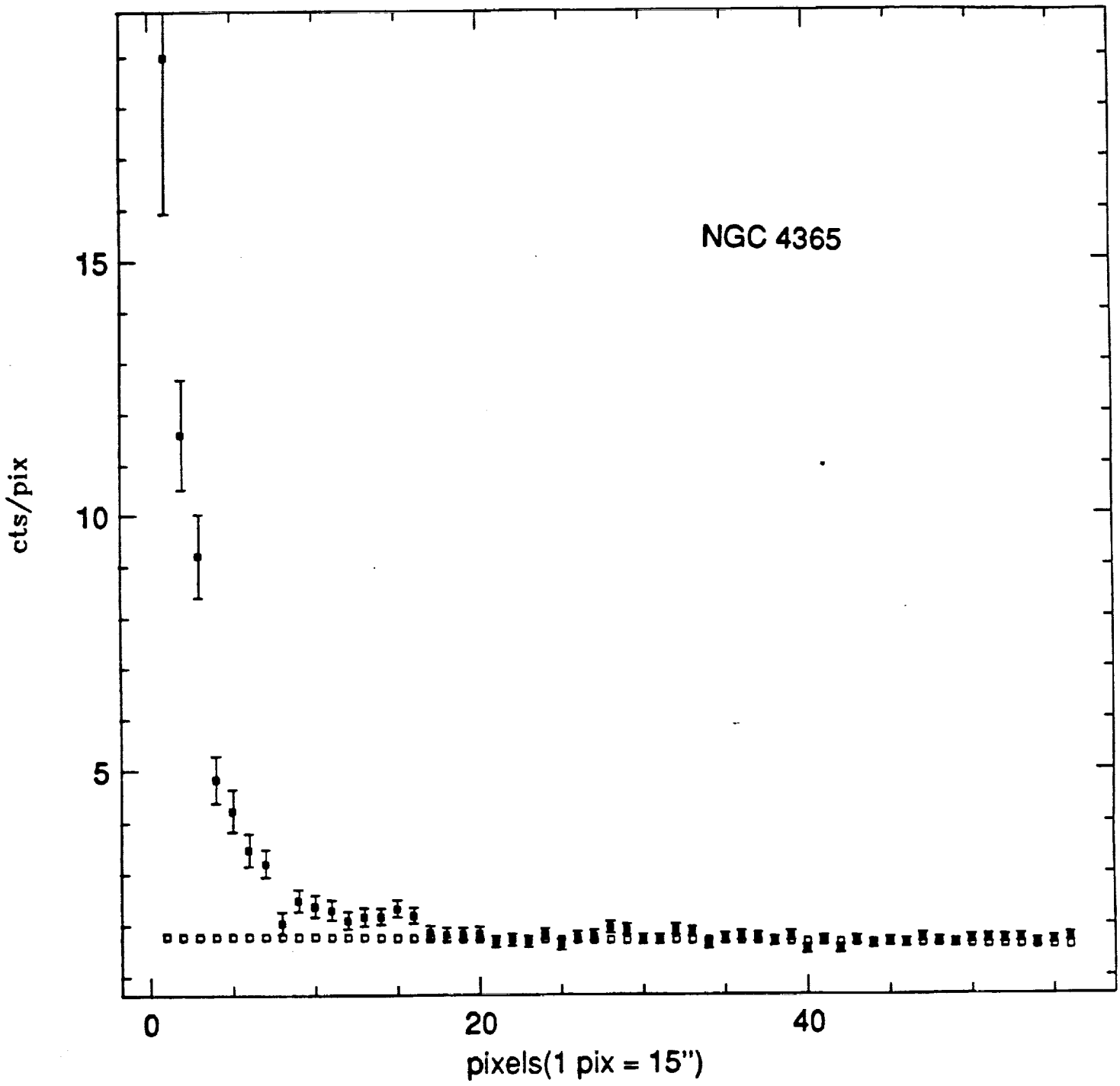
NGC 4365
15
10
5
cts/pix
0
20
40
pixels(1 pix = 15")

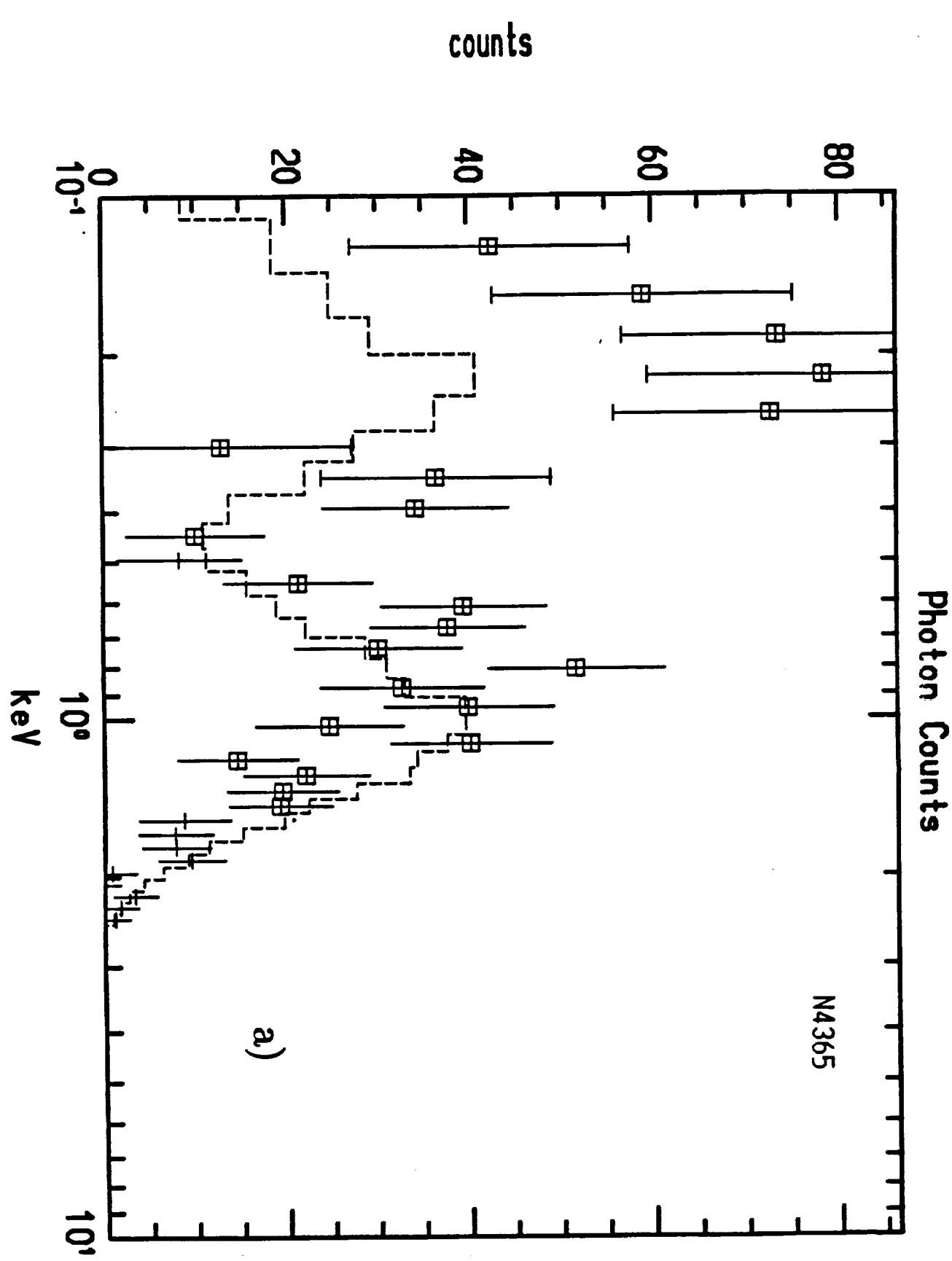
counts
0
20
40
60
80
10^{-1}
10^{0}
10^{1}
keV
Photon Counts
N4365
a)

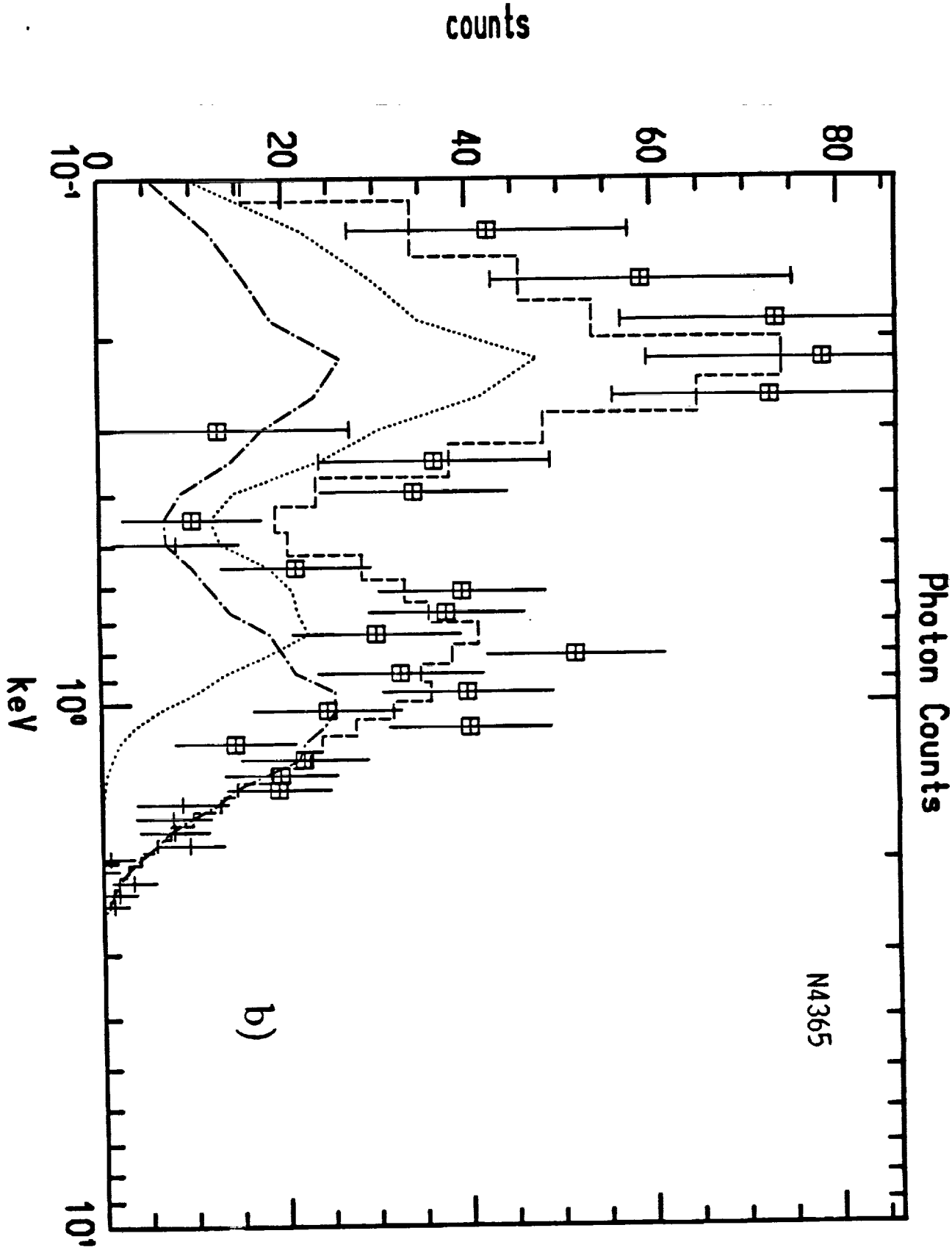
counts
0
20
40
60
80
10^{-1}
10^{0}
10^{1}
keV
Photon Counts
(b)
N4365

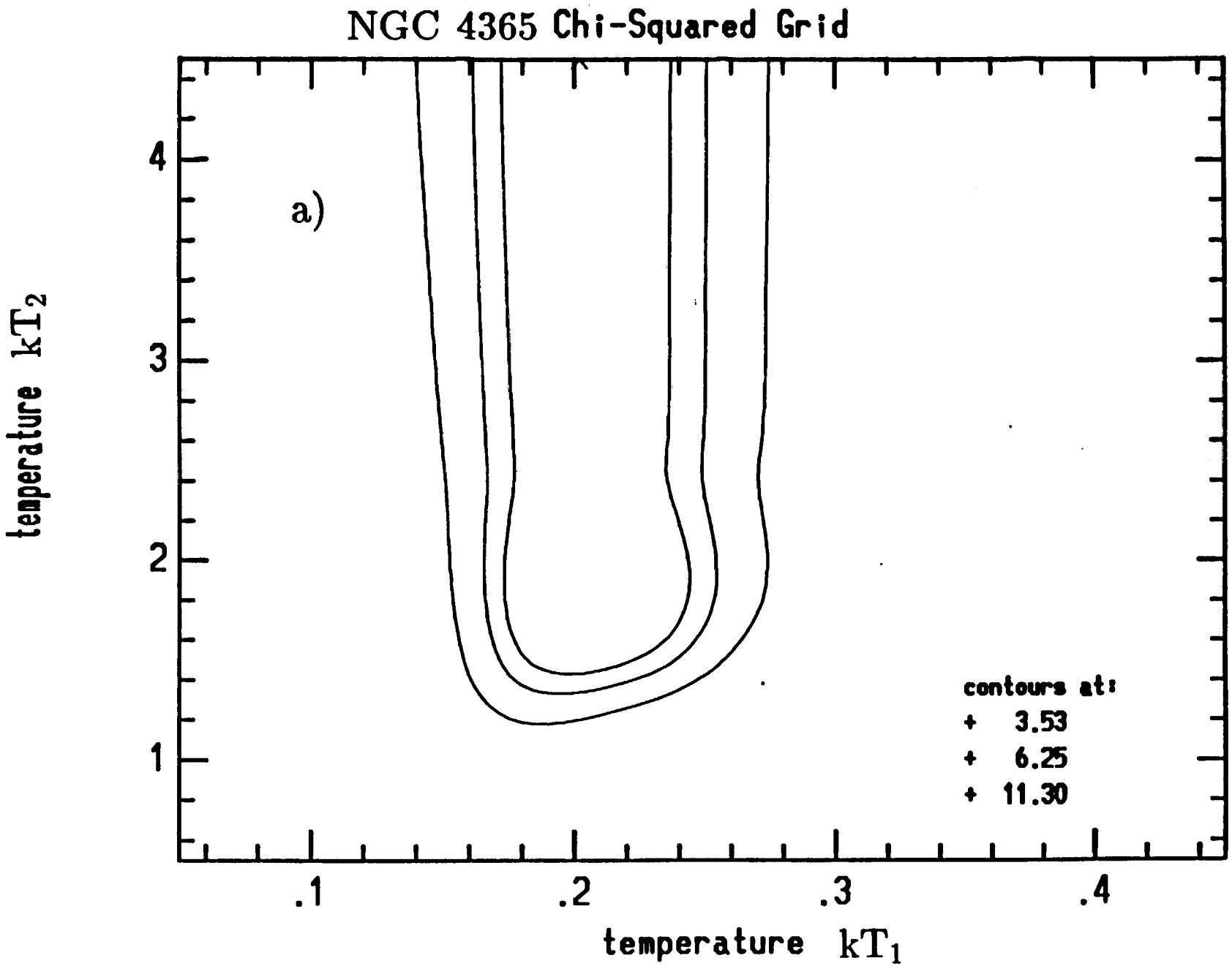
NGC 4365 Chi-Squared Grid
a)
temperature kT_2
temperature kT_1
1
2
3
4
.1
.2
.3
.4
contours at:
+ 3.53
+ 6.25
+ 11.30

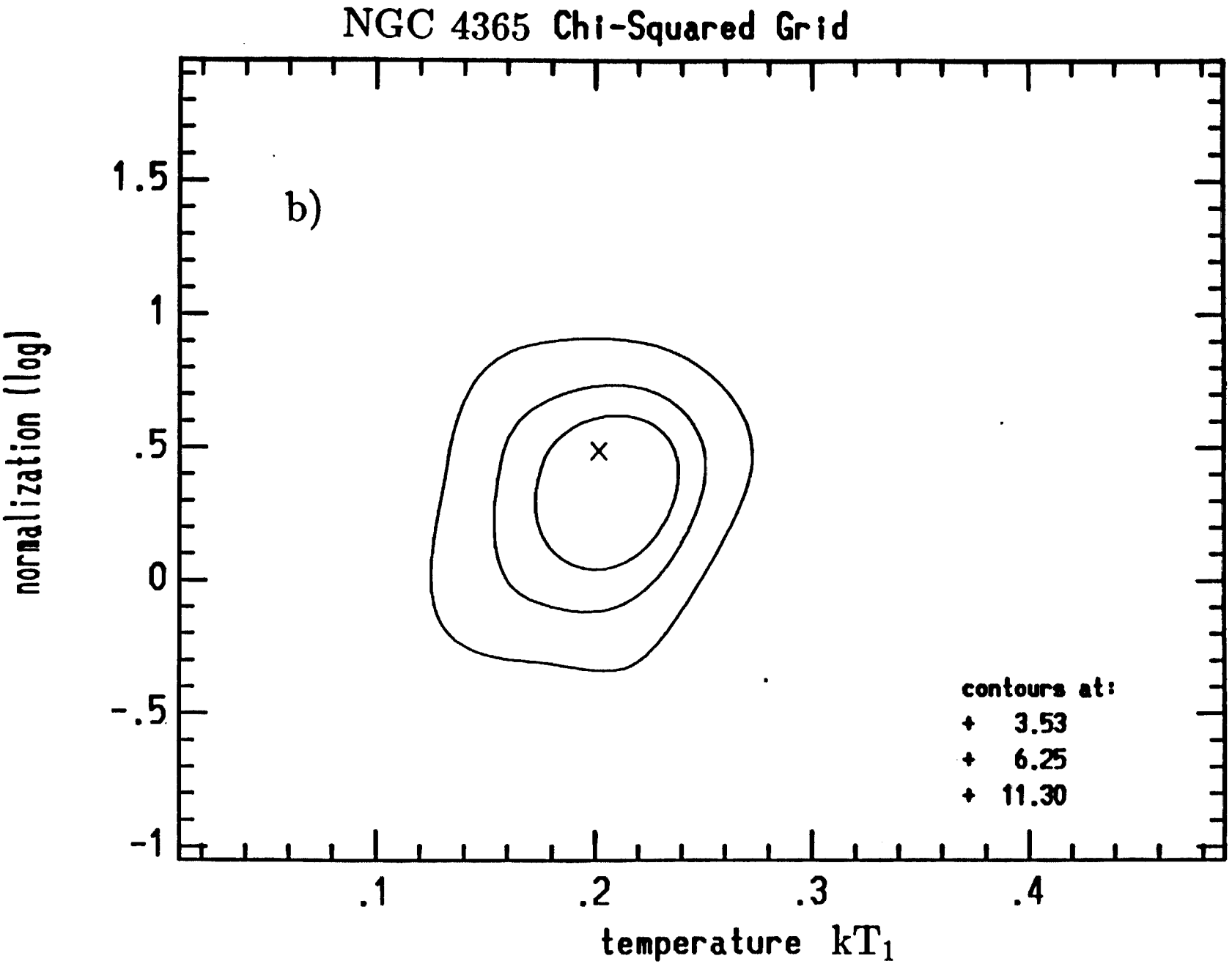
NGC 4365 Chi-Squared Grid
b)
1.5
1
.5
0
-.5
-1
.1
.2
.3
.4
normalization (log)
temperature kT_1
contours at:
+ 3.53
+ 6.25
+ 11.30

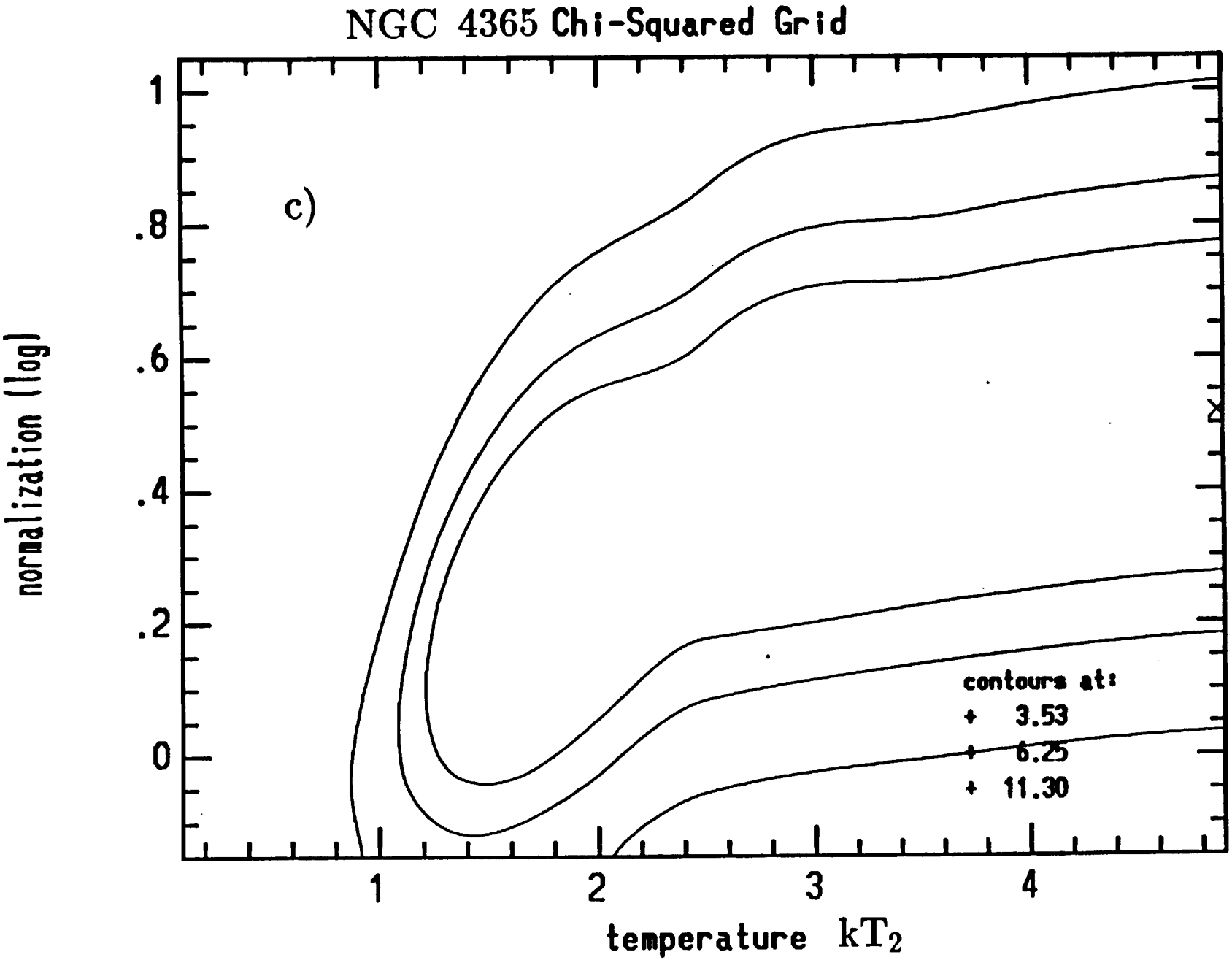
NGC 4365 Chi-Squared Grid
c)
normalization (log)
1
.8
.6
.4
.2
0
1
2
3
4
temperature kT_2
contours at:
+ 3.53
+ 6.25
+ 11.30

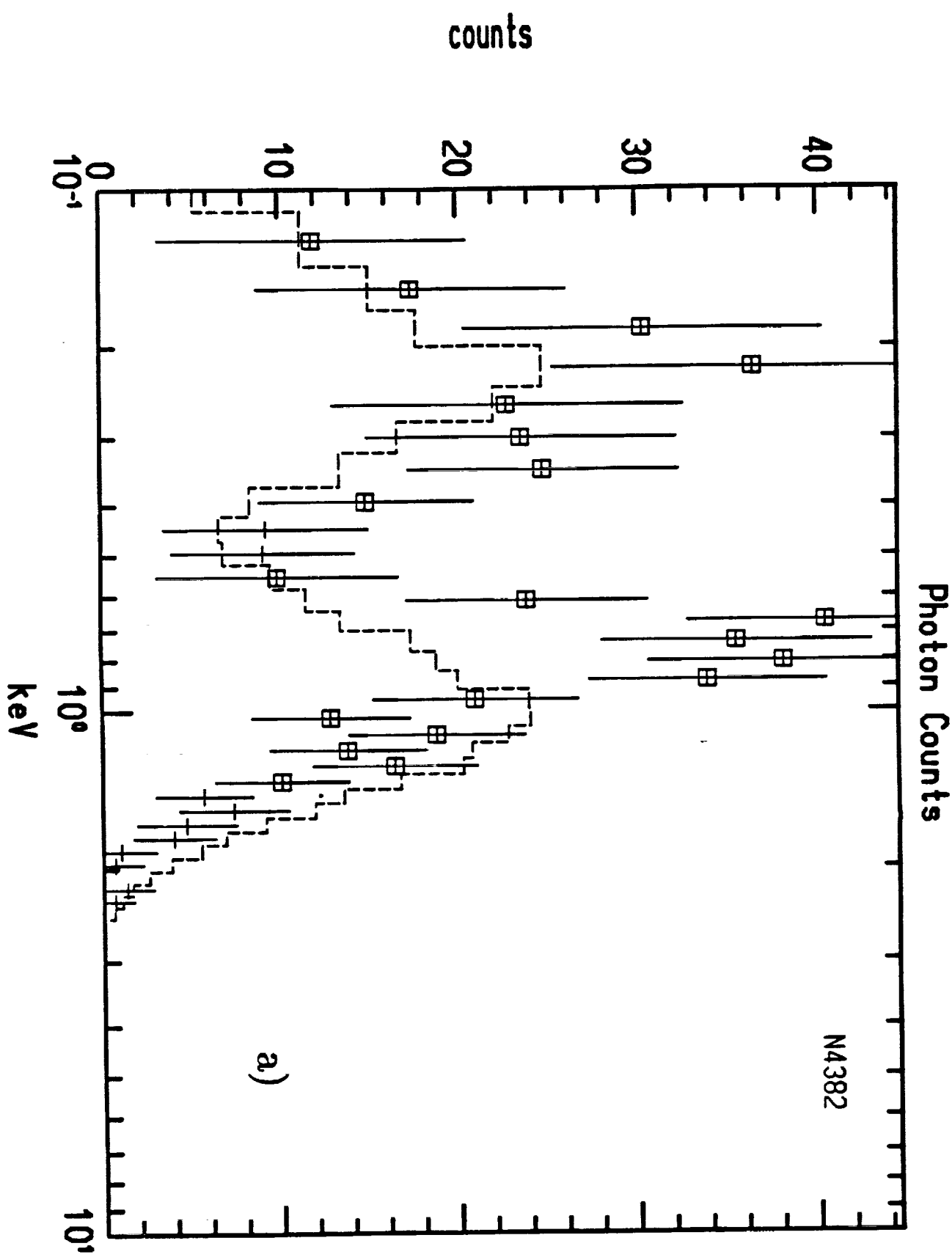
counts
0
10
20
30
40
10⁻¹
10⁰
10¹
keV
Photon Counts
N4382
a)

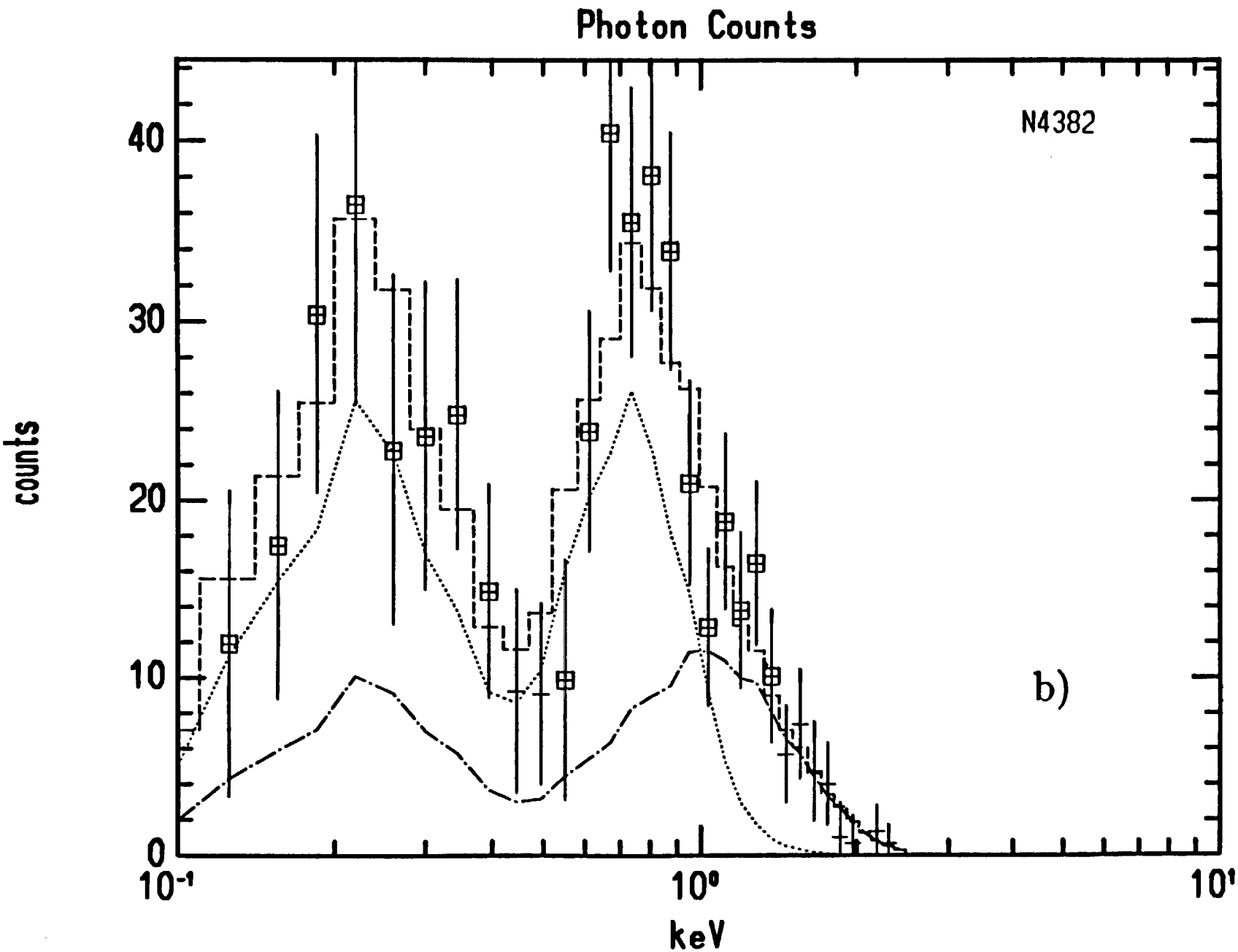
Photon Counts
N4382
b)
counts
keV
0
10
20
30
40
10^{-1}
10^{0}
10^{1}

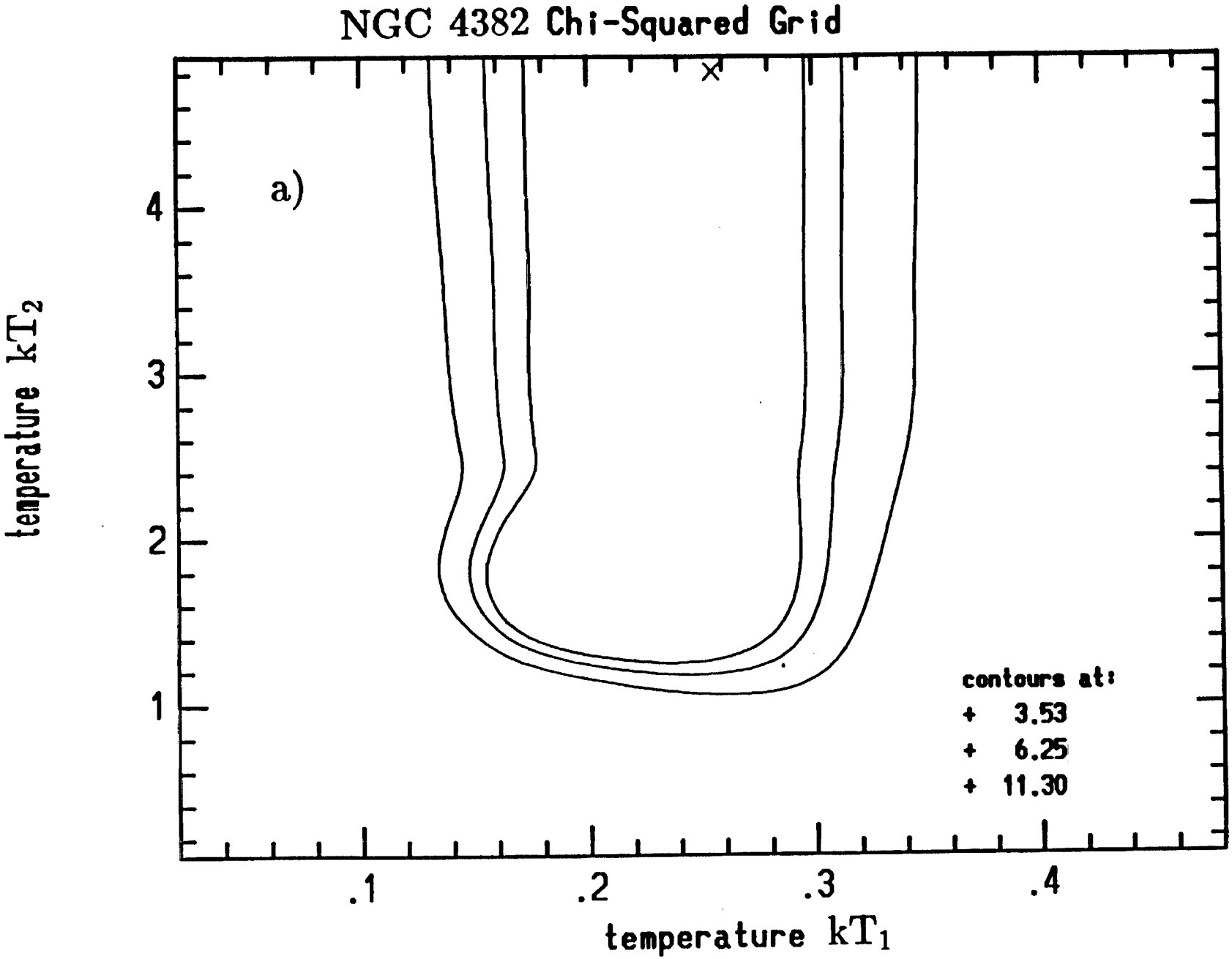
NGC 4382 Chi-Squared Grid
a)
temperature kT_2
temperature kT_1
1
2
3
4
.1
.2
.3
.4
contours at:
+ 3.53
+ 6.25
+ 11.30

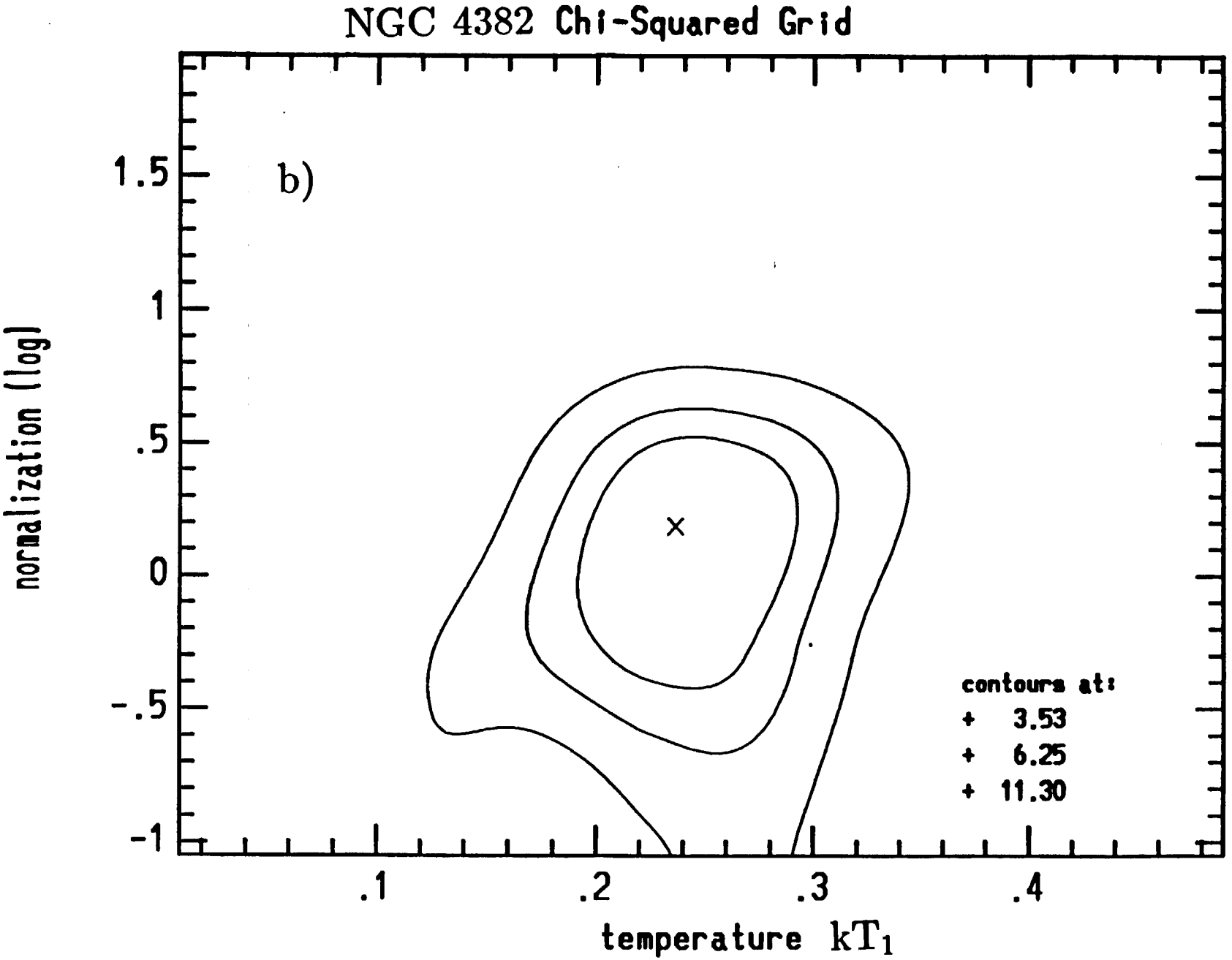
NGC 4382 Chi-Squared Grid
b)
1.5
1
.5
0
-.5
-1
normalization (log)
.1
.2
.3
.4
temperature kT1
contours at:
+ 3.53
+ 6.25
+ 11.30

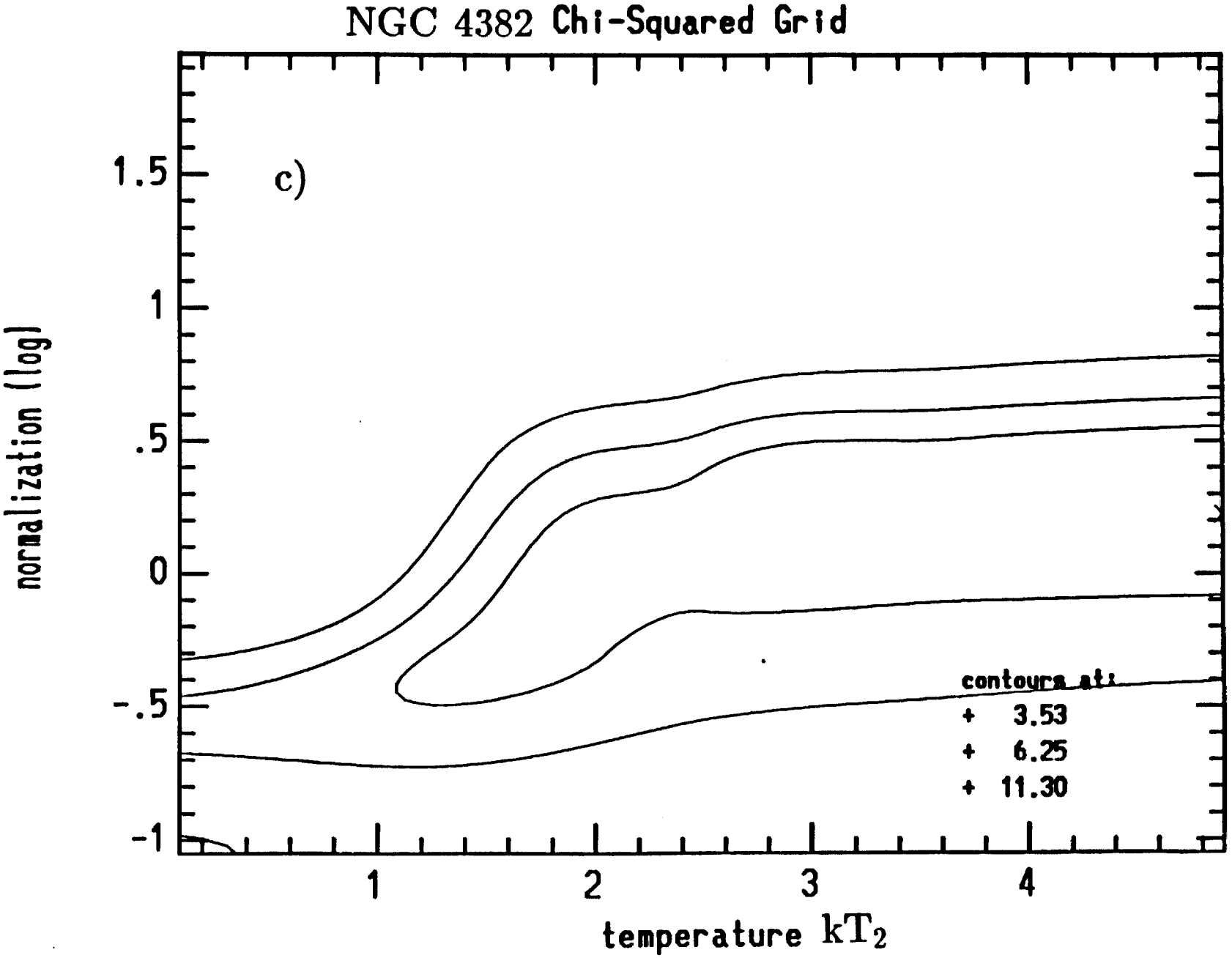
NGC 4382 Chi-Squared Grid
c)
1.5
1
.5
0
-.5
-1
normalization (log)
1
2
3
4
temperature kT_2
contours at:
+ 3.53
+ 6.25
+ 11.30

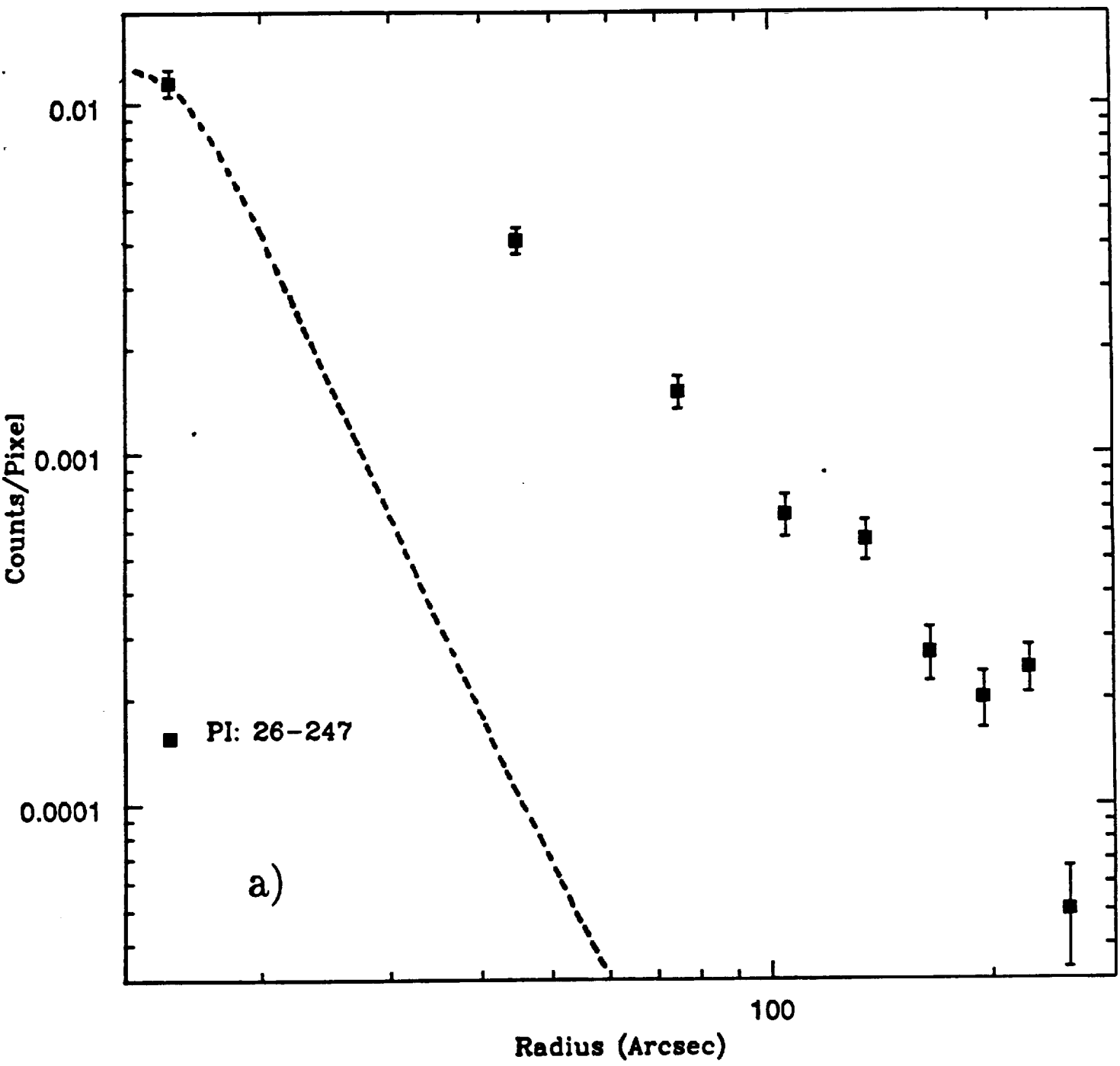
NGC 4365 – HARD BAND
0.01
0.001
0.0001
Counts/Pixel
PI: 26–247
a)
100
Radius (Arcsec)

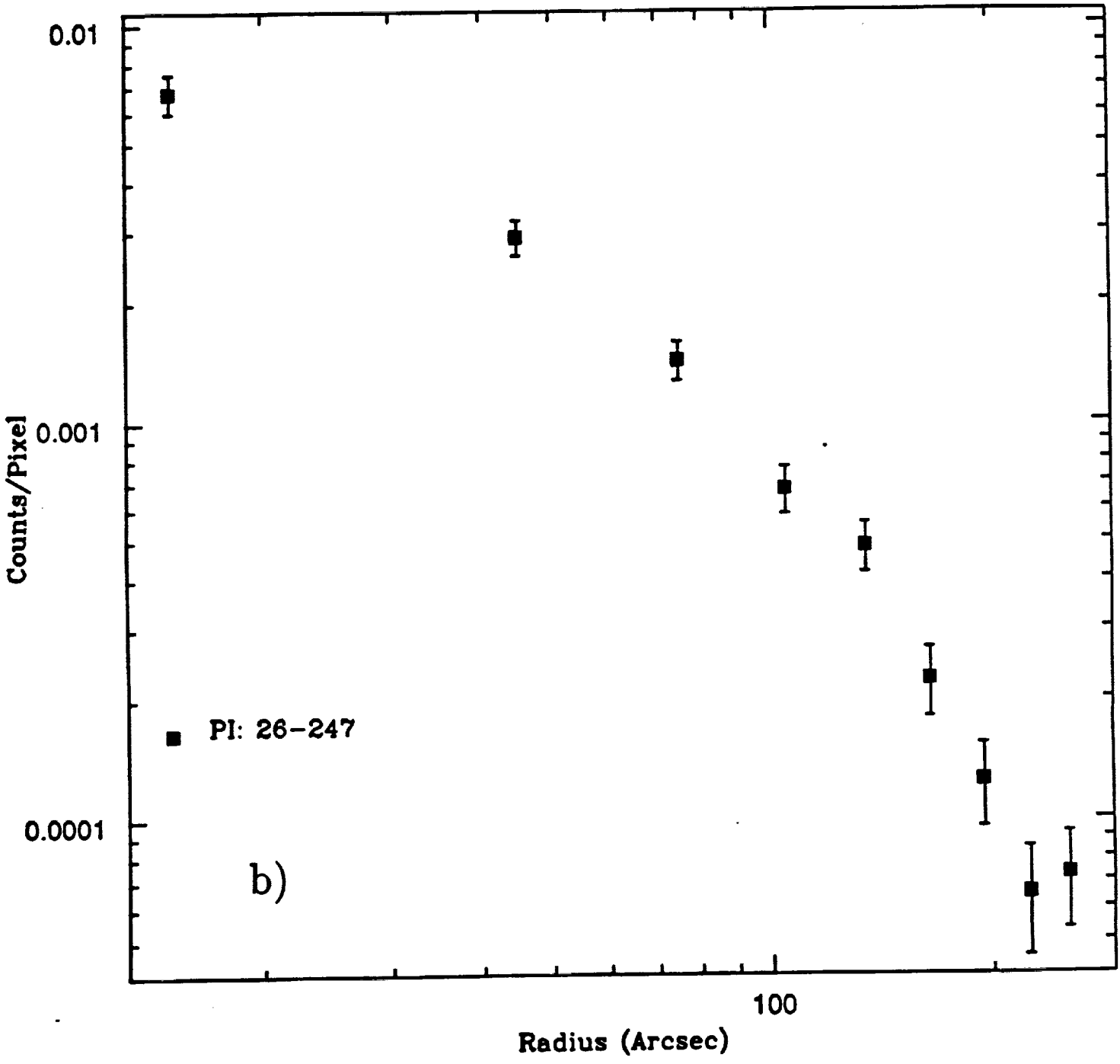
NGC 4382 – HARD BAND
0.01
0.001
0.0001
Counts/Pixel
PI: 26–247
b)
100
Radius (Arcsec)

THE VERY-SOFT X-RAY EMISSION OF X-RAY FAINT EARLY-TYPE GALAXIES

S. Pellegrini
European Southern Observatory

and

G. Fabbiano
Harvard-Smithsonian Center for Astrophysics

August 31, 1993

submitted to Ap. J.

ABSTRACT

A recent re-analysis of *Einstein* data, and new *ROSAT* observations, have revealed the presence of at least two components in the X-ray spectra of X-ray faint early-type galaxies: a relatively hard component ($kT > 1.5$ keV), and an ultra-soft component ($kT \sim 0.2-0.3$ keV). In this paper we address the problem of the nature of the ultra-soft component, and whether it can be due to a hot interstellar medium (ISM), or is most likely originated by the collective emission of very soft stellar sources. To this purpose, hydrodynamical evolutionary sequences for the secular behavior of gas flows in ellipticals have been performed, varying the type Ia supernovae rate of explosion, and the dark matter amount and distribution. The results are compared with the observational X-ray data: the average *Einstein* spectrum for 6 X-ray faint early-type galaxies (among which are NGC4365 and NGC4697). and the spectrum obtained by the *ROSAT* pointed observation of NGC4365. The ultra-soft component could be entirely explained with a hot ISM only in galaxies such as NGC4697, i.e. when the depth of the potential well – on which the average ISM temperature strongly depends – is quite shallow; in NGC4365 a diffuse hot ISM would have a temperature larger than that of the ultra-soft component, because of the deeper potential well. So, in NGC4365 the softest contribution to the X-ray emission comes certainly from stellar sources. As stellar soft X-ray emitters. we consider late-type stars coronae, supersoft sources such as those discovered by *ROSAT* in the Magellanic Clouds and M31, and RS CVn systems. All these candidates can be substantial contributors to the ultra-soft emission, though none of them, taken separately, plausibly accounts entirely for its properties.

We finally present a model for the X-ray emission of NGC4365, to reproduce in detail the results of the *ROSAT* pointed observation, including PSPC spectrum and radial surface brightness distribution. Since the X-ray surface brightness appears more extended than the optical profile, a straightforward explaination in terms of

stellar sources is not satisfactory. We find that the available data can be explained with three different contributions: a very soft component of stellar origin, a hard component from X-ray binaries, and a ~0.6 keV hot ISM. The latter can explain the extended X-ray surface brightness profile, if the galaxy has a dark-to-luminous mass ratio of 9, with the dark matter very broadly distributed, and a SNIa explosion rate of ~0.6 the Tamman rate.

1. Introduction

After the launch of the *Einstein* satellite (Giacconi *et al.* 1979), it was first realized through X-ray measurements that elliptical galaxies may retain a large amount ($\sim 10^8 - 10^{11} M_\odot$) of hot ($T \sim 10^7$ K) interstellar gas (e.g. Forman, Jones, and Tucker 1985; Canizares, Fabbiano, and Trinchieri 1987; see the review of Fabbiano 1989). This conclusion was supported by the presence of X-ray emission displaced from the optical body in some cases, by the relatively soft (~1 keV) X-ray spectra of X-ray bright ellipticals, and by the steep correlation between X-ray and optical luminosity ($L_X \propto L_B^{1.5-2}$), see Fig. 1. In contrast in spiral galaxies, where the X-ray emission can be attributed to a population of evolved stellar sources (see Fabbiano 1989, and references therein), the X-ray spectra tend to be harder. and $L_X \propto L_B$. Besides suggesting a steep relationship between L_X and L_B. the L_X–L_B diagram of early-type galaxies shows a substantial amount of scatter: the range of L_X for a given optical luminosity spans about two orders of magnitude. for $L_B > 3 \times 10^{10} L_\odot$ (Fig. 1).

Many theoretical models were developed to explain the L_X–L_B diagram. including numerical simulations for the behavior of gas flows fed by stellar mass loss and heated to X-ray temperatures by type Ia supernovae (SNIa; see the review of Fabbiano 1989; Loewenstein and Mathews 1987; Sarazin and White 1987. 1988; D'Ercole *et al.* 1989; David *et al.* 1991; Ciotti *et al.* 1991, hereafter CDPR). The most successful models are those explaining the scatter in the L_X–L_B diagram in terms of different dynamical phases for the hot gas flows, ranging from winds to inflows (CDPR). These authors, assuming that the SNIa explosion rate is declining with time slightly faster than the rate with which mass is lost by stars, find that in the beginning the energy released by SNIa's can drive the gas out of the galaxies through a supersonic wind. As the collective SNIa's energy input decreases, a subsonic outflow takes place, and this gradually slows down until a central cooling

catastrophe leads to the onset of an inflow. An attractive feature of this scenario is that any of the three phases wind/outflow/inflow can be found at the present epoch, depending only on the various depths and shapes of the potential wells of the galaxies: in X-ray faint ellipticals the gas is still in the wind phase, and the emission is mostly accounted for by stellar sources; in the bulk of galaxies the gas flows are in the outflow phase; in X-ray brightest galaxies the soft X-ray emitting gas dominates the emission, being in the inflow phase. In this latter case, the gas flow resembles a "cooling flow" (e.g. Sarazin and White 1987, 1988).

The knowledge of the actual contribution of discrete sources to the total X-ray emission is an important *tool* for constraining the gas flow phase, especially in X-ray faint galaxies. Unfortunately, even the amount of the hard contribution coming from accreting low-mass binaries, which should be substantial, is still a matter of debate, due to the impossibility of estimating it directly from the available *Einstein* X-ray spectra (Forman, Jones, and Tucker 1985; Canizares, Fabbiano, and Trinchieri 1987). Progress in this field comes from a recent systematic investigation of the X-ray spectra of early-type galaxies obtained by the Imaging Proportional Counter (IPC) on board of the *Einstein* satellite, by Kim, Fabbiano, and Trinchieri 1992 (see Fig. 1). These authors find that on the average the X-ray emission temperature increases with decreasing X-ray to optical ratio (L_X/L_B), until the dominant contribution to the total emission comes from a hard component, similar to that dominating the emission in spirals, which can be fitted with a $kT > 3$ keV bremsstrahlung model. These findings are in agreement with the CDPR scenario, in which the emission of X-ray faint early-type galaxies is due mainly to a stellar component (these galaxies would be in the wind phase), while the gaseous emission becomes dominant in X-ray bright galaxies, which would be in the inflow phase.

In the group of galaxies with the lowest values for L_X/L_B (Group 1, which includes 6 early-type galaxies with $29.3 < \log(L_X/L_B) < 30.0$, with L_X in erg s^{-1},

L_B in $L_\odot$), Kim, Fabbiano, and Trinchieri 1992 find that a very soft ($kT \approx 0.2$ keV) thermal X-ray component (hereafter VSC) is present in addition to the hard thermal component. The VSC emission has been estimated to amount approximately to one third to half ($\sim 10^{40}$ erg s^{-1}) of the total X-ray luminosity in the 0.2–3.5 keV band. With the available data, it remains possible that this VSC is present in all early-type galaxies. Recent *ROSAT* PSPC observations of two galaxies of Group 1 (NGC4365 and NGC4382, Fabbiano *et al.* 1993) confirm the existence of a VSC.

Investigating the nature of the VSC is the principal aim of this paper. We present hydrodynamical evolutionary sequences for the secular behavior of gas flows – in the frame of the CDPR models – specific to the Group 1 galaxies NGC4697 and NGC4365, to explore whether such flows can account for the observed VSC characteristics. These two galaxies were chosen because of their different central stellar velocity dispersions σ_*; σ_*^2 is proportional to the central depth of the galaxy potential well, on which the gas temperature strongly depends. In our models we adopt the observed optical characteristics of the galaxies, and we vary the SNIa's rate of explosion, and the amount and distribution of dark matter. The *ROSAT* results on NGC4365 allow us to make more secure conjectures on the various components of the X-ray emission, considering both the X-ray spectrum and the X-ray surface brightness profile. We also consider whether the VSC could originate in the collective emission of discrete very soft sources, such as late-type stellar coronae, ultrasoft accreting binaries like those detected by *ROSAT* in the Magellanic Clouds and M31 (Greiner *et al.* 1991; Kahabka and Pietsch 1992; Schaeidt *et al.* 1993), and RS CVn systems.

This paper is organized as follows: in §2 we summarize and re-examine the observational properties of the VSC in X-ray faint early-type galaxies; in §3 we investigate whether these properties are consistent with the expected characteristics of gas flows in Group 1 galaxies; in §4 we show the results of the numerical sim-

ulations to model the observations of NGC4697 and NGC4365; in §5 we consider stellar sources as origin of the VSC; in §6 we present a detailed model for the X-ray emission of NGC4365; in §7 we summarize our conclusions.

2. The VSC from *Einstein* and *ROSAT* Observations

For an accurate theoretical investigation, we need to have the best definition of the VSC characteristics which is possible within the observational boundaries. So, our first step was to re-analyze in detail the average spectrum obtained from *Einstein* data for Group 1 galaxies by Kim, Fabbiano, and Trinchieri 1992. to determine the range of the VSC temperature (T_{VSC}) and the VSC contribution to the total X-ray emission ($L_{X,VSC}$) allowed by the data. To this purpose, we used the PROS ('xray') package of *IRAF*, developed at *SAO* for the analysis of reduced X-ray data. Following Kim, Fabbiano, and Trinchieri 1992, we adopt an average value for the hydrogen column density along the line of sight $N_H = 3.2 \times 10^{20}$ cm^{-2}. Acceptable fits (at the 90% confidence level, for three interesting parameters: the two temperatures, and the ratio of the normalizations) are obtained when the spectrum is modeled by the superposition of a hard thermal component ($kT > 1$ keV), and a soft thermal component ($kT < 0.5$ keV). for solar abundance of the emitting gas[1]. The temperatures are not well constrained for very low and high values, due to the *Einstein* IPC sensitivity (Figs. 2 and 3).

The uncertainties in Group 1 data are such that the normalizations of the two thermal components are not well determined. If we put the constraint $kT > 0.1$ keV on the VSC temperature, we have that $0.15 < L_{X,VSC}/L_X < 0.50$ at the 90%

[1] With these data we cannot model temperatures and metal abundance of the ISM meaningfully. However the *ROSAT* observations of two Group 1 galaxies (Fabbiano *et al.* 1993) suggest that the two temperature model is the more likely representation of the data.

confidence level. Assuming that this range is representative of all Group 1 galaxies, we derive the range of $L_{X,VSC}$ values given in Table 1 for NGC4697.

Recent *ROSAT* observations of two Group 1 galaxies (NGC4382 and NGC4365, Fabbiano *et al.* 1993) confirm the presence of a VSC with better spectral data. The combination with a hard ($kT > 1.5$ keV) thermal component gives a best fit emission temperature $kT_{VSC} = 0.2$ keV, and its estimated range of variation at 90% confidence is between 0.15 and 0.3 keV. The soft and the hard contributions to the total X-ray luminosity in the *ROSAT* band are comparable in the best fit case. The spectral counts distribution of NGC4365 together with the two best fit components and their sum are shown in Fig. 4. We report in Table 1 the main results of the analysis concerning NGC4365, for which we perform numerical simulations of the hot gas behavior (we do not simulate the S0 galaxy NGC4382. because our spherically symmetric models cannot handle the presence of a disk).

3. Can a hot ISM be the origin of the VSC?

In this section we examine whether the observed VSC characteristics are in principle compatible with a hot ISM origin. As an outcome of this investigation. we will also find what input parameters are needed for the numerical simulations of the gas flow behavior. We first introduce our galaxy models.

3.1 The galaxy models

The galaxy structure adopted for the hydrodynamical simulations of the hot gas evolution is that of CDPR: it is a superposition of a King 1972 model for the luminous matter distribution, and of a quasi-isothermal halo for that of the dark matter; both distributions are truncated at the same tidal radius r_t. We adopt r_t/r_{c*}=180, where r_{c*} is the stellar core radius, so that the projection of the luminous matter distribution gives a good fit to the observed optical surface brightness

profiles of ellipticals (Kormendy 1982). The observed quantities are L_B, σ_*, and r_{c*}; from these the central stellar density ρ_{0*} is derived through the virial condition (e.g. Binney and Tremaine 1987). The stellar mass-to-light ratio is assumed to be constant with radius. The dark matter distribution can be described by the ratios of the dark/luminous masses ($R = M_h/M_*$), the dark/luminous core radii ($\beta = r_{ch}/r_{c*}$), and the dark/luminous central densities ($\gamma = \rho_{0h}/\rho_{0*}$), only two among these three parameters being independent. The problem of the physical consistency of the proposed mass distribution – whether it represents a self-consistent solution of the Poisson and Vlasov equations (see, e.g., Binney and Tremaine 1987) with two components – was addressed by Ciotti and Pellegrini 1992, in the hypothesis of stellar orbits with various anisotropies. In this paper we just want to derive the physical properties of the gas flows, and possible constraints on the amount and distribution of the dark matter, starting from reasonable shapes for the potential wells.

The time-evolving input ingredients of the numerical simulations are the rate of stellar mass losses, and the SNIa's heating; these too are calculated as in CDPR. In particular, the stellar mass loss rate is parameterized as $\dot{M}_*(t) \simeq -1.5 \times 10^{-11} L_B (t/15\,\mathrm{Gyrs})^{-1.3}\ M_\odot\,\mathrm{yr}^{-1}$; the SNIa's heating is parametrized as $L_{SN}(t) \simeq 7.1 \times 10^{30} \vartheta_{SN} L_B (t/15\,\mathrm{Gyrs})^{-1.5}$ erg s^{-1}, with $0 < \vartheta_{SN} < 1$. The value $\vartheta_{SN} = 1$ gives the present rate of SNIa explosion in ellipticals estimated by Tammann 1982: this is $0.88h^2$SNU, where $h = H_\circ/100$, and 1 SNU=1 event/100 yrs/$10^{10}\ L_\odot$ (we adopt $H_\circ = 50$ km/sec/Mpc throughout this paper). Van den Bergh and Tammann 1991 give an estimate which translates into $\vartheta_{SN} = 1.1$, close to that of Tammann 1982; Cappellaro *et al.* 1993 give a value 4 times lower ($\vartheta_{SN} \sim 0.3$), which illustrates the present range of uncertainty in the SNIa rate of explosion in ellipticals. L_{SN} is assumed here to be decreasing with time just faster than the stellar mass loss rate (Renzini 1989). This assumption produces the wind/outflow/inflow secular evolution of the gas dynamical state (CDPR).

The effects introduced by the possible presence of population gradients can be neglected without affecting our conclusions. Age and/or metallicity gradients – such as those that can be estimated from observations – introduce a variation of $\dot{M}_*(t)$ within $\sim 10\%$ (Renzini and Buzzoni 1986), while many uncertainties already affect $L_{SN}(t)$.

In summary, our parameter space for each galaxy model consists of (R, β, ϑ_{SN}).

3.2 $L_{X,gas}$ and $L_{X,VSC}$

Here we address the question of which gas flow phase can reproduce the observed $L_{X,VSC}$. Global inflows are far too luminous ($L_{X,gas} \gtrsim 10^{41}$ erg s^{-1}) with respect to $L_{X,VSC}$, while during winds the X-ray luminosity of the gas is very low ($< 10^{39}$ erg s^{-1}); during the outflow phase $L_{X,gas}$ can vary by orders of magnitude, going from wind values to inflow values. The duration of this transient phase is very sensitive to the input parameters, and it can last up to ~10 Gyrs; this means that any of the L_X values, from those typical of winds to those typical of inflows, can be shown by gas flows in outflows *at the present epoch*, depending on the input parameters. Another dynamical state in which $L_{X,gas} \sim L_{X,VSC}$ is the "partial wind" (hereafter PW). In this case radiative losses suppress an outflow in the center of the galaxy, causing a small inflow region, but a wind can be sustained in the external regions, where the gas density is much lower and the gas is also less tightly bound (MacDonald and Bailey 1981; §4.1.1). Clearly, the smaller is the central inflow region, and the higher is the wind velocity, the lower is the gas mass inside the galaxy, and so the X-ray luminosity.

Which gas flow phase is expected in Group 1 galaxies? They show a large range of σ_* (σ_*=186–284 km s^{-1}; Whitmore, McElroy, and Tonry 1985), reaching particularly low values with respect to the average Faber-Jackson relation. This is important because σ_* is one of the key parameters regulating the gas flow phase:

together with the amount of dark matter (R), and its concentration (β), it measures the binding energy of the gas. Following CDPR, we can summarize the gas flow energetic balance as a function of σ_*, and the introduced parameters (R, β, ϑ_{SN}), by using the parameter χ. This is defined as the ratio of the power required to steadily extract the gas shed by stars from the potential well of the galaxy, to the energy made available by SNIa's explosions: $\chi \propto \sigma_*^2(A + \beta^{-0.14}R)/\vartheta_{SN}$, at any epoch ($A$ is a constant). When $\chi > 1$, inflows are expected, while when $\chi < 1$, we expect winds; if $\chi \approx 1$ we have outflows. In Table 2 we show the values assumed by χ at the present epoch, for $\vartheta_{SN} = 1$ and for the σ_* values of the two galaxies in Table 1, NGC4697 and NGC4365; the dark matter amount (R) and concentration (β) have been varied. We can see how winds are expected in both galaxies, if $\vartheta_{SN} = 1$, even for large R values. So, we have to lower ϑ_{SN} to obtain outflows, especially for NGC4697, which has the smaller σ_*.

The parameter χ cannot be used to make predictions on the PW phase: the gas could be in PW with χ either larger or smaller than 1, because this parameter describes the global energetic balance of the gas, while in PW the gas behaves differently in the center and in the outskirt of the galaxy (these regions become "decoupled"). We expect PW solutions for small amounts of dark matter – since we assume it is distributed mainly at large radii – and this is confirmed by the numerical simulations (see also §4.1.1 and 4.2.1).

In conclusion, we have to explore through numerical simulations of the gas flow evolution which region of the parameter space (R, β, ϑ_{SN}) is populated by gas flow phases with $L_{X,gas} \sim L_{X,VSC}$, at the present epoch. We can just anticipate we need $\vartheta_{SN} < 1$.

3.3 T_{gas} and T_{VSC}

We explore here whether the VSC temperature is compatible with that of the hot ISM in ellipticals. As it was the case for the X-ray luminosity, the average gas

flow temperature depends strongly on σ_*. For instance, during the inflow phase predictions on the temperature profile of the gas can be made where the following simplifying assumptions hold: 1) the gas is in quasi-hydrostatic equilibrium in the galaxy potential well (i.e. $t_{sound}(r) << t_{cool}(r)$, with t_{sound} the sound speed crossing time, and t_{cool} the gas cooling time); 2) the flow is dominated by gravity rather than by the supernovae energy input (the gas is in inflow); 3) the cooling is just a small fraction of the global energetic balance of the gas flow. Under these hypotheses, from the momentum equation one derives $T_{in}(r) \propto |\phi(r)|$, ϕ being the galaxy gravitational potential. Just outside the central region of the galaxy, as soon as the infall velocity becomes small, one has $kT_{in}(5r_{c*}) \approx 3.6\mu m_P \sigma_*^2 (0.46 \div 1.6)$, respectively for $R = 0 \div 10$, and $\beta = 2$ (μm_P is the average gas particle mass). So we have $kT_{in}(5r_{c*}) \gtrsim 0.3$ keV if $\sigma_* \gtrsim 180$ km s^{-1}.

In conclusion, we can expect flows characterized by temperatures of the order of T_{VSC} only for low σ_* values. However the temperature estimates given above refer to the central regions of the galaxy, while the gas radial temperature distribution decreases outward, unless a sizable external pressure is effective. So. a detailed calculation of the gas X-ray spectrum in the sensitivity bands of the satellites is required. The extent to which the dark matter presence and distribution, the SNIa's rate, and the cooling of the gas determine the past flow evolution – and then its present temperature and density profiles – can be derived only through numerical simulations.

4. Numerical simulations for an ISM origin of the VSC

In this section we explore the gas flow evolution in the parameter space (R, β, ϑ_{SN}), to find whether there are regions in which gas flows have the observed VSC characteristics at the present epoch. To this purpose we construct hydrodynamical evolutionary sequences specific to the galaxies in Table 1, NGC4697 and NGC4365;

these have been chosen because, in Group 1, they have respectively the lowest and one of the highest values for σ_*, on which $L_{X,gas}$ and T_{gas} mostly depend (§3). To tailor the model structures to these galaxies, we adopt also the observed values of the blue luminosities (Table 1) and of the core radii (King 1978). Initially only the two fundamental parameters R (dark-to-light mass ratio) and ϑ_{SN} (SNIa's rate) vary, while the dark-to-luminous core radii ratio $\beta = 2$; we explore later the effect of a variation of β. The mass profiles of such galaxy models are shown in Fig. 5, for $\beta = 2$ and $\beta = 10$.

The time-dependent equations of hydrodynamics with source terms, and the numerical code to solve them, are described in CDPR. The cooling curve is an analytical fit to the results given by the Raymond code for the thermal emission of a hot, optically thin plasma, at the collisional ionization equilibrium, and with solar abundance (Raymond and Smith 1977). The gas flow evolution is followed for 15 Gyrs.

The characteristics of the flows (X-ray luminosities in the *Einstein* and *ROSAT* sensitivity bands, spectral energy distributions, and X-ray surface brightness profiles) are compared directly to the data, after they are transformed into predicted "observed" quantities, as follows. Using the Raymond code, the spectral energy distribution in the bands of sensitivity of the satellites is computed in each one of the 100 grid points used for the hydrodynamical simulation. After projection, the energy distribution of the photon flux is corrected for the interstellar absorption along the line of sight, using the photo-absorption cross sections of Morrison and McCammon 1983. Finally the model spectral distribution is convolved with the *Einstein* IPC (Harnden *et al.* 1984) or *ROSAT* PSPC spectral response and effective area, to obtain the predicted counts distribution. The model X-ray surface brightness profile is convolved with the energy dependent PSPC point spread function (Hasinger *et al.* 1992).

4.1 NGC4697

4.1.1 The X-ray Luminosity

In Fig. 6 we show how the various gas flow phases, at the end of the simulation, populate the (R, ϑ_{SN}) plane; the regions where $L_{X,gas}$(15 Gyrs)$\sim L_{X,VSC}$ are also shown. Due to the low σ_* value, a large region of the plane is occupied by global winds; to obtain χ(15Gyrs)$\approx$1, that is to expect an outflow at the present epoch, we need a dark-to-light mass ratio $R \approx 40$, if $\vartheta_{SN} = 1$.

For $R > 6$ the gas flow evolution is the "classical" one: wind/outflow/inflow; as anticipated in §3.2, $L_{X,gas}$(15 Gyrs)$\approx L_{X,VSC}$ during the outflow. The ϑ_{SN} value for this is very critical, because the flow is very sensitive to the global energetic balance. As an example, for (R=9, ϑ_{SN}=0.38) the gas is in outflow, and its L_X can vary by a factor of 8 with ϑ_{SN} varying by only 1%.

If $R \lesssim 6$ the flow doesn't follow the evolutionary history wind/outflow/inflow. If $\vartheta_{SN} \lesssim 0.3$, i.e. excluding the cases when a global wind lasts up to the present epoch, a cooling catastrophe takes place in the first few Gyrs (Fig. 7) in the central regions of the galaxy, while the gas escapes the external regions at a high velocity up to the present, and we have a PW. This is due to the SNIa's heating being too low to prevent an inflow in the gas dense and tightly bound central regions, while it is high enough to drive out the gas in the external regions. The tendency is however to evolve into a subsonic outflow, and then eventually into an inflow, even for the outer regions, as the specific heating secularly declines.

The flow behavior across the (R, ϑ_{SN}) plane can be explained looking at how the structure of the models changes across it. In the central regions of the galaxy the amount of luminous matter is always larger than that of the dark matter (see Fig. 5); increasing R, we bring to inner radii the dominance of the dark matter over the luminous one, but even for R=9, we have $M_h(< r)/M_*(< r) > 1$ only for $r > 11 r_{c*}$. So, the central regions are always dominated (from a gravitational point

of view) by the stellar structure, which is fixed across the plane. At low values of R, to avoid winds we decrease ϑ_{SN}, until it reaches a critical value ϑ^c_{PW} which is too low to prevent an inflow in the central regions, and we have a partial wind. At high values of R, ϑ^c_{PW} cannot prevent a global inflow, because also the external regions become very tightly bound.

The above results are sensitive to variations of the parameter β expecially during the outflow phase: a larger value for β – decreasing the dark matter concentration: $M_h(< r)/M_*(< r) > 1$ for $r > 21 r_{c*}$, if $R = 9$ and $\beta = 10$ (Fig. 5) – has the effect of retarding the onset of the global inflow. As a consequence, the values of ϑ_{SN} corresponding to outflows should be slightly decreased in Fig. 6. In PW cases – when R is low, and the luminous matter concentration is already high enough to cause a central inflow – a $\beta > 2$ has little influence. Values of β smaller than ~ 2 are not plausible, since dark matter halos around galaxies (if present) seem to be diffuse (Mathews 1988; Bertin, Saglia,and Stiavelli 1992).

4.1.2 The X-ray Spectrum

The spectral energy distribution of the flows having $L_{X,gas}(15\ \mathrm{Gyrs}) \approx L_{X,VSC}$ is in good agreement with that derived for the VSC, from a best fit of the *Einstein* IPC data (see Fig. 8). This is especially true for those cases with low values of ϑ_{SN} and R, i.e. PWs, when the gas temperature is lower. For $R \gtrsim 5$ the peak in the counts distribution of the gas flow models takes place at energies higher than observed, and it is clearly displaced for $R = 9$, $\vartheta_{SN} = 0.38$. However, all these distributions lie within that corresponding to $kT = 0.5$ keV, the 90% confidence upper limit on the VSC temperature, because the average X-ray emission temperature of gas flows is $kT = 0.2 - 0.3$ keV. In Fig. 9 we show the comparison of the average Group 1 spectrum with that of the ($R = 3$, $\vartheta_{SN} = 0.2$) model, to which a hard thermal component has been added.

In conclusion, for a galaxy with the optical characteristics of NGC4697, an ISM origin of the VSC is in principle possible; the strongest constraints in the parameter space come from the required $L_{X,gas}$ value, not from that of the gas emission temperature. In fact the latter cannot vary much for fixed σ_*, and the *Einstein* spectral data for Group 1 galaxies have large uncertainties, which don't allow any discrimination between the effects of R and ϑ_{SN} on the average gas emission temperature.

4.2 NGC4365

This galaxy, belonging to the Virgo cluster, has been observed also by the *ROSAT* PSPC. In the modelling we try to reproduce the results of these more accurate observations.

4.2.1 The X-ray Luminosity

In Fig. 10 we show the (R, ϑ_{SN}) plane for NGC4365. The main features of the gas flow behavior are the same as in the case of NGC4697; here we point out the main differences, and some characteristics of the gas flows which have been investigated in more detail, since more accurate observations are available.

Due to the larger value of σ_*, a larger region of the (R, ϑ_{SN}) plane is occupied by global inflows, and even with $R \sim 0$ the flows can be luminous enough (or even too luminous); the ϑ^c_{PW} values are higher than for NGC4697; the models with $L_{X,gas}$(15 Gyrs)$\sim L_{X,VSC}$ are in PW up to $R \approx 5$. For $3 \lesssim R < 5$ the global wind phase is actually followed by a global outflow phase, but the emission of the latter is never sufficiently high: a central cooling catastrophe develops, originating a PW, *before* the outflow phase can reach $L_{X,VSC}$ (Fig. 11). Global outflows can have $L_{X,gas} \gtrsim 6 \times 10^{39}$ erg s^{-1} only for $R \gtrsim 5$. The ϑ_{SN} value to have $L_{X,gas}$(15 Gyrs)$\sim L_{X,VSC}$ is specially critical if $R = 5 - 6$, the lowest R values for which

the outflow can be luminous enough: enough gas mass has accumulated within the galaxy only just before the central cooling catastrophe occurs (see the $R = 5$ case in Fig. 11).

As for NGC4697, changing the value of β has some effect only during outflows; for instance, if $R = 9$ and we increase β from 2 to 10, ϑ_{SN} goes from 0.68 to 0.59; if $R = 6$, increasing β from 2 to 20 lowers ϑ_{SN} from 0.55 to 0.43.

4.2.2 The X-ray Spectrum

In Table 3 we show the average emission temperatures for a few representative models having $L_{X,gas}(15\ \mathrm{Gyrs}) \sim L_{X,VSC}$ in the *ROSAT* band; the emission region considered is the same used by Fabbiano *et al.* 1993 to derive the observed spectral counts distribution. Going from PW's to outflows, kT varies from 0.4 to 0.7 keV.

In Fig. 12a we plot the observed counts distribution, together with the superposition of the spectrum of the gas flow - corresponding to a galaxy model with $R = 3$ and $\vartheta_{SN} = 0.35$ - and the spectrum of a bremsstrahlung component with $kT \sim 4$ keV, both convolved with the *ROSAT* response. The interstellar absorption is fixed at the line of sight value given in Table 1; the temperature and normalization of the hard component have been chosen so as to minimize the χ^2 of the fit with the observed counts distribution. From Fig. 12a we see how difficult it is to reproduce the observed peak at energies around 0.2 keV; this is true for every galaxy model. The case in Fig. 12a can be brought into much better agreement with the observational data if a column density $N_H = 3 \times 10^{19}$ cm^{-2} is assumed (Fig. 12b).

In conclusion, the gas spectrum is not as soft as that of the VSC, and cannot explain the observed counts distribution at low energies, under reasonable conditions, even when no dark matter is present, and with a very low SNIa rate (see the $R = 0$ and $\vartheta_{SN} = 0.18$ case in Table 3), because of the value of σ_*.

4.3 Conclusions

The numerical simulations we have performed, tailored precisely on a couple of galaxies in which the VSC has been measured, show that hot gas flows can easily be characterized by a luminosity $L_{X,gas} \sim L_{X,VSC}$, for acceptable values (within the present uncertainties) of the input parameters describing the amount and distribution of dark matter, and the SNIa explosion rate. The analysis of the X-ray spectra of gas flows reveals instead that they can be responsible for the VSC only in those galaxies having a low value of σ_* ($\lesssim$200 km s^{-1}), such as NGC4697. Among these galaxies, the requirement $L_{X,gas} \sim L_{X,VSC}$ implies a low value of ϑ_{SN} ($\lesssim$0.4 if $R \lesssim 10$).

ROSAT observations, confirming the existence of a VSC, indicate that its temperature doesn't depend on the σ_* value of the host galaxy: at 90% confidence level $kT_{VSC} < 0.3$ keV in NGC4365, whose σ_* value prevents the average gas emission temperature from falling below 0.4 keV. This fact leads us to conclude that by itself a hot ISM cannot generally explain the VSC.

5. Stellar Sources as Origin of the VSC

In the following we explore the alternative possibility that discrete sources have the required spectral characteristics and luminosity to account for the very soft emission in ellipticals. *ROSAT* has observed ultra-soft sources in M31 and the Magellanic Clouds, and the presence of a soft component in RS CVn systems has been well established, while late type stellar coronae have been known to be sources of very soft X-ray emission since the *Einstein* observations.

5.1 Supersoft Sources

ROSAT observations, during the All-Sky Survey and deep pointings, have revealed strong supersoft X-ray emission in several stellar sources; in a fraction of

them such emission had been revealed previously by *Einstein* observations. In the Large Magellanic Cloud (LMC) the supersoft sources are CAL 83 and CAL 87, optically identified with close binary systems, and RXJ 0527.8-6954 (Greiner *et al.* 1991), the variable RXJ0513.9-6951 (Schaeidt *et al.* 1993), and RXJ 0537.7-7034 and RXJ 0534.6-7056 (Orio and Ögelman 1993). In the Small Magellanic Cloud (SMC) supersoft sources are PN67 (at the location of a planetary nebula), 1E0035.4-7230, and SMC3 , a symbiotic star (Wang and Wu 1992; Kahabka and Pietsch 1992). In our Galaxy *ROSAT* detected GQ Mus, a recent nova (Ögelman *et al.* 1993). These are among the softest X-ray sources observed, and it has been suggested that they form a separate new class of X-ray objects, not previously encountered in our Galaxy because of the interstellar extinction (Schaeidt *et al.* 1993). Their similar spectra – the bulk of the X-ray emission is below 0.5 keV – can be described by black body radiation with $kT_{bb} = 20 - 50$ eV and X-ray luminosity from a few$\times 10^{37}$ erg s^{-1} up to $\sim 10^{38}$ erg s^{-1}. Many strong supersoft sources have also been discovered in M31 where they seem to show a larger range in $kT_{bb} = 20 - 70$ eV, and $L_X = (0.1 - 1) \times 10^{38}$ erg s^{-1} (R. Supper 1993, private comm.).

The origin of the soft spectra and the nature of the compact object in such supersoft sources are still unclear: they could be neutron stars accreting matter at or above the Eddington rate (Greiner *et al.* 1991), or they might represent a long sought class of white dwarfs (WDs) burning accreted matter (van den Heuvel *et al.* 1992). This second interpretation seems more likely, thanks also to the nature of the accreting object optically identified in a few cases (see for example the case of SMC3 or that of the nova GQ Mus). In the van den Heuvel *et al.* model for CAL83 and CAL87 the X-ray emission is produced by steady nuclear burning on the surface of a $0.7 \div 1.2\ M_\odot$ WD; the accreted matter is not ejected in thermonuclear nova flashes, thanks to the high accretion rate [(1–4)$\times 10^{-7} M_\odot$yr^{-1}].

5.1.1 Can Supersoft Sources Be the VSC Origin?

We examine here whether the presence of supersoft sources can explain the X-ray spectra of those early-type galaxies where the VSC was discovered. Fitting the average Group 1 X-ray spectrum with a black body component of $kT_{bb} = 50$ eV, instead of a 0.2 keV thermal component, the goodness of the fit remains the same; $kT_{bb} = 150$ eV at the best fit. The contribution of the black body component is approximately half of the total flux in the (0.2–4) keV band, and so, for example, ≈ 500 supersoft sources are needed to explain the soft emission of NGC4697.

Fitting the X-ray spectrum of NGC4365 with a black body component of $kT_{bb} \sim 50$ eV, instead of a 0.2 keV thermal component, the fit gets worse; if kT_{bb} is allowed to vary, at the best fit $kT_{bb} \sim 110$ eV, and still the fit is slightly worse than with a 0.2 keV thermal component. In this last case, $L_{X,bb} \sim 3 \times 10^{40}$ erg s^{-1}, and so we need ≈ 300 supersoft sources to account for the soft emission of NGC4365.

In conclusion, the supersoft sources can plausibly account only for a fraction of the very soft emission of early-type galaxies, because they are slightly too soft. Also, something more needs to be discovered concerning their nature (stellar components, origin and duration of the soft phase, variability) to investigate whether their collective emission can be significant in early-type galaxies. For example, the interpretation model of van den Heuvel *et al.* 1992 requires as donor stars respectively a normal F-G star with mass $\sim 1.4 - 1.5\ M_{\odot}$ for CAL 87, and either an evolved main sequence star of $\sim 1.9 - 2.M_{\odot}$, or a post main sequence subgiant of lower mass ($M \gtrsim 1.5 M_{\odot}$) for CAL 83. Such companions are unlikely to be present in the old population of an elliptical galaxy. In other cases the estimated companion mass is much lower [see, e.g., the case of GQ Mus, a classical nova, where the mass of the secondary is $< 0.2\ M_{\odot}$, Ögelman *et al.* 1993].

Finally, it is interesting to note that were the supersoft sources WDs burning accreted matter, they would represent a long sought class of sources, which could also be the progenitors of type Ia supernovae (Munari and Renzini 1992, Kenyon

et al. 1993). In this case the accreting WD would explode after having grown to the Chandrasekhar limit, or even before (helium detonation SNIa's). We estimate here what SNIa rate of explosion (R_{exp}) is expected if $L_{X,VSC}$ comes entirely from WDs accreting matter and then exploding as SNIa's: $R_{exp} \approx 10^{-52} L_{X,VSC}/\alpha M_{acc}$ s^{-1}, where α is the fraction of the *bolometric* luminosity produced by the hydrogen burning, collected by the *ROSAT* satellite; M_{acc} is the mass which has to be accreted before explosion, in solar masses; and the energy yield per unit mass by hydrogen burning, for 0.7 hydrogen mass fraction, is $\sim 4.5 \times 10^{18}$ erg g^{-1}. On average, the progenitor WD has to accrete $\sim 0.2\ M_{\odot}$ before exploding (Munari and Renzini 1992), or even less if it undergoes helium detonation (Woosley and Weaver 1993); so $R_{exp} \approx 1.5 \times 10^{-11}/\alpha$ s^{-1} in NGC4365. Since the observed rate is $R_{SN} \approx 4.5 \times 10^{-10} \vartheta_{SN}$ s^{-1} for this galaxy (from §3.1), to reproduce it we need $\alpha \lesssim 0.03/\vartheta_{SN}$. Note that $\alpha = 0.01, 0.24, 0.82$ for $kT_{bb} = 10, 20, 50$ eV, and so most of $L_{X,VSC}$ should come from objects with quite low temperatures. This requires to make another check, i.e. whether the UV flux that would be produced is consistent with that observed. Greggio and Renzini (1990) derive for ellipticals $L_{UV}/L_{BOL} < 0.02$; imposing this constraint on the UV emission of supersoft sources, we derive $\alpha > 2 \times 10^{-3}$ in NGC4365. So, the possible link between $L_{X,VSC}$, supersoft sources, and SNIa's is not ruled out by current observational constraints.

5.2 Late Type Stars

In comparison to other types of stellar X-ray sources which are powered by accretion, normal stars are very faint sources of X-ray emission ($L_X \approx 10^{26} - 10^{30}$ erg s^{-1}). Their collective emission can still be substantial, because dwarfs of all spectral types from F to M are sources of X-ray emission (e.g. Schmitt *et al.* 1990); particularly, it is interesting to consider the X-ray properties of K and M dwarfs. These stars are the most numerous in a single burst old stellar population like that of elliptical galaxies. In such stars the X-ray emission is thermal, and originates

in the stellar coronae. From a systematic investigation of *Einstein* IPC data, Schmitt *et al.* 1990 find that a two-temperature description is always required for the coronae of K and M dwarfs when high signal-to-noise spectra are available. The values of these temperatures cluster around $kT \sim 1.4$ keV and $kT \sim 0.2$ keV.

We can estimate the collective emission due to the lower temperature component of K and M dwarfs in ellipticals by multiplying their expected number (N_K and N_M respectively) by their average X-ray luminosity ($< L_X >_K$ and $< L_X >_M$). Assuming that K and M dwarfs were generated with the Salpeter initial mass function, their expected number in a single burst stellar population is:

$$N_K = \int_{0.6}^{0.85} A \cdot M^{-2.35} dM \qquad (1)$$

and

$$N_M = \int_{0.08}^{0.6} A \cdot M^{-2.35} dM \qquad (2)$$

where $A = 2.9 L_B$ (CDPR), $M = 0.85 M_\odot$ is the turn-off mass after 15 Gyrs, $M_{inf} = 0.08 M_\odot$. So we derive $N_M = 60.7 L_B$ and $N_K = 1.61 L_B$, with L_B in $L_\odot$; in the following we consider just the M dwarf contribution, since $< L_X >_M$ and $< L_X >_K$ are similar. Adopting $< L_X >_M = 2 \times 10^{28}$ erg s^{-1} (Rosner *et al.* 1981), we obtain $L_{X,M} = N_M < L >_M = 1.2 \times 10^{30} L_B$. This means $L_{X,M} \approx 2 \times 10^{41}$ erg s^{-1} for NGC4697, and $L_{X,M} \approx 8 \times 10^{40}$ erg s^{-1} for NGC4365: even if just a fraction of $L_{X,M}$ is due to the 0.2 keV component, M dwarfs seem to be able to explain the VSC in early-type galaxies. In general, $\log(L_{X,M}/L_B) \approx 30$, while for Group 1 galaxies $\log(L_{X,VSC}/L_B) = 29.0 - 29.7$.

Two comments are however in order. The first is that in late-type stars the emission is strongly dependent on the rotation rate (Pallavicini *et al.* 1981), because coronal heating is strongly related to the presence of a magnetic dynamo (Rosner 1991). Probably an "age effect", reducing the angular momentum. also reduces the X-ray luminosity, and this is particularly crucial for population II M

dwarfs. Barbera *et al.* 1993 have systematically investigated the presence of this effect: using all the available *Einstein* IPC data, they have identified a subsample representative of the population of M dwarfs in the solar neighborhood; using a kinematic criterion to determine the age, they have confirmed the decrease in X-ray luminosity going from young-disk to old-disk population. For old M dwarfs they find $< L_X >_M = (0.8 - 1) \times 10^{27}$ erg s^{-1} (going from late to early M). We derive then $\log(L^{old}_{X,M}/L_B) \approx 28.7$; for NGC4365 $L^{old}_{X,M} \sim 3.5 \times 10^{39}$ erg s^{-1}, while $L_{X,VSC} \sim 2.7 \times 10^{40}$ erg s^{-1}. So the age effect probably rules out the M dwarfs as the main origin of the VSC in ellipticals; the contribution of these stars could even be much lower, when we consider that the *ROSAT* pointed observation of an old M dwarf such as the Barnard star shows that its $L_X = 3 \times 10^{25}$ erg s^{-1} (T. Fleming 1993, private communication).

The second consideration is that the Salpeter initial mass function probably doesn't hold down to stellar masses as low as 0.08 $M_\odot$. Tinney *et al.* 1992 find that in the solar neighborhood the initial mass function clearly flattens for stellar masses $< 0.2 M_\odot$. If this is the case also in early-type galaxies, we have overestimated N_M. Unfortunately we don't really know what the IMF is in ellipticals; we can just note that the adopted Salpeter IMF would imply a mass-to-light ratio of $M_*/L_B \approx 13$, within the range of values recently estimated by Guzman, Lucey, and Bower 1993 ($M_*/L_B = 8 \div 25$, assuming $L_V = 1.67 L_B$ as Greggio and Renzini 1990). If we want to explain the VSC with old M dwarfs, we have to increase N_M by at least of a factor of 4 (8 in NGC4365). This implies an IMF steeper than the Salpeter function, with slope > 2.6 in eq. (2), which in turn implies $M_*/L_B > 19$.

In conclusion, late type stellar coronae do have the required spectral characteristics to explain the VSC in ellipticals, but due to an age effect we expect their collective emission to be too low to account for it all, unless the IMF for M dwarfs is much steeper than the Salpeter function, and hence is at variance with the IMF

in the solar neighborhood.

5.3 RS CVn systems

RS Canum Venaticorum (RS CVn) systems are chromospherically active objects, typically consisting of a G or K giant or subgiant, with a late type main sequence or subgiant companion (Linsky 1984). As *Einstein* observations have shown, RS CVn's are the most X-ray luminous late type stars ($L_X \sim 10^{29} - 10^{31.5}$ erg s^{-1}), and their quiescent coronae can be well modeled by a thermal plasma with two temperatures (see e.g. Schmitt *et al.* 1990). Recently, Dempsey *et al.* 1993 presented the results of their analysis of X-ray spectra of 44 RS CVn systems obtained during the *ROSAT* All-Sky Survey with the PSPC. They find that a bimodal distribution of temperatures centered near 0.2 and 1.4 keV fit the data best.

We examine here the soft X-ray emission expected from RS CVn systems in early type galaxies. Though most of Dempsey *et al.* 's systems belong to population I, we take 4×10^{30} erg s^{-1}as an average value for the soft X-ray luminosity of a system (Dempsey *et al.* 's Fig. 3). The spatial density of RS CVn's has been estimated by Ottmann and Schmitt 1990 for the Galaxy; here we estimate it for an old stellar population as follows. The number of RS CVn is a fraction of the number of G or K giants and subgiants (respectively N_{giant} and N_{subg}); N_{giant} and N_{subg} can be calculated from the knowledge of the time spent by stars in such evolutionary phases (see e.g. Renzini 1989). Assuming that low mass metal rich stars spend approximately 1 Gyr on the subgiant branch, and 1 Gyr on the red giant branch, we have $N_{subg} + N_{giant} \approx 0.1 L_B$. Taking half this number for those in binary systems, and another factor (a) for those which become RS CVn, we derive the collective contribution $L_{X,RSCVn} = 4 \times 10^{30}(N_{subg} + N_{giant}) \approx 2 \times 10^{29} a L_B$; or $\log (L_{X,RSCVn}/L_B) = 28.6$ if $a = 0.2$. So we conclude that RS CVn systems represent another class of likely contributors to the VSC in early-type galaxies, especially thanks to their spectral characteristics, but they are certainly not the

unique explanation of the phenomenon.

6. A Model for the X-ray Emission of NGC4365

We propose here a model for the X-ray emission of NGC4365, to explain the results obtained from the *ROSAT* pointed observation of this galaxy (Fabbiano *et al.* 1993). The X-ray spectrum and surface brightness profile ($\Sigma_X(R)$) allow us to investigate in detail what is the dynamical phase of the gas flow, and what are the different components of the X-ray emission. From the resulting model we also obtain information on the dark matter content of this galaxy, its distribution, and the SNIa rate.

6.1 The X-ray surface brightness profile

$\Sigma_X(R)$ obtained by *ROSAT* is shown in Fig. 13. Assuming that the hard component present in the X-ray spectrum (§2) is due to low-mass accreting binaries, its spatial distribution probably follows that of the stars; the same holds for the VSC, if it comes from stellar sources. In Fig. 13 we also plot the superposition of two brightness profiles, having each the spectral energy distribution and the normalization of the two components derived from the best fit to the observed spectrum; their spatial distribution is the same as that of the optically luminous matter, and has been convolved with the PSPC response. The observed $\Sigma_X(R)$ is clearly less peaked than that of this model.

The discrepancy could be fixed if some cold material is present at the center of the galaxy to absorb the X-ray radiation (see, e.g., White *et al.* 1991). In this case, the 'observed' $\Sigma_X(R)$ could look like that in Fig. 14, where the absorbing material is confined within a spatial radius of 4 kpc, and produces a column density of $\sim 5\times10^{21}$ cm^{-2} (the spectral counts distribution is that observed by construction). The required cold gas mass would be $M_{HI} \approx 2\times10^9\ M_\odot$; from observations (Knapp

et al. 1985) an upper limit of 1.5×10^8 $M_\odot$ for the HI mass has been estimated. Based on these results, we consider the hypothesis of an intrinsic absorption unlikely.

6.2 X-ray Emission Sources in NGC4365

A hot ISM doesn't need to be distributed as the stars; indeed, its $\Sigma_X(R)$ can be very flat, during the outflow phase (*Ciotti et al.* 1992). So, introducing the presence of hot gas (as discussed earlier, this gas would be hotter the the observed VCS, and therefore its presence is not required by the X-ray spectral analysis) could help reproduce the particular shape of the observed $\Sigma_X(R)$. The amount and distribution of dark matter then play an important role, because – as simulations show – the gas density profile is flatter for larger and more extended (large β values) dark matter halos.

The gas flow that allows the best agreement with both the observed X-ray spectrum and $\Sigma_X(R)$ must have the following characteristics: its $\Sigma_X(R)$ is mostly flat, and its L_X is not larger than $\sim 2 \times 10^{40}$ erg s^{-1}, since a higher value cannot be reconciled with the observed spectrum. To reproduce the latter at high (> 1 keV) and low (< 0.5 keV) energies, two further components must be added to the spectrum of the gas flow: a hard component, and a very soft component. The temperature and normalization of these additional components are determined by a best fit to the observed spectrum.

After an accurate exploration of the $(R, \beta, \vartheta_{SN})$ parameter space, we found that the galaxy model best reproducing the data has ($R = 9$, $\beta = 9.4$, $\vartheta_{SN} = 0.59$). The X-ray properties of the three components are summarized in Table 4. $L_{X,VSC}$ strongly depends on the assumed N_H value; here the value in Table 1 is assumed. The very soft emission can also be produced by a black body component of $kT_{bb} = 50$ eV, rather than by a Raymond thermal component, and so the VSC temperature in this model is close to that of the supersoft sources (§5.1). To reproduce the whole $L_{X,VSC}$ in this way we need ~ 200 supersoft sources.

The resulting "best fit" spectrum is plotted in Fig. 15; $\chi^2/\nu = 1.6$, where $\nu = 19$ is the number of degrees of freedom (the lower and higher energy spectral bins have been excluded from the fit, see e.g. Fabbiano *et al.* 1993). The $\Sigma_X(R)$ resulting from the superposition of the three components is plotted in Fig. 16 ($\chi^2/\nu = 1.3$, for $\nu = 11$); the spatial distribution of the 0.1 keV and the 5 keV components is the same as that of the stars.

In conclusion, we suggest for this galaxy a SNIa's explosion rate of ≈ 0.6 the Tammann 1982 rate, and a mass model in which there is a considerable amount of dark matter, distributed mostly at large radii. The stellar velocity dispersion profile is observed only within the central $\sim 30''$ (Bender and Surma 1992), so a useful comparison with the dark matter effects is not possible. The above authors also find that NGC4365 might have suffered a merging process in the past, based on the presence of a kinematically decoupled core component. If this is true, and a starburst followed the merger, the stellar population of NGC4365 might be peculiar.

7. Conclusions

In this paper we have investigated possible origins for the very soft X-ray emission ($kT \sim 0.2$ keV) recently discovered in low L_X/L_B early-type galaxies. We considered both an origin in gas flows, performing numerical simulations of their behavior tailored to two galaxies (NGC4697 and NGC4365), and an origin in stellar sources. Our findings are as follows:

1) The X-ray luminosity of gas flows can be comparable to that of the very soft emission during the outflow or the partial wind dynamical phases. Both phases can be found at the present epoch only if the SNIa rate of explosion is lower than the standard (Tammann 1982) rate. The PW phase occurs only for values of the dark/luminous matter ratio up to 5–6, and the outflow for larger values.

The average emission temperature of gas flows is comparable to that of the

very soft emission only in galaxies with quite shallow potential wells, i.e. with low values of the central stellar velocity dispersion ($\sigma_* \lesssim 200$ km s^{-1}). Due to the larger σ_* value, the average emission temperature of gas flows in NGC4365 ($kT > 0.4$ keV) is higher than that of the very soft emission ($kT < 0.3$ keV at 90% confidence level) determined from the *ROSAT* pointed observation of NGC4365. So, by itself a hot ISM cannot generally explain the very soft emission.

2) Concerning stellar sources, we investigated the possible contributions to the very soft emission coming from supersoft sources, late type stellar coronae, and RS CVn systems.

The typical emission temperature of supersoft sources ($kT_{bb} < 70$ eV) is too low to explain entirely the very soft emission of early-type galaxies, although these objects might make an important contribution. In principle, if their nature is that of accreting white dwarfs, they could also account for the observed SNIa explosion rate.

M dwarf stars' coronae possess a thermal component at a temperature close to that of the very soft emission of early-type galaxies, but they are not likely to account entirely for it, because an age effect which reduces their X-ray luminosities is expected in old stellar populations. The initial mass function of M dwarfs should be much steeper than the Salpeter IMF to compensate for the age effect, but this may conflict with the observed M_*/L_B ratios of ellipticals.

RS CVn systems can also give a contribution, being the most X-ray luminous late type stellar sources, and possessing a soft ($kT \approx 0.2$ keV) thermal component.

3) We construct a detailed model for the X-ray emission of NGC4365, which can account for the results of the *ROSAT* pointed observation. We suggest the presence of three contributors, approximately equally important: evolved stellar sources such as low-mass X-ray binaries, producing the hard emission (energies > 1 keV); a hot ISM, necessary to reproduce the X-ray surface brightness profile ($kT_{gas} \sim 0.6$ keV);

stellar sources with very soft emission ($kT \approx 0.1$ keV). A major fraction of the latter could come from supersoft sources such as those in 2). The galaxy model that produces a gas flow with the required properties has a dark-to-luminous mass ratio of 9, with the dark matter very broadly distributed, and a SNIa explosion rate of ~ 0.6 the Tammann rate.

4) The ISM of NGC4697 is in a wind regime for the galaxy parameters giving the best agreement with the observations of NGC4365. If we don't assume that considerable variations from galaxy to galaxy exist in the amount of dark matter and SNIa rate, the very soft emission should come entirely from stellar sources in NGC4697. This can be tested by future *ROSAT* pointed observations of this galaxy.

Acknowledgements

We are grateful to A. D'Ercole for the hydrodynamical routines, F. Fiore for enlightments on the instrumental responses, D.W. Kim for the Group 1 X-ray spectrum, and J. Raymond for having kindly provided his thermal X-ray emission code; we thank J. Bookbinder, L. Ciotti, P. Eskridge, T. Fleming, J. Orszak and M. Birkinshaw for discussions and comments, and A. Renzini for useful suggestions. This work was supported by a Smithsonian Institution pre-doctoral fellowship. and by NASA LTSA grant NAGW-2681.

REFERENCES

Avni, Y., 1976. Ap. J., 210, 642

Barbera, M., Micela, G., Sciortino, S., Vaiana, G., Harnden, F.R., Rosner, R., 1993. Ap. J., in press

Bender, R., Surma, 1992. Astron. and Ap., 258, 250

Bertin, G., Saglia, R.P., and Stiavelli, M., 1992. Ap. J., 384, 423

Binney, J., and Tremaine, S., 1987. *Galactic Dynamics* (Princeton University press)

Canizares, C., Fabbiano, G., and Trinchieri, G. 1987. Ap. J., 312, 503

Cappellaro, E., and Turatto, M., 1988. Astron. and Ap., 190, 10

Cappellaro, E., Turatto, M., Benetti, S., Tsvetkov, D. Y., Bartunov, O.S.. and Makarova, I.N., 1993. Astron. and Ap., in press

Ciotti, L., D'Ercole, A., Pellegrini, S., and Renzini, A., 1991. Ap. J., 376, 380 (CDPR)

Ciotti, L., and Pellegrini, S., 1992. MNRAS, 255, 561

Ciotti L., D'Ercole A., Pellegrini S., and Renzini A., 1992. In *Morphological and Physical Classification of Galaxies*, ed. M. Capaccioli, G. Longo. (Dordrecht: Kluwer), p. 179

Dempsey, R.C., Linsky, J.L., Schmitt, J.H.M.M., and Fleming, T.A., 1993. Ap. J., in press

D'Ercole, A., Ciotti, L., Pellegrini, S., and Renzini, A., 1989. Ap. J., 341, L9

Fabbiano, G., 1989. Ann. Rev. Astron. Ap., 27, 87

Fabbiano, G., Kim, D.W., and Trinchieri, G., 1992. Ap. J. Suppl. Series, 80, 531

Fabbiano, G., Kim, D.W., and Trinchieri, G., 1993. Ap. J. submitted

Faber, S., and Jackson, R., 1986. Ap. J., 204, 668

Forman, W., Jones, C., and Tucker, W., 1985. Ap. J., 293, 102

Greggio, L., and Renzini, A., 1990. Ap. J., 364, 35

Greiner, J., Hasinger, G., Kahabka, P., 1991. Astron. and Ap., 246, L17

Guzmán, R., Lucey, J.R., and Bower, R.G., 1993. Ap. J., in press

Harnden, F.R., Fabricant, D.G., Harris, D.E., and Schwarz, J., 1984. *Smithsonian Ap. Obs. Spec. Rept.*, No. 393

Hasinger, G., Turner, J.T., George, I.A., and Boese, G., 1992. OGIP Calibration Memo CAL/ROS/92-001, NASA/GSFC

Kahabka, P., and Pietsc, W., 1992. In *New Aspects of Magellanic Cloud Research*, Heidelberg, June 1992.

Kenyon, S.J., Livio, M., Mikolajewska, J., and Tout, C.A., 1993. Ap. J., 407, L81

Kim, D.W., Fabbiano, G., and Trinchieri, G., 1992. Ap. J., 393, 134

King, I., 1972. Ap. J., 174, L123

King, I., 1978. Ap. J., 222, 1

Knapp, G., Turner, E.L., and Cunnife, P., 1985. Astron. J., 90, 454

Kormendy, J., 1982. In *Morphology and Dynamics of Galaxies*, ed. L. Martinet. and M. Mayor (Sauverny: Geneva Observatory), p. 113

Linsky, J.L., 1984. In *Cool Stars, Stellar Systems and the Sun*, eds. S.L. Baliunas and L. Hartmann (Berlin: Springer Verlag), p.244

Loewenstein, M., and Mathews, W., 1987. Ap. J., 319, 614

MacDonald, J., and Bailey, M., 1981. MNRAS, 197, 995

Mathews, W., 1988. Astron. J., 95, 1047

Morrison, R., and McCammon, D., 1983. Ap. J., 270, 119

Munari, U., and Renzini, A., 1992. Ap. J., 397, L87

Ögelman, H., Orio, M., Krautter, J., and Starrfield, S., 1993. Nature, 361, 331

Orio, M., and Ögelman, H., 1993. Astron. and Ap., 273, L56

Ottmann, R., and Schmitt, J.H.M.M., 1992. Astron. and Ap., 256, 421

Pallavicini, R., Golub, L., Rosner, R., Vaiana, G., Ayres, T., Linsky, J.L., 1981. Ap. J., 248, 279

Raymond, J.C., and Smith, B.W., 1977. Ap. J. Suppl. Series, 35, 419

Renzini, A., 1989. in *Evolutionary Phenomena in Galaxies*, ed. J. Beckman, and B. Pagel (Cambridge University Press), p. 422

Rosner, R., Avni, Y., Bookbinder, J., Giacconi, R., Golub, L., Harnden, F.R., Maxson, C.W., Topka, K., and Vaiana, G., 1981. Ap. J., 249, L5

Rosner, R., 1991. In *Mechanisms of Chromospheric and Coronal Heating*, ed. P. Ulm-Schneider, E. Priest, and R. Rosner, p. 287

Sarazin, C., and White, R., 1987. Ap. J., 320, 32

Sarazin, C., and White, R., 1988. Ap. J., 331, 102

Schaeidt, G., Hasinger, G., and Trümper, J., 1993. Preprint

Schmitt, J., Collura, A., Sciortino, S., Vaiana, G., Harnden, F.R., Rosner, R.. 1990. Ap. J., 365, 704

Stark, A., *et al.* , 1992. Ap. J. Suppl. Ser., 79, 77

Tammann, G., 1982. In *Supernovae: A Survey of Current Research*, ed. M. Rees and R. Stoneham (Dordrecht: Reidel), p. 371

Tinney, C.G., Mould, J.R., and Reid, I.N., 1992. Ap. J., 396, 173

van den Bergh, S., and Tammann, G., 1991. Ann. Rev. Astron. Ap., 29, 332

White, D.A., Fabian, A., Johnston, R.M., Mushotzky, R.F., Arnaud, K.A., 1991. MNRAS, 252, 72

Whitmore, B.C., McElroy, D.B., and Tonry, J.L., 1985. Ap. J. Suppl. Series, 59. 1

Woosley, S.E., and Weaver, T.A., 1993. In preparation

FIGURE CAPTIONS

Figure 1: The L_X–L_B diagram for early-type galaxies; data (detections only) are from Fabbiano, Kim, and Trinchieri (1992). The dashed line is the luminosity expected from SNIa heating L_{SN}, assuming the Tammann (1982) rate of explosion. The four groups of galaxies chosen by Kim, Fabbiano and Trinchieri (1992), to investigate the behavior of the average X-ray emission temperature, are indicated with different symbols (full squares are Group 1 galaxies; stars, full circles, and open circles with a cross are the other Groups, in order of increasing L_X/L_B values).

Figure 2: The average spectral energy distribution of Group 1 galaxies, obtained by the *Einstein* IPC (open squares with errorbars). Also plotted are the two thermal components which best fit this distribution (dotted and dashed lines), and their superposition (solid line).

Figure 3: 68% and 90% probability confidence contours for the temperatures (in keV) of the two components which best fit the average spectrum of Group 1 galaxies: the VSC (abscissa) and the hard component (ordinate). The increments above the χ^2_{min} value correspond to 3 interesting parameters, as explained in the text (Avni 1976).

Figure 4: The *ROSAT* PSPC X-ray spectrum of NGC4365, together with the VSC (dotted line), the hard component (dashed line), and their superposition (solid line), at the best fit (from Fabbiano *et al.* 1993).

Figure 5: The radial trend of the dark to luminous mass ratio $M_h(< r)/M_*(< r)$, for the cases $R = 1$ (lower lines) and $R = 10$ (upper lines); $\beta = 2$ for the dashed lines, and $\beta = 10$ for the dot-dashed lines.

Figure 6: The (R, ϑ_{SN}) plane for NGC4697. The dashed lines enclose the region of PWs. The solid lines enclose the region where the models have $L_{X,gas} \sim L_{X,VSC}$; they are coincident in the outflow regime, when a small variation of ϑ_{SN} causes a large variation of $L_{X,gas}$.

Figure 7: The time evolution of the fundamental hydrodynamical quantities describing the gas properties: velocity (v<0 for inflows, v>0 for outflows), temperature T and number density n. Plotted is the PW case (R = 5, ϑ_{SN} = 0.27) for NGC4697. Dashed lines refer to t=0.75 Gyrs, dotted lines to t=4.5 Gyrs, and solid lines to the present epoch (t=15 Gyrs).

Figure 8: The X-ray spectrum of the VSC from the analysis of *Einstein* spectral data (solid line), and that of a thermal component with kT = 0.5 keV, the 90% confidence upper limit on the VSC temperature (dotted line). The other lines are the gas spectra (convolved with the IPC response) for the following models for NGC4697: R = 9, ϑ_{SN} = 0.38 (dashed line); R = 6, ϑ_{SN}=0.28 (long dashed line): R = 4, ϑ_{SN} = 0.23 (dot-dashed line); R = 3, ϑ_{SN}=0.2 (dot-long dashed line). In order to compare the shapes, each spectrum has been normalized to the number of counts in the channel where it has the maximum.

Figure 9: The observed spectral count distribution for Group 1 galaxies (open squares with errorbars) compared with the superposition (solid line) of the convolved spectral distributions of the gas flow in NGC4697, for a model with R = 3. β = 2 and ϑ_{SN} = 0.2 (dotted line), and of a hard ($kT \sim 5$ keV) thermal component (dashed line).

Figure 10: The (R, ϑ_{SN}) plane for NGC4365. The solid lines enclose the region where the models have $L_{X,gas} \sim L_{X,VSC}$, and the dashed lines the PW region.

Figure 11: The time evolution of the X-ray luminosity in the *ROSAT* sensitivity band for the following models for NGC4365: R=1, ϑ_{SN} = 0.25 (solid line); R=2, ϑ_{SN} = 0.3 (dotted line); R = 3.5, ϑ_{SN} = 0.36 (dashed line); R=9, ϑ_{SN} = 0.68 (dot-dashed line). The three PWs can be recognized from the early cooling catastrophes (peaks in L_X). To show the strong sensitivity to ϑ_{SN} during the outflow phase, the case of R = 5 has also been plotted (long dashed lines): in order of increasing $L_{X,gas}$, the models have ϑ_{SN} = 0.500, 0.498, 0.495 (this last is an inflow at the

present epoch). The parallel solid lines represent the range of $L_{X,VSC}$ values allowed by the data.

Figure 12: The observed spectral counts distribution for NGC4365 (open squares with errorbars) together with the superposition (solid line) of the distribution of a gas flow of the ($R = 3$, $\vartheta_{SN} = 0.35$) model (dotted line), and that of a hard component with $kT = 5$ keV (dashed line), both convolved with the PSPC instrumental response. In a $N_H = 1.6 \times 10^{20}$ cm^{-2}, and in b $N_H = 3.2 \times 10^{19}$ cm^{-2}.

Figure 13: The observed X-ray surface brightness profile of NGC4365 (open squares with errorbars), from Fabbiano *et al.* 1993; unbinned PI channels 26–247 have been considered, to eliminate ghost effects. Also plotted are the surface brightness profiles of the hard (long dashed line) and soft (short dashed line) thermal components, derived from the best fit of the observed X-ray spectrum, and their superposition (solid line). The thermal components are distributed as the optical profile, and have been convolved with the PSPC response, appropriate for their respective spectral energy distribution.

Figure 14: The same as in figure 13, but an intrinsic absorption corresponding to $N_H = 5 \times 10^{21}$ cm^{-2} has been applied within the central 30″ (see §6.1).

Figure 15: The observed spectral energy distribution of NGC4365 (open squares with errorbars), together with the three components of the "best fit" model (§6.2) after convolution with the PSPC response: the hot ISM (dotted line), the very soft component ($kT \approx 0.1$ keV, dot-dashed line), and the hard component ($kT = 5$ keV, dashed line); the solid line is their superposition.

Figure 16: The X-ray surface brightness profile (solid line) of the superposition of the three components which best fit the observed X-ray properties of NGC4365 (§6.2). Open squares are the observed counts, the long dashed line is the hard thermal component, the short dashed line is the very soft $kT \approx 0.1$ keV thermal component, and the dotted line is the hot gas.

TABLE 1

Observational Properties

NAME	L_B[a] ($10^{11} L_\odot$)	σ_*[b] (km s^{-1})	d[a] (Mpc)	N_H[c] (10^{20}cm^{-2})	log L_X[d] (erg s^{-1})	$\frac{L_{X,VSC}}{L_X}$[e]	kT_{VSC}[e] (keV)
NGC4697	1.95	186	37.4	2.1	40.97	0.15 – 0.50	$\lesssim$0.5
NGC4365	0.65	262	27	1.6	40.74	0.3 – 0.7	0.15–0.26

[a] from Fabbiano, Kim, and Trinchieri 1992

[b] from Whitmore, McElroy, and Tonry 1985

[c] from Stark *et al.* 1992

[d] NGC4697 X-ray luminosity is the estimate derived from *Einstein* data by Fabbiano, Kim, and Trinchieri 1992, in the (0.2–4) keV range; L_X for NGC4365 is derived from *ROSAT* data by Fabbiano *et al.* 1993, in the (0.1–2.0) keV range. From *Einstein* data, Fabbiano, Kim, and Trinchieri 1992 derived logL_X=40.42 for NGC4365, in the (0.2–4) keV range, assuming 1 keV thermal emission.

[e] 90% confidence range (from Fabbiano *et al.* 1993 in the case of NGC4365).

TABLE 2

χ(15 Gyrs), with $\vartheta_{SN} = 1$

	$\sigma_\bullet = 186$ km s^{-1}			$\sigma_\bullet = 262$ km s^{-1}		
R / β	0	5	10	0	5	10
1	0.12	0.36	0.60	0.25	0.71	1.18
6	0.12	0.31	0.49	0.25	0.61	0.98
11	0.12	0.29	0.46	0.25	0.58	0.92

TABLE 3

NGC4365: gas flows average emission temperatures

(t=15 Gyrs)

R	ϑ_{SN}	flow [a] phase	kT_{gas} (keV)
9	0.68	O	0.7
5	0.498	O	0.5
3	0.35	PW	0.4
0	0.18	PW	0.4

[a] O= outflow; PW= partial wind

TABLE 4

X-ray emission components for NGC4365

	kT (keV)	$L_X(0.1-2$ keV) (10^{40} erg s^{-1})	$L_X/L_{X,tot}$
soft sources	≈ 0.1	2.0	0.35
hard sources	5	2.1	0.37
hot ISM	0.6	1.6	0.28

Note: the X-ray luminosities, and the average X-ray emission temperature of the hot gas, are calculated considering the same region used by Fabbiano *et al.* 1993 (a circle of 250″ radius).

FIG. 1

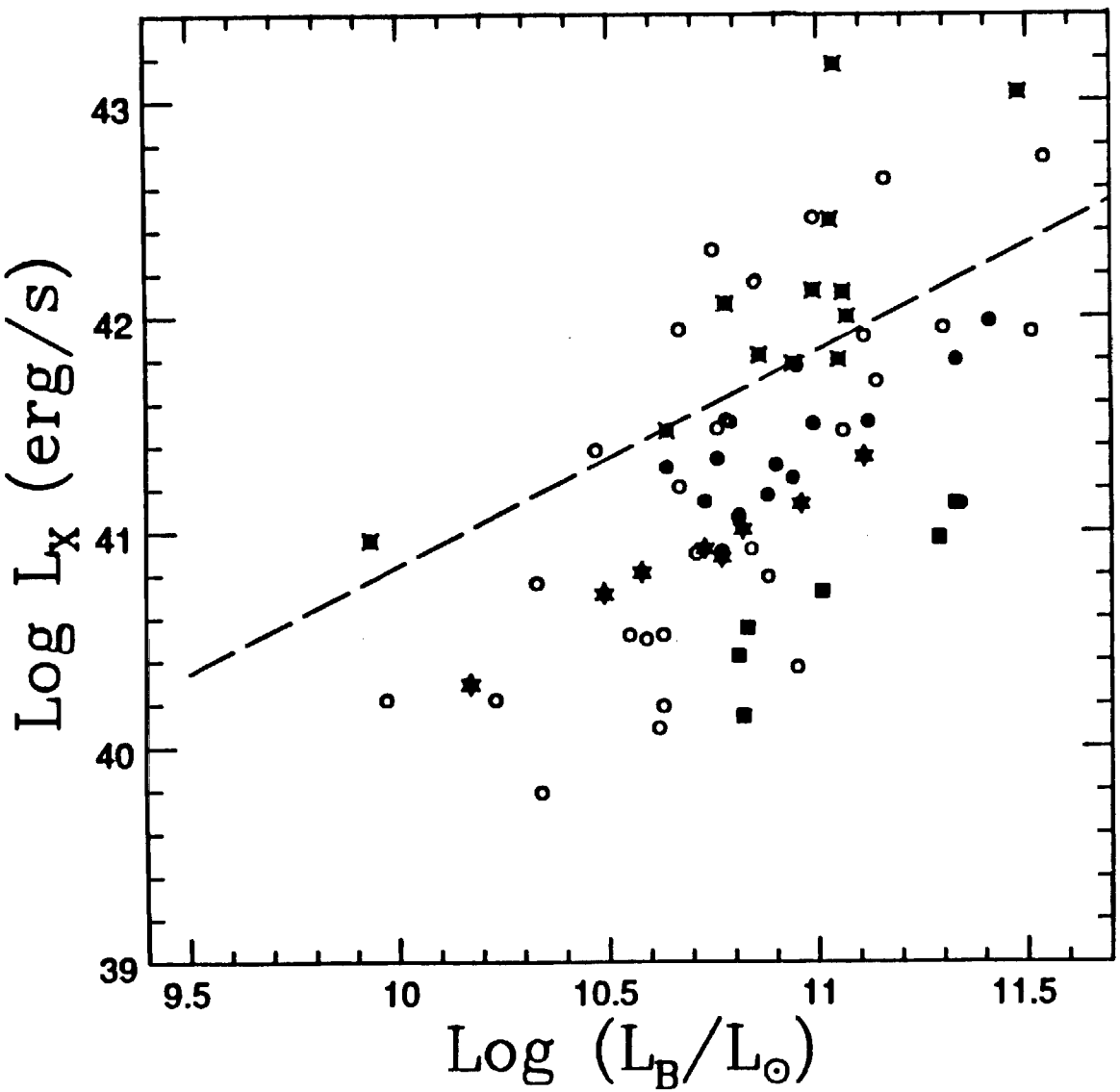

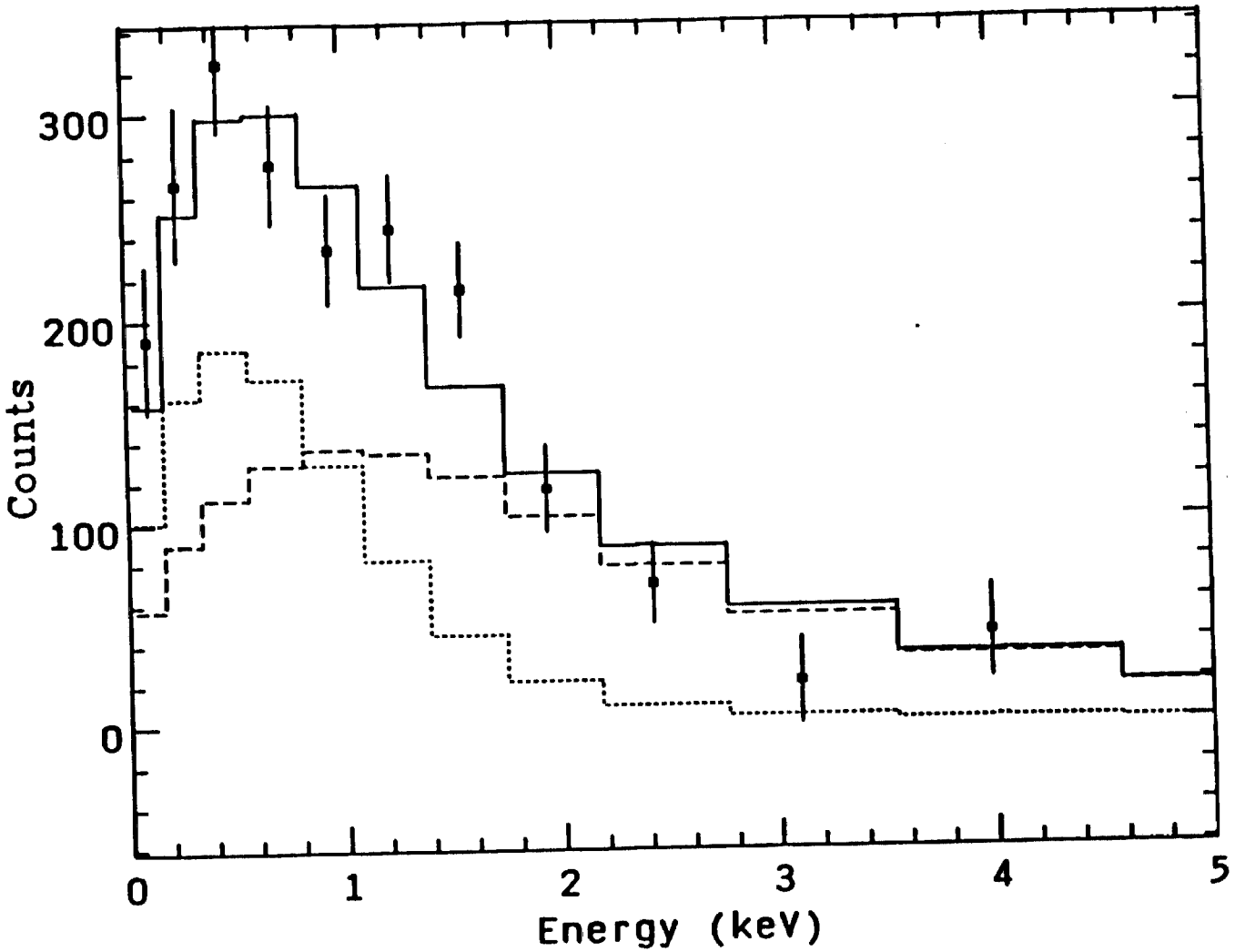

FIG. 2

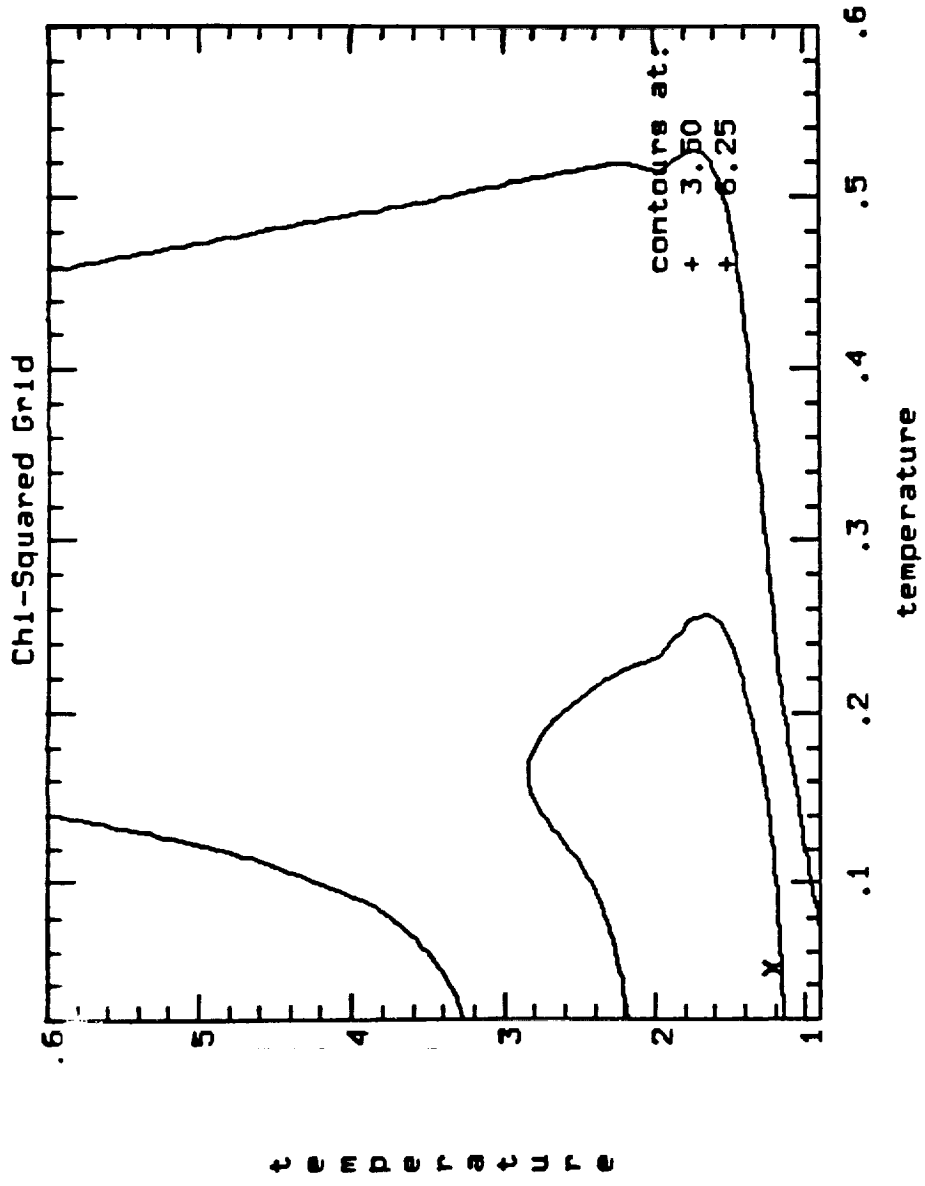
Chi-Squared Grid
contours at:
+ 3.50
+ 6.25
temperature
.1
.2
.3
.4
.5
.6
1
2
3
4
5
.6
temperature

FIG. 3

FIG. 4

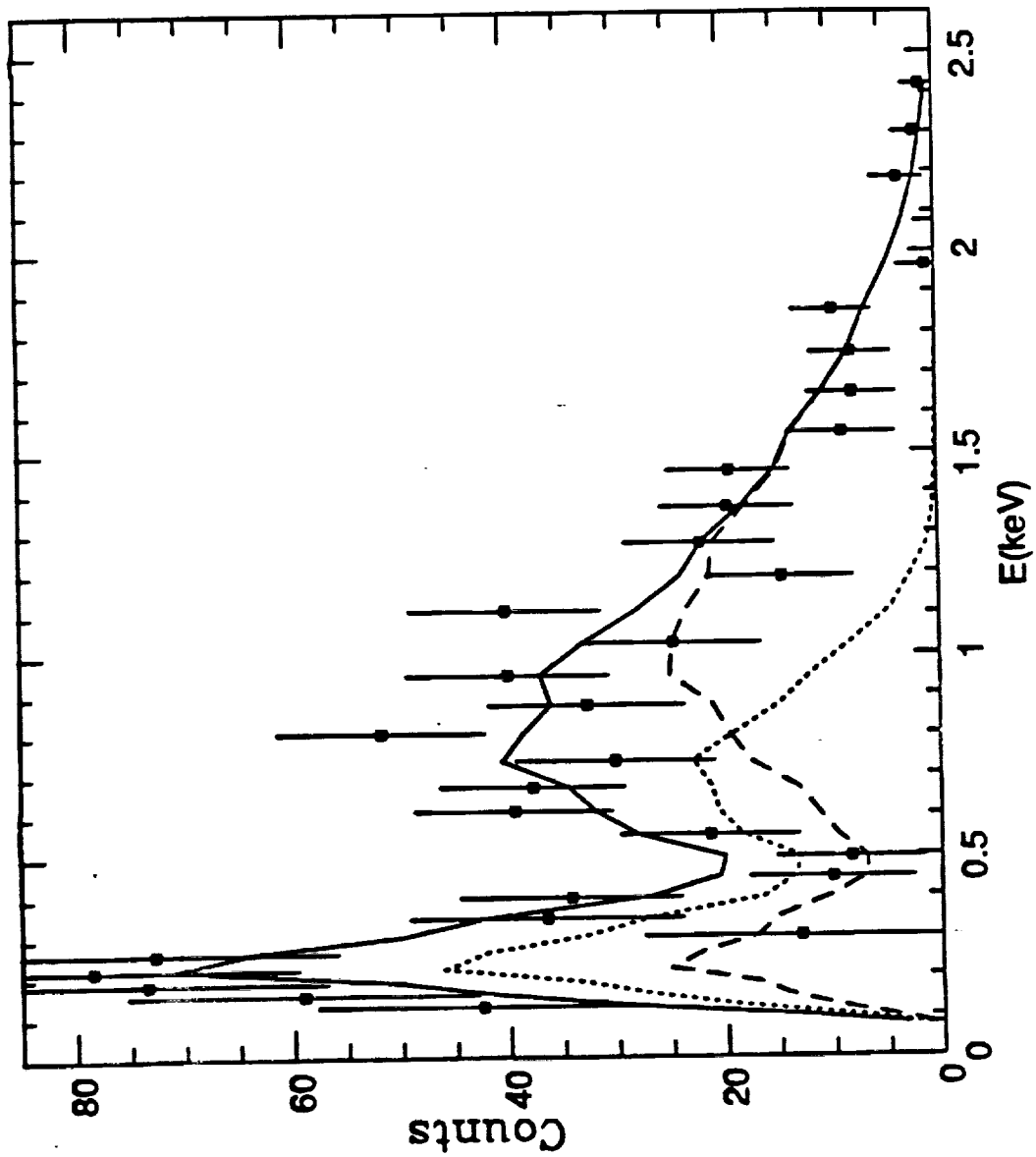

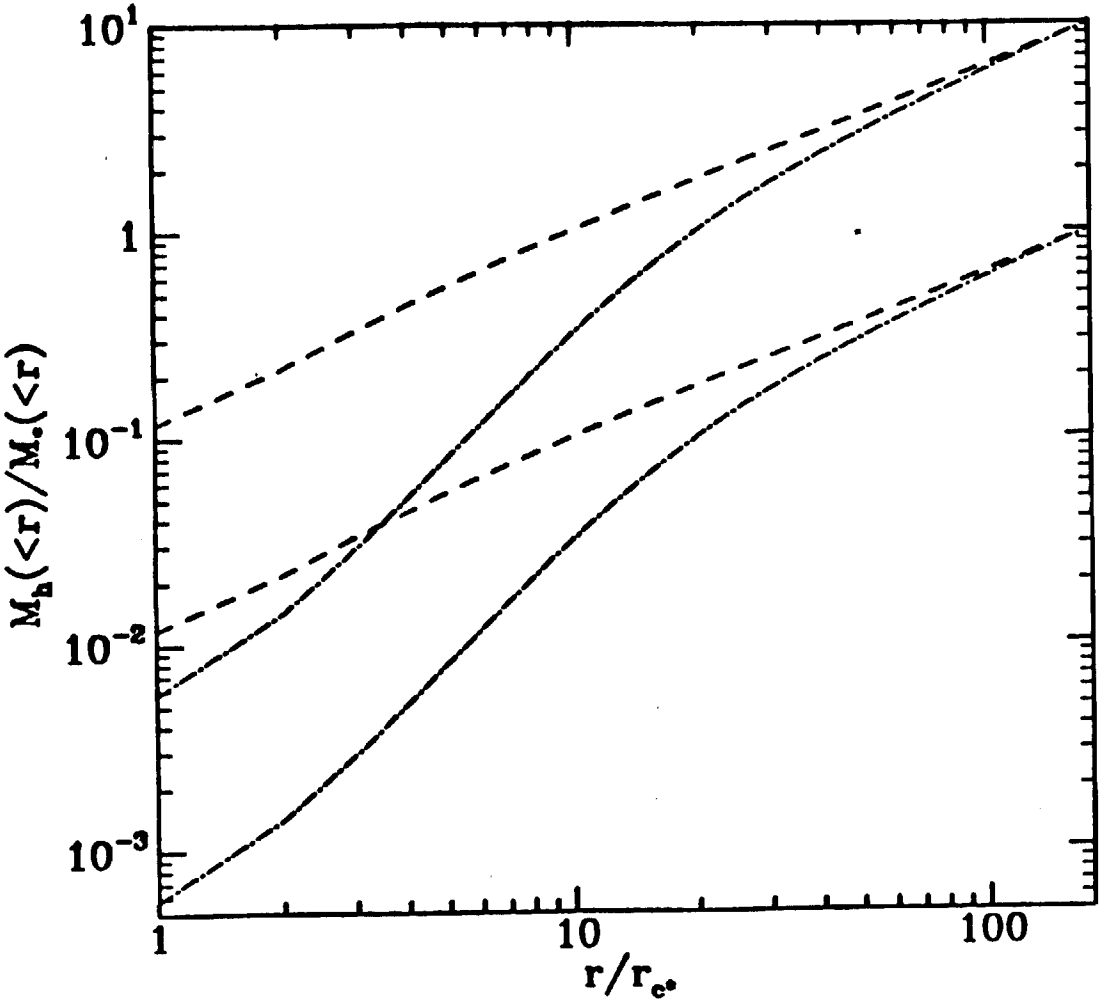

FIG. 5

FIG. 6

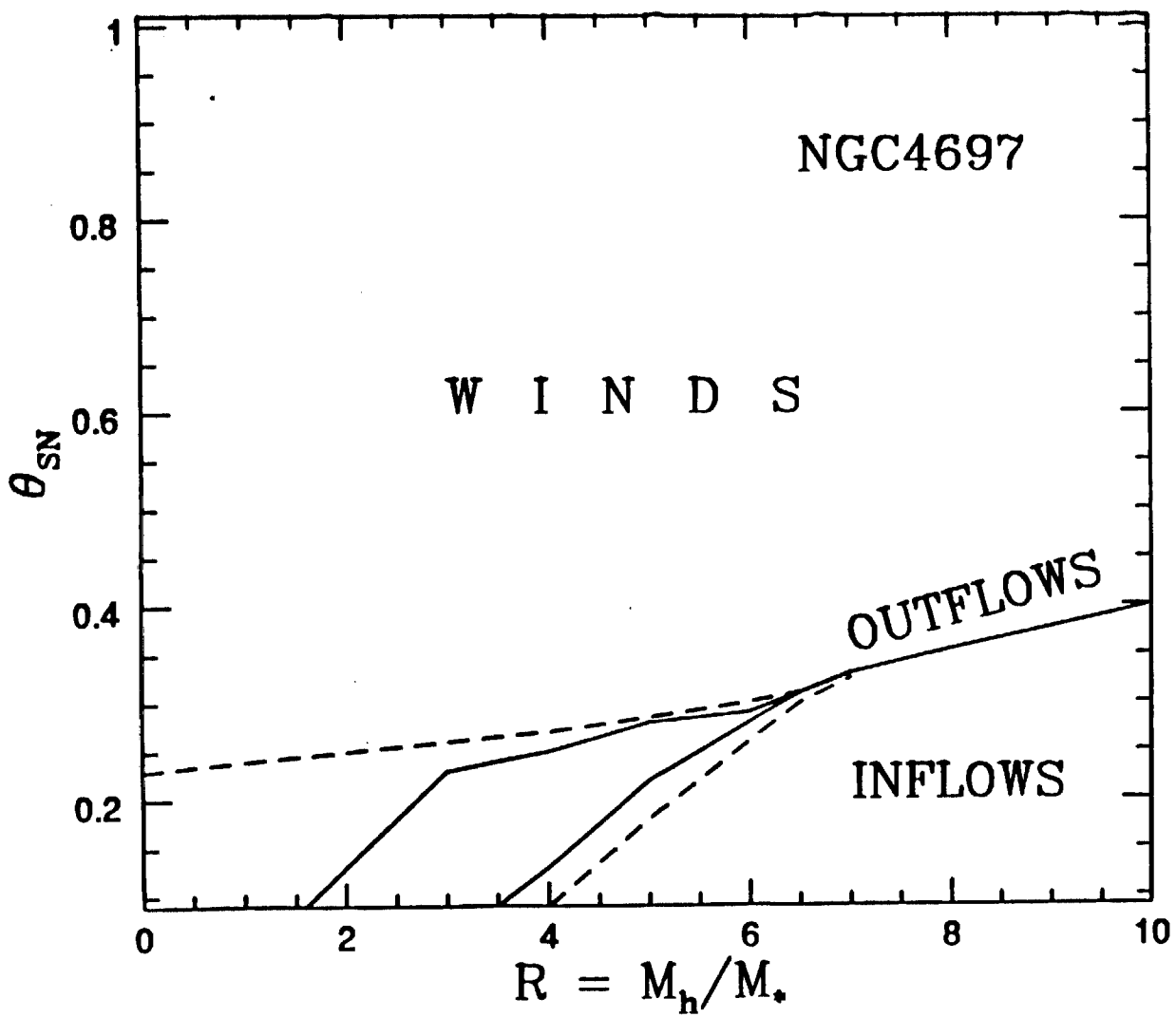
NGC4697
W I N D S
OUTFLOWS
INFLOWS
θ_{SN}
1
0.8
0.6
0.4
0.2
0
2
4
6
8
10
$R = M_h/M_*$

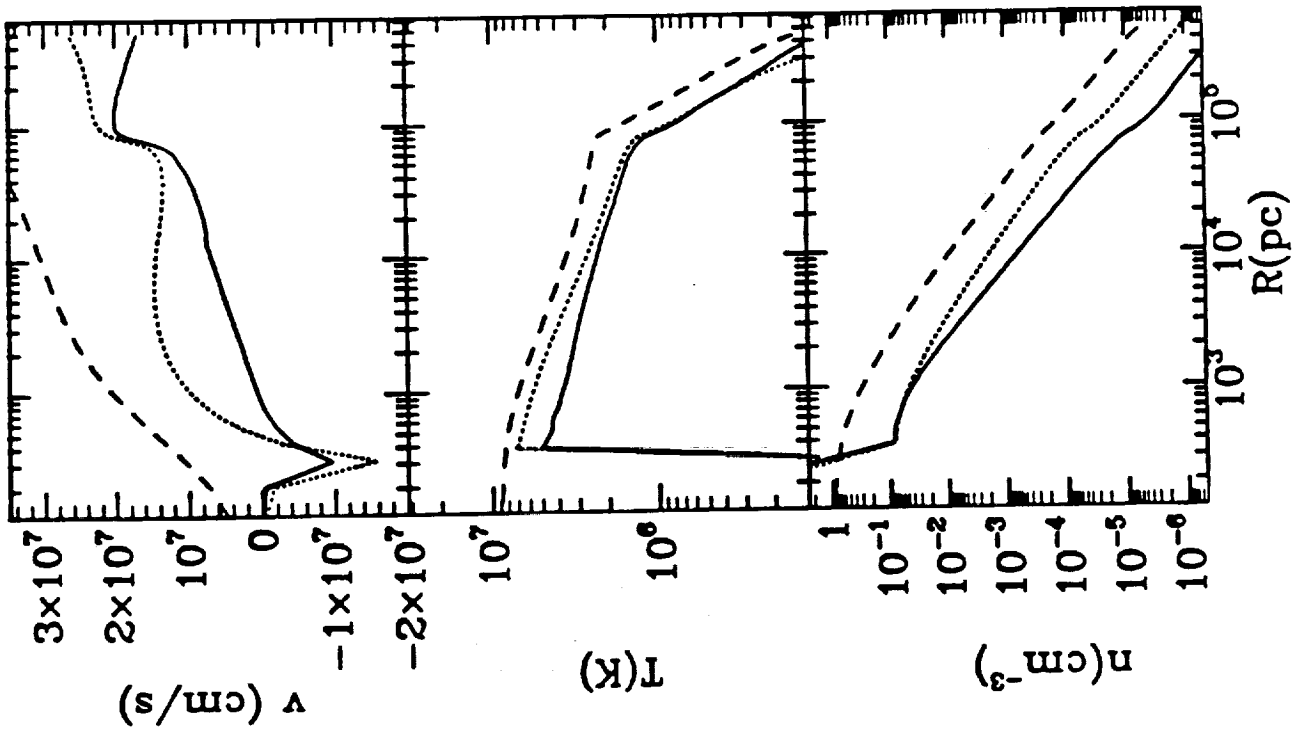
v (cm/s)
3×10^7
2×10^7
10^7
0
−1×10^7
−2×10^7
T(K)
10^7
10^6
n(cm^-3)
1
10^-1
10^-2
10^-3
10^-4
10^-5
10^-6
10^3
10^4
10^5
R(pc)

FIG. 7

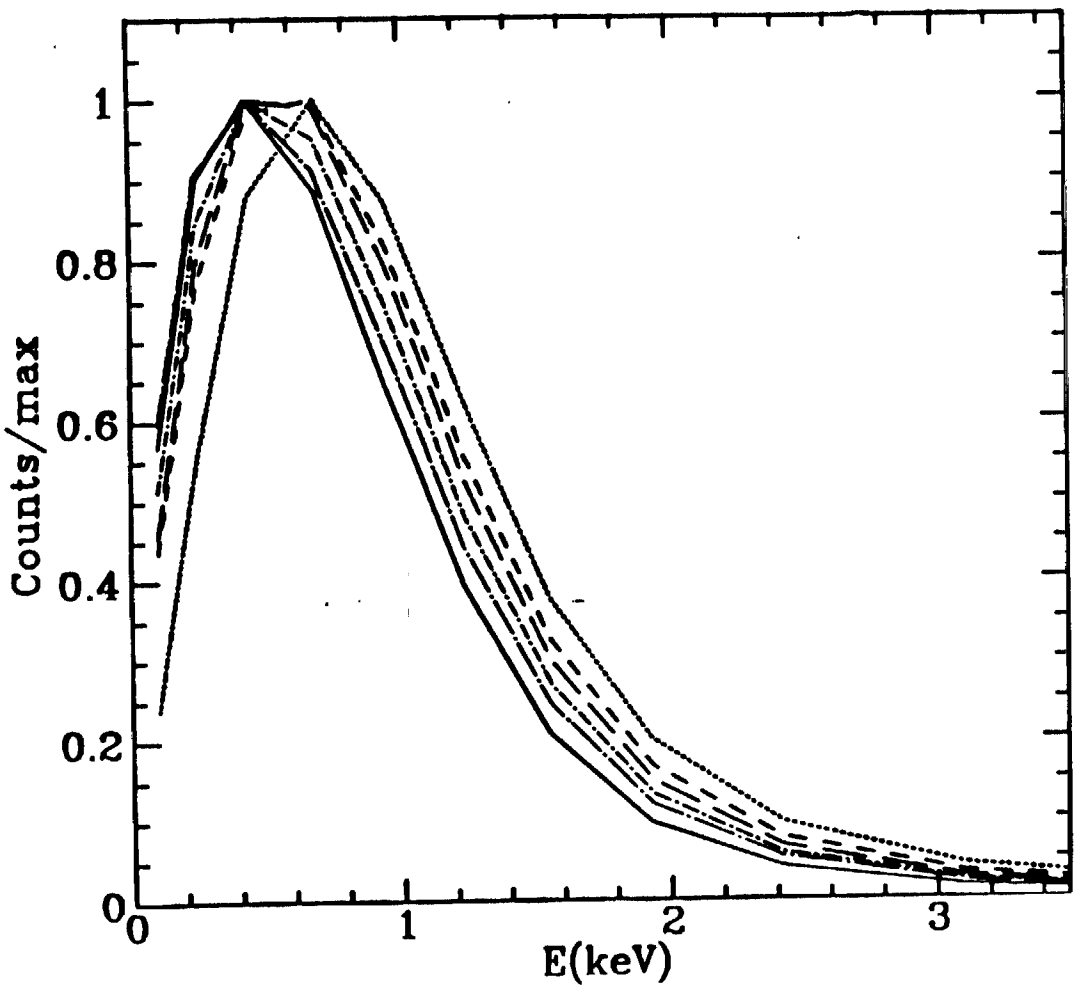

FIG. 8

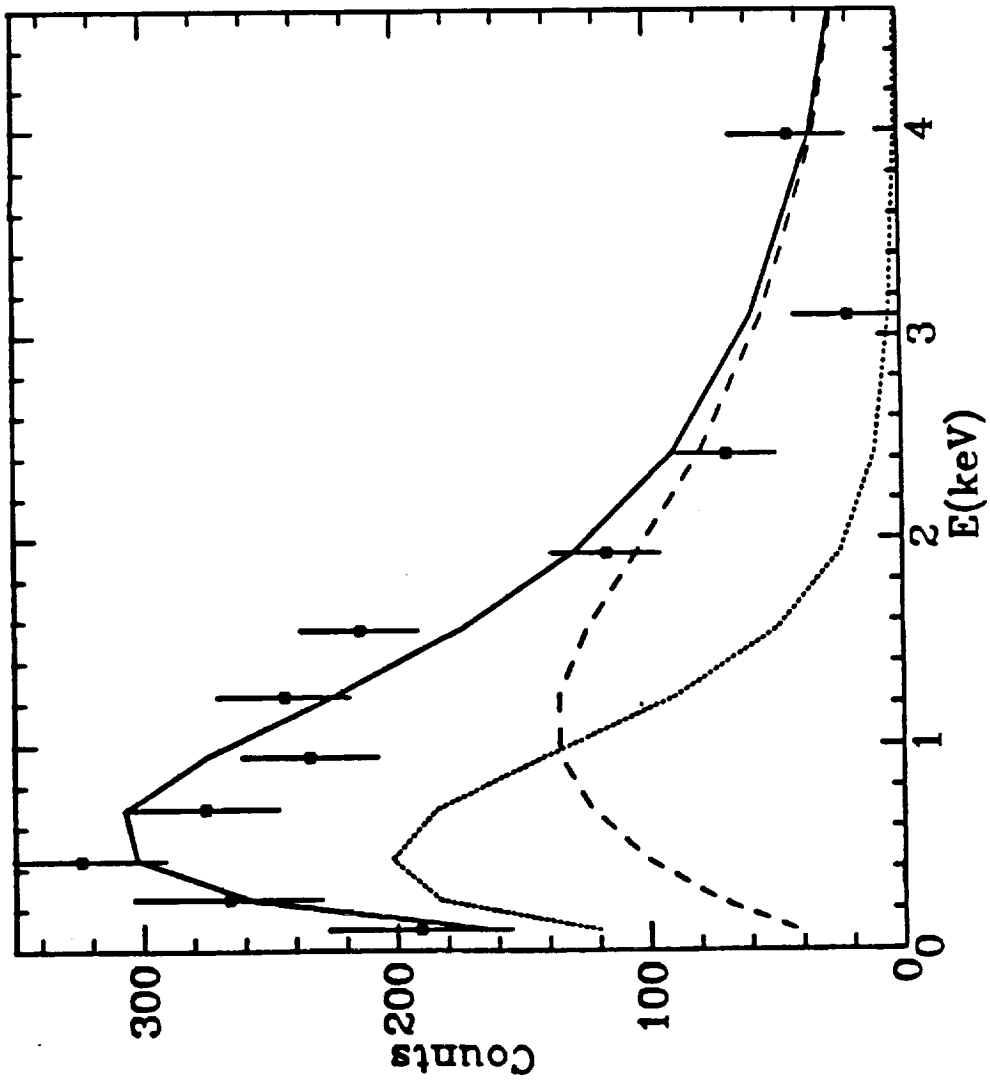

FIG. 9

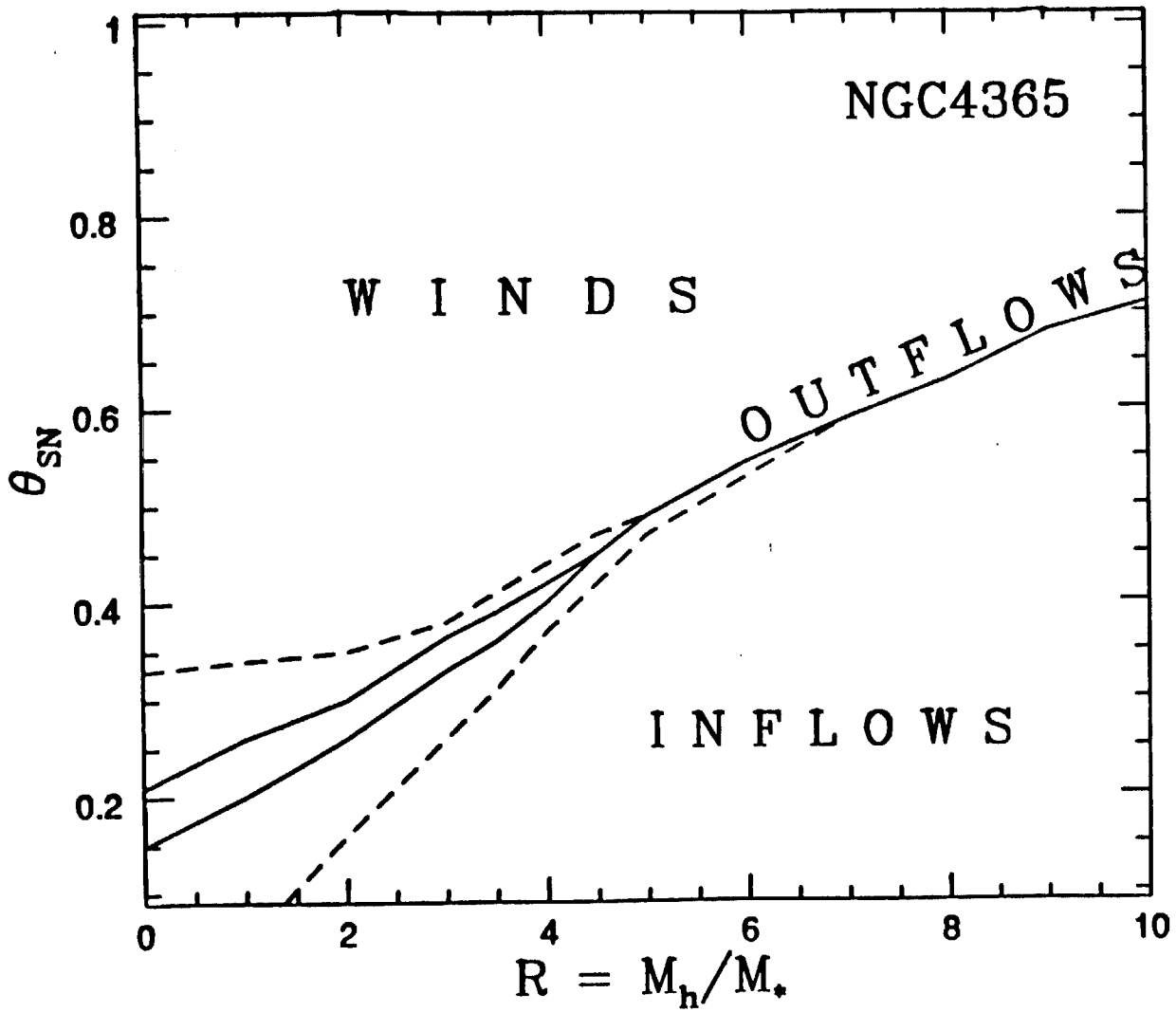
NGC4365
W I N D S
O U T F L O W S
I N F L O W S
θ_{SN}
1
0.8
0.6
0.4
0.2
0
2
4
6
8
10
R = M_h/M_*

FIG. 10.

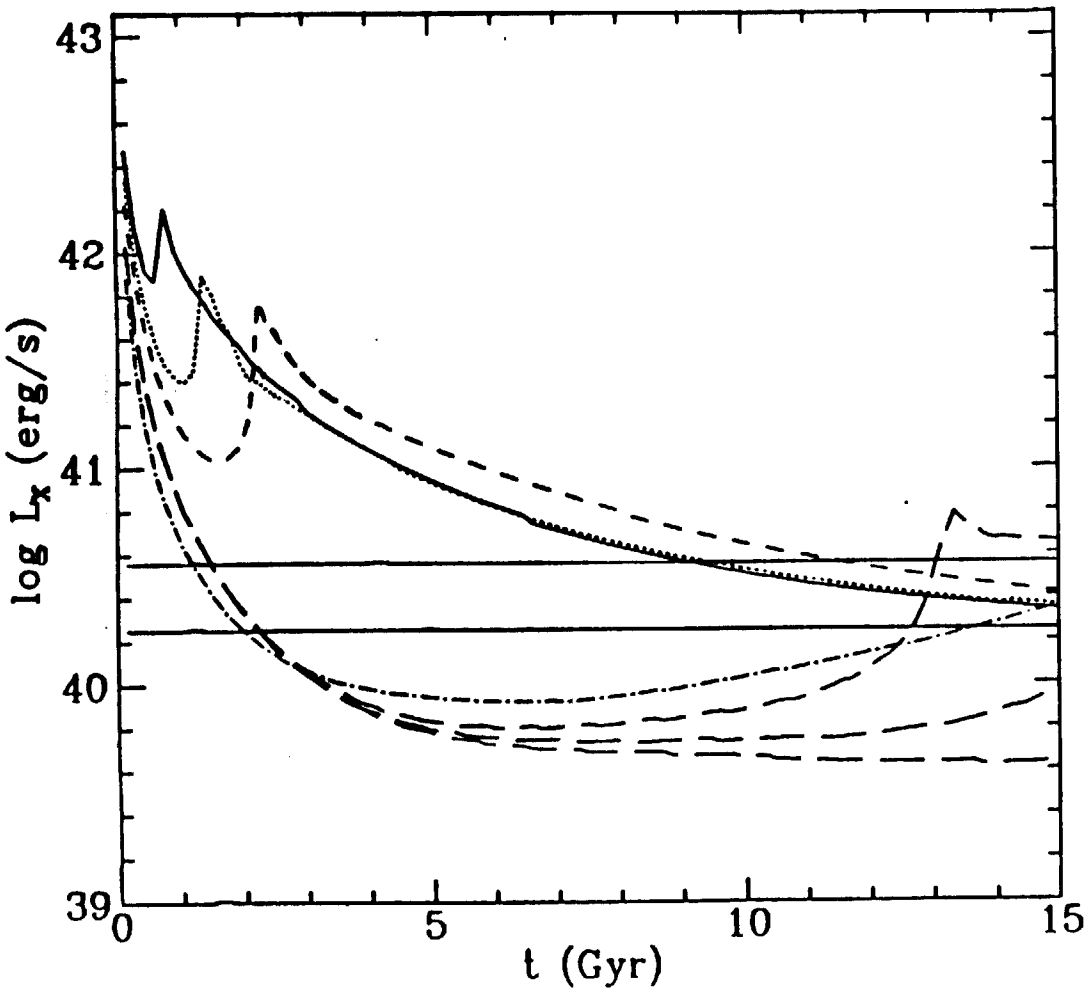

FIG. 11

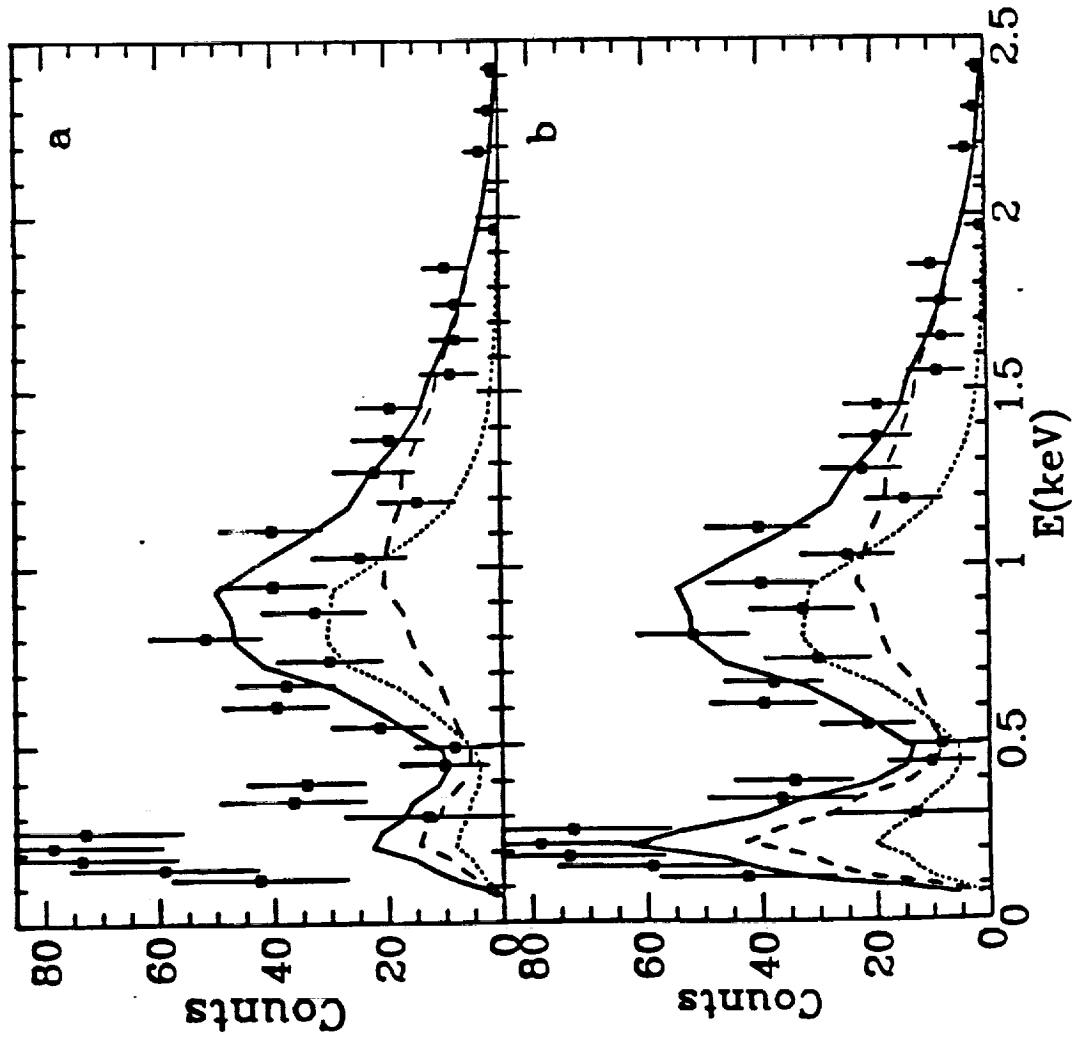

FIG. 12

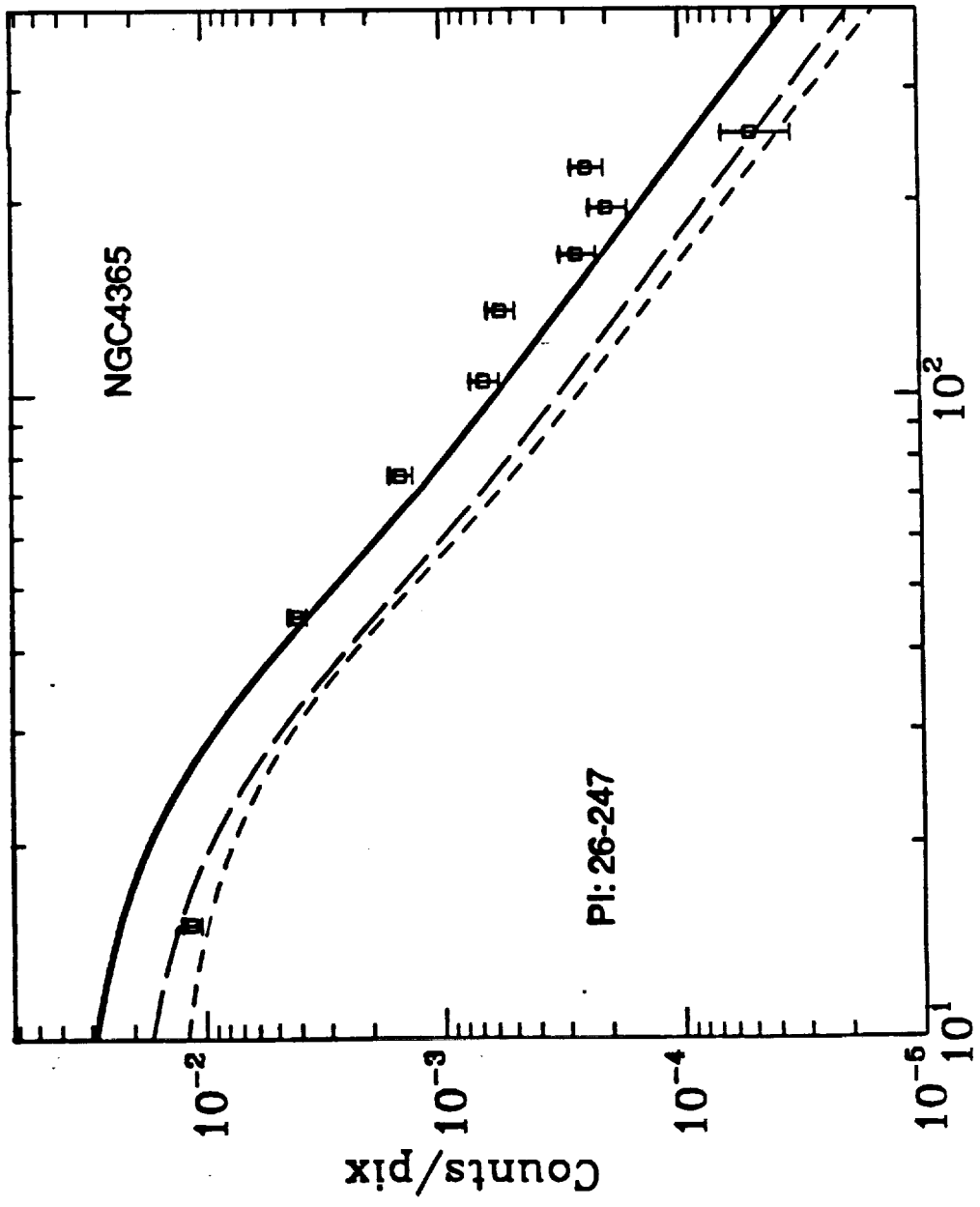

FIGURE 12

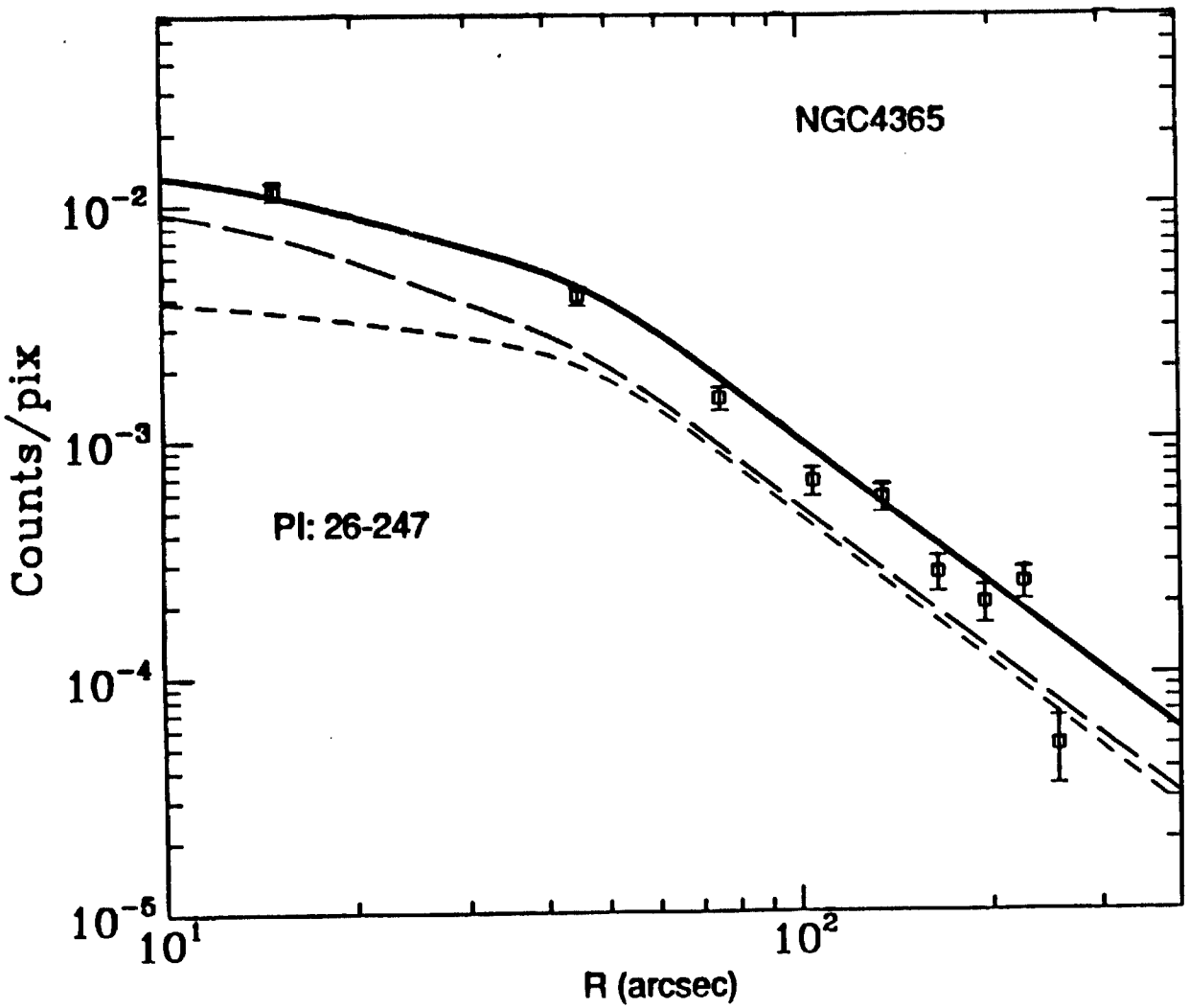

FIG. 14

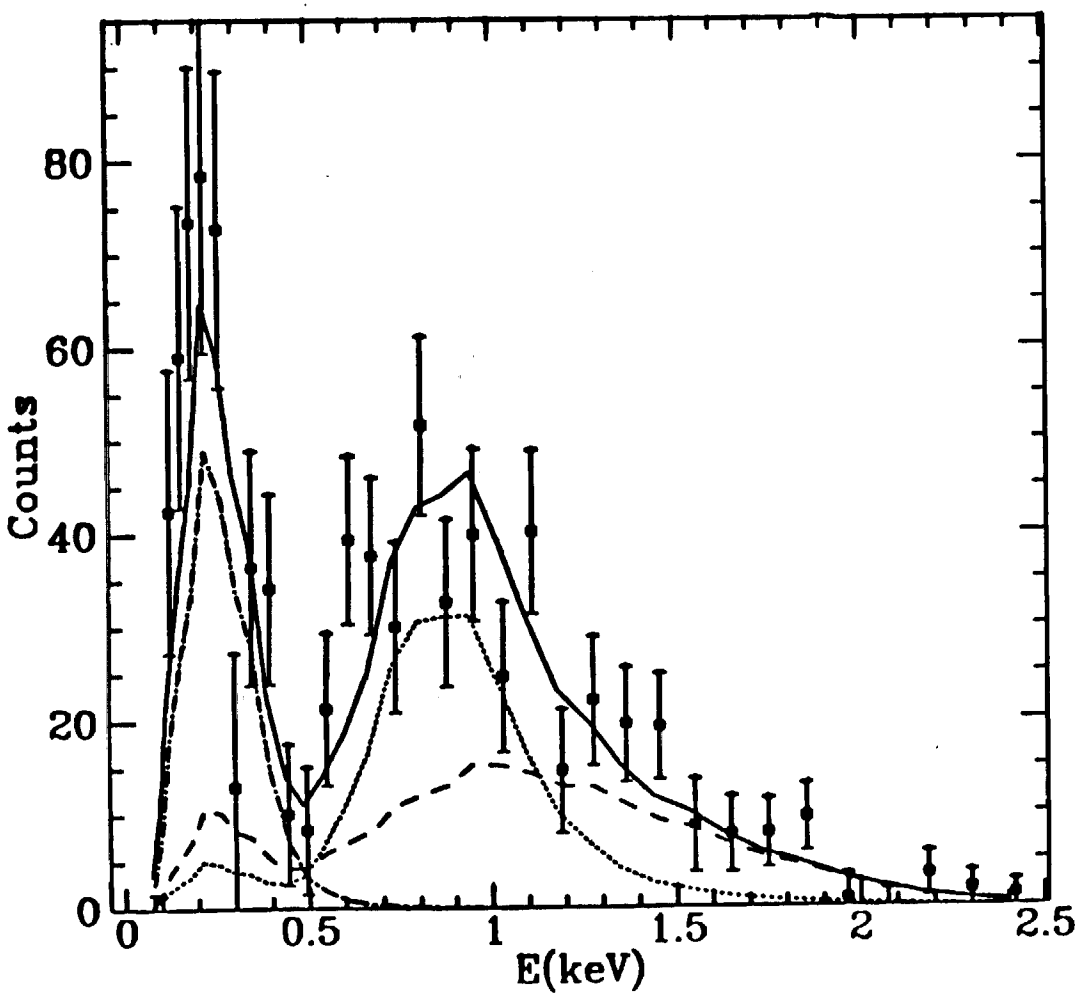

FIG. 15

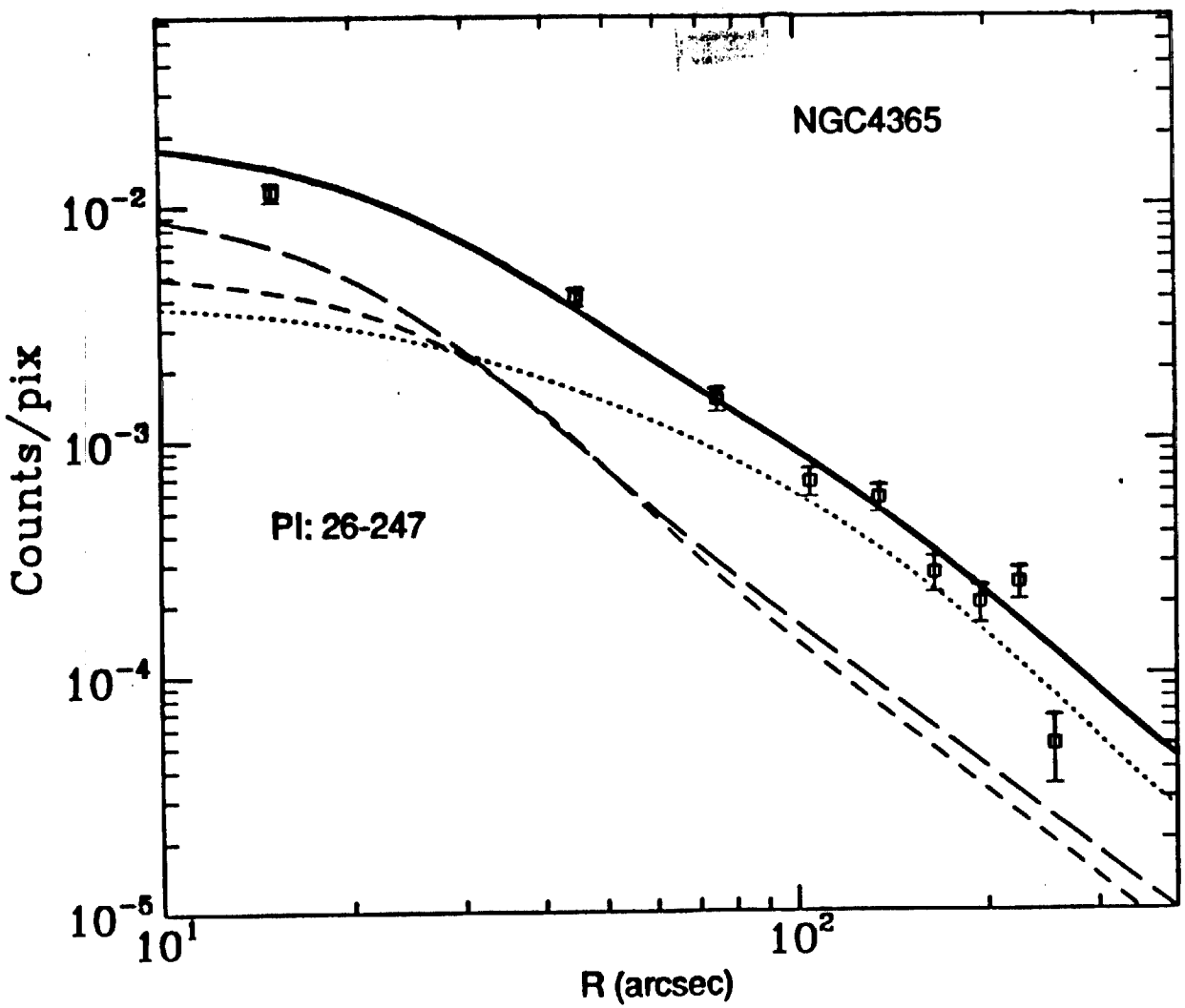

END DATE APRIL 5. 1994

FIG.